공학박사 학위논문

Isogeometric Configuration Design Optimization of Built-up Structures in Generalized Curvilinear Coordinates

일반곡면좌표계에서 조립구조물의

아이소-지오메트릭 배치 최적설계

2017년 8월

서울대학교 대학원

산업·조선공학부

이 승 욱

Isogeometric Configuration Design Optimization of Built-up Structures in Generalized Curvilinear Coordinates

일반곡면좌표계에서 조립구조물의 아이소-지오메트릭 배치 최적설계

지도 교수 조 선 호

이 논문을 공학박사 학위논문으로 제출함
2017년 8월

서울대학교 대학원
산업·조선공학부
이 승 욱

이승욱의 공학박사 학위논문을 인준함
2017년 6월

위 원 장 _____ (인)

부위원장 _____ (인)

위 원 _____ (인)

위 원 _____ (인)

위 원 _____ (인)

Isogeometric Configuration Design Optimization of Built-up Structures in Generalized Curvilinear Coordinates

by

Seung-Wook, Lee

A dissertation submitted for the degree of
DOCTOR OF PHILOSOPHY

in the
Department of Industrial Engineering and Naval Architecture
of
SEOUL NATIONAL UNIVERSITY, KOREA

August 2017

Abstract

Seung-Wook Lee
Department of Industrial Engineering and Naval Architecture
College of Engineering
Seoul National University

In the thesis, an isogeometric configuration design optimization method for built-up which consists of plate and shell structures based on generalized curvilinear coordinate (GCC) is developed. We derive the isogeometric configuration sensitivity of the Mindlin plates by using the material derivative and adjoint approaches. This is utilized in the configuration design optimization that includes a variation of design components in its shape and orientation. Due to the non-interpolatory property of the Non-Uniform Rational B-Spline(NURBS) basis functions, a mismatch of patches in the built-up structures could occur during the isogeometric design optimization, which can be easily resolved using transformed basis functions. Also, isogeometric configuration sensitivity of shell structures is derived with separating shape and orientation effect. For the shell structures, the design is generally affected by the coupled effect of shape and orientation variations. But, at each material point, exact rotational transformation can be calculated using GCC system and isogeometric approach. An orientation variation is identified as rotational transformation of body-

fixed local curvilinear coordinate system. Configuration design sensitivity of shell structure is verified by comparing finite difference sensitivity. And, configuration design optimization is performed for built-up structure.

The built-up structure is made by combining various elements such as plate, beam and shell. When optimizing the built-up structure, configuration design sensitivity is necessary because shape and orientation variations simultaneously happen. Moreover, in the isogeometric analysis (IGA), the control points play the role of design variables so that no more design parameterization is necessary. Hence, the IGA-based one is suitable for the configuration optimization of the built-up structures

By the IGA, the NURBS basis function in computer aided design (CAD) system is directly utilized in the response analysis, which enables the seamless incorporation of higher continuity and exact geometry such as curvature and normal vector into the computational framework. IGA provides a more accurate sensitivity of complex geometries including higher order geometric effects such as normal and curvature information. The impact of exact curvature in the bending problem of Mindlin plates on the configuration design sensitivity is demonstrated through numerical examples. The obtained design sensitivity is further utilized in the configuration design optimization of built-up structures.

Configuration design sensitivity analysis (DSA) for shell structure based on GCC system is formulated using direct differentiation method (DDM). In the design sensitivity of the curved structure such as curved

beam and shell, it is difficult to separate shape and orientation contributions. They affect design variation at the same time. We divide shape and orientation effects through exact transformation between two local curvilinear coordinate in the original design and perturbed design. It can be possible to calculate accurate sensitivity in spite of geometrically complex structures.

Keywords: Isogeometric analysis, Configuration design sensitivity, Built-up structure, Configuration design optimization, Transformed NURBS basis function

Student number : 2010-21111

Table of Contents

List of Tables

List of Figures

Nomenclature

ξ	Knots
$\boldsymbol{\Xi}$	Set of knots
R_i^p	NURBS basis function
N_i^p	B-spline basis function
$\mathbf{B}_i$	Control point
Ω	Open domain
$\mathbf{b}$	Body force
$\mathbf{t}$	Traction on the surface
$\hat{\mathbf{x}}$	Material point in RCC system
$\hat{\mathbf{z}}$	Displacement in RCC
E	Young's modulus
h	Thickness of structures
ν	Poisson's ratio
μ, λ	Lame constants
τ_{ij}	Stress tensor
$\hat{\varepsilon}_{ij}$	Strain tensor
$\varepsilon_{\alpha\beta}$	Strain measure of membrane part
$\omega_{\alpha\beta}$	Strain measure of bending part
γ_α	Strain measure of shear part
$\mathbf{d}$	Set of nodal displacements

u_α	In-plane displacement at mid-surface
w	Out-of-plane displacement at mid-surface
θ_α	Rotational angle at mid-surface
$c^m_{\alpha\beta\mu\lambda}$	Membrane part of material tensor
$c^b_{\alpha\beta\mu\lambda}$	Bending part of material tensor
$c^s_{\alpha\beta}$	Shear part of material tensor
Z	*d*-dimensional variational space
Γ_D	Displacement boundary
Γ_N	Traction boundary
$\mathbf{y}_I$	Response coefficient
$\mathbf{n}$	Normal vector
κ	Curvature
V_Ω	Shape design velocity field
V_θ	Orientation design velocity field
ψ	General performance measure
$\mathbf{g}_i$	Covariant base vector
$\mathbf{g}^i$	Contravariant base vector
g_{ij}	Covariant coefficient of metric tensor

g^{ij}	Contravariant coefficient of metric tensor
$\left\|\mathbf{J}\right\|$	Determinant of Jacobian matrix
Γ_{ij}^{k}	Second-kind Chrisoffel symbol
$\hat{\mathbf{x}}^{*}$	Material point in physical domain
$\mathbf{a}_{\alpha}$	Covariant base vector on the neutral surface
$\mathbf{a}^{\alpha}$	Covariant base vector on the neutral surface
b_{α}^{β}	Mixed curvature tensor
$b_{\alpha\beta}$	Covariant curvature tensor
$E_{\alpha\beta}$	Strain tensors in shell tangent plane
$C^{\alpha\beta\mu\lambda}$	Membrane and bending part of material tensor in curvilinear coordinates
$C^{\alpha 3\mu 3}$	Transverse shear part of material tensor in curvilinear coordinates
N	Axial force
M	Bending moment
Q	Shear force
$\mathbf{p}$	Distributed load intensity vector
$\mathbf{q}$	Boundary resultant vector
$\delta\alpha, \delta\beta$	Euler angle
$\tilde{\mathbf{V}}_{\theta}$	Material derivative of transformation matrix
$\mathbf{\Omega}_{\alpha}$	Initial curvature matrix
$\mathbf{E}_{\alpha}$	Component of the perturbed tangential vector
k_1, k_2	Initial bending curvature

k_{61}, k_{62}	Initial twisting curvature
k_4, k_5	Spiral curvature
$\mathbf{\Lambda}_\tau$	Transformation between original design and perturbed design
$\mathbf{A}(\delta a, \delta\beta)$	Transformation matrix by Euler angle
ϕ	Generalized basis function
δ	Generalized response coefficient
$\mathbf{X}_J$	Physical collocation point
$\Xi_{\mathbf{x}_J}$	Parametric collocation point

Chapter 1. Introduction

1.1 Motivation

1.1.1 Configuration design sensitivity analysis in curved structures

The configuration DSA includes both shape and orientation variation of design components. Twu and Choi (1992) present continuum-based configuration DSA for built-up structures which include trusses, beam, plane elastic solids, and plate for linear elastic problems. For a straight or flat design component, they described the configuration design change as a dynamic process of moving the design component in three steps: rigid body translation, rigid body rotation, and shape variation. They noted that a rigid body translation of the design component does not contribute to the design sensitivity and considered shape and orientation design variables.

It is necessary to compute configuration design sensitivity when design optimization is performed in three dimensional space. The built-up structure which consists of one or two dimensional elements accompanies the combination of shape and orientation design variation during design is changed toward optimal model. Therefore a configuration design is applicable to built-up structure with structural design components such as truss, beam plate and shell. The orientation change yields a different structural response

The configuration design sensitivity formulations are limited to linear geometric perturbation, such that a line component remains straight and a surface component remains flat during the design change. For the curved structures, however, the design is affected by the coupled effect of shape and orientation variations. Therefore, it is difficult to distinguish shape from orientation variation at the configuration design change.

In this thesis, configuration design sensitivity analysis for the curved structures is proposed by regarding a change of body-fixed local coordinate systems as orientation variation. The generalized curvilinear coordinate is used to represent geometry of the curved structures. The rotational transformation of curvilinear coordinate system between the original and perturbed designs is exactly expressed. Also, through configuration design sensitivity and optimization of built-up structure using plate and shell elements, we can extend optimization problems to real engineering structures.

1.1.2 Advantages of isogeometric framework

Advantages of isogeometric analysis are investigated by many researchers. In aspect of analysis, isogeometric analysis is usually compared with finite element analysis (FEA) which is one of widely used numerical analysis method and has difficulties in dealing with curved structures due to geometric approximation which is inherent in the finite element mesh. IGA framework is introduced to overcome this difficulty.

The framework of IGA, which handles exact geometry with the NURBS basis function, is introduced by Hughes et al. (2005). The IGA that employs the same basis functions used in a CAD model has shown many advantages over the standard FEA. It enables the seamless incorporation of higher order continuity and exact geometry such as curvature and normal vector into the computational framework. IGA provides a more accurate sensitivity of complex geometries including higher order geometric effects such as normal and curvature information. The NURBS functions of higher continuity offer a much more compact representation of the response and sensitivity of systems than the standard FE functions do, yielding more accurate results, even at the same order of basis functions. Therefore, it is possible for the IGA to obtain a more accurate solution than from the polynomial-based FEA, even with fewer degrees of freedom. In the curved structure, exact geometric property is important. This study is suitable to show advantage of IGA. Also, GCC frame gives many higher order terms. Therefore, IGA can exactly evaluate higher order terms and their sensitivities.

In view of design optimization, IGA has significant superiority. In many shape design optimization for real engineering cases, an initial model usually comes from a CAD modeler. Therefore, if the shape design optimization is based on FEA, the designer should convert this CAD model into finite element (FE) mesh. During this conversion process, often there are numerical errors, due to the approximation of model geometry. But, IGA adopts the NURBS function, which is used in CAD modeling, as a basis function of analysis. Therefore, an exact

geometry can be described by using exactly the same basis functions. In shape design optimization sense, a design boundary is already expressed by the NURBS curve, so that an additional design parameterization is not necessary. Also, the optimal shape is easily obtained without the help of mesh regeneration. Thus, the isogeometric shape DSA is free from re-meshing during the optimization process. But, to apply real engineering problem, it is necessary to extend practical elements such as shell, plate and built-up structures. In a sense, this research has much significance. Therefore, the isogeometric configuration design optimization can approach to practical numerical examples.

1.2 Literature survey

1.2.1 Configuration design sensitivity analysis

There are few papers regarding the configuration DSA method that includes both shape and orientation variations of design components. A continuum-based configuration DSA method was developed for built-up structures, where both shape and orientation variations were made for each structural component (Twu and Choi, 1992). Cho and Choi (2000) performed the configuration DSA and optimization for beam design components in transient dynamic and path-dependent problems. In order to obtain accurate design sensitivity, they employed angular design velocity fields with Euler angles to represent the orientation design variations. Also, Choi (2002) presented that a general formulation for configuration design sensitivity analysis about a three-dimensional beam structure is developed based on a variational formulation of the original Euler beam theory in linear elastic problem and using the material derivative and adjoint variable method. For the curved structure, Kim *et al*. (2002) suggested DSA formulation for shell structures considering sizing, shape and orientation design variables using meshfree discretization. In their formulation, strain-displacement and constitutive relations are given in global and local coordinate system, respectively. They bridged this gap through adopting the rotational transformation of constitutive matrix, and defined the change of this transformation relation as an orientation design variation.

The configuration optimization for a surface design component is

rarely applied to IGA. Since we have considered the shape and orientation variations, the parameterization of design is quite difficult and complicated but, in the IGA, the control points play the role of design variables so that no more design parameterization is necessary. Hence, the IGA-based one is suitable for the configuration optimization of the built-up structures (Lee and Cho 2015). Choi and Cho (2014) considered an orientation variation of crack as a change of crack-tip local coordinate system for the DSA of stress intensity factors in curved crack problems. The NURBS-based exact tangential and normal vectors enables us to exactly define a local coordinate system at the crack-tip, whose shape dependency naturally leads to configuration design variations that include the change of crack orientation. Yoon et al. (2015) applied configuration design sensitivity to boundary integral equation method which employs the shape variation of a domain naturally result in both shape and orientation variation. Therefore, the tangential and the normal design velocity fields should have been taken into account in the IGA using boundary integral equation. Also, Choi *et al*. (2016) developed that displacement field is described in a GCC system whose change in design variation process is defined as an orientation design variation. Also, the rotational transformation of GCC system between the original and perturbed designs is exactly expressed, through employing the kinematical description of geometrically exact beam theory, regardless of perturbation amount. In this paper, configuration DSA based on straight and curved surface structure is formulated. In their DSA formulation, the orientation design variation can be considered as a

change of body-fixed local coordinate system.

1.2.2 Isogeometric framework

Ever since the framework of the IGA method was established by Hughes *et al*. (2005), the isogeometric method that employs the same basis functions as used in the CAD model has shown many advantages over the standard finite element method (FEM). The isogeometric method has a major feature, the CAD based parameterization of field variables in an isoparametric manner, and thus requires no further communication with the CAD systems during the refinement processes. Moreover, analogue to the *h*- and *p*-refinements in the standard FEM, a new efficient *k*-refinement scheme was proposed without any change in the model geometry. Later, these refinement issues were more extensively discussed by Cottrell *et al*. (2007). It was found that the increased smoothness by *k*-refinement yielded a more accurate solution than classical C^0-continuous *p*-refinement. k-refinement method is a new concept containing characteristics in the *h*- and p-refinements of the FEM. The importance of inter-element continuity in the isogeometric analysis is highlighted by Cottrell *et al*. (2006) in the structural vibration, and by Akkerman *et al*. (2008) in the multiscale analysis, where C^1-continuous discretization outperform the C^0 counterparts in FEM. Evans *et al*. (2009) proposed the first mathematical study of *k*-refinement in the IGA. IGA method has now been widely applied to many different fields, such as fluid mechanics (Zhang *et al*. 2007), fluid-structure interactions

(Bazilevs *et al*. 2008) and contact treatment (Temizer *et al*. 2008).

In applying the IGA to shape design optimization problems, accurate DSA is essential Based on the shape DSA theory (Komkov et al., 1986), Cho and Ha (2009) performed shape optimization based on IGA and showed that IGA has shown two significant benefits addressed. *First*, the accurate sensitivity of complex geometries including the higher order effect originated from the exact representation of the geometry such as curvature as well as normal and tangential vectors. The NURBS functions of higher order continuity offer a much more compact representation of response and sensitivity of structures than the standard Lagrangian polynomial functions do, yielding better accuracy even at the same polynomial order. *Second*, the vast simplification of design parameterization utilizing the direct variation of CAD geometry. Since the NURBS basis functions are used in both isogeometric response and sensitivity analysis, design modifications are easily obtainable using the adjustment of control points which represent the geometric model. Similar to the approach in FEM-based optimization, the design variables are defined at boundary control points. Unlike the FEM, the boundary of the isogeometric model is already expressed by NURBS curves, and every perturbation of boundary control points preserves the smooth change of the design boundary. Although isogeometric shape optimization provides simple and useful parametrization, the updates of interior control points are still challenging since CAD typically represents the boundary information. The movement of internal control points may be related to the change in boundary control points through

simple algebraic constraints (Wall *et al*. 2008). Qian (2010) derived shape design sensitivity equation with respect to positions and weights of NURBS control points. Isogeometirc shape optimization for shell structures is also presented using sensitivity weighting and semi-analytical sensitivity analysis. A sensitivity weighting scheme is presented which eliminates certain effect of the chosen discretization on the design update. (Kiendl *et al*. 2014). Also, Yoon (2015) presented that utilizing the generalized formulation in the isogeometric framework, both of response and sensitivity analysis methods for the geometrically exact shear deformable shell are developed in the curvilinear coordinates. The developed isogeometric shape optimization scheme applied to the various fields such as heat conduction (Yoon *et al*. 2013), geometrically nonlinear structures (Koo *et al.* 2013) and boundary integral equation (Yoon and Cho 2016)

1.2.3 Shell structures based on curvilinear coordinate

In many engineering applications on a wide scale, curved geometries represented by shell components have been employed. The degenerated solid approach has been widely used for finite element shell analysis ever since Ahmad et al. (1970). Alternatively, Simo and Fox (1989) introduced the geometrically exact shell formulation based on the classical shell theory. Although the degenerated solid approach and classical shell theory share the same hypothesis for shell structures, the resultant formulation is typically derived numerically in the former, and

analytically in the latter. Avoiding the mathematical complexities associated with classical shell theory, the degenerated solid approach would be better for the numerical implementation. On the other hand, the geometrically exact formulation describes the mathematical model of a shell naturally by curvilinear coordinates (Roh and Cho 2003). Employing the degenerated solid approach, Benson *et al*. (2010) and Hosseini *et al*. (2014) have developed the isogeometric shell analysis in the rectangular Cartesian coordinate system: a set of orthogonal unit base vectors has been employed as the basis for representation of vectors and tensors. Bouclier *et al*. (2013) have proposed the locking free isogeometric degenerated solid model with mixed formulation. Indeed, the parametric knot representations of the NURBS geometries are rather suited to describe curved geometries in curvilinear coordinate systems: arbitrary bases, with base vectors not necessarily orthogonal nor of unit length, are considered. Thus the isogeometric analysis of the geometrically exact shell models has been formulated in curvilinear coordinate systems (Kiendl *et al*. 2009; Echter *et al*. 2013; Nagy *et al*. 2013).

In this study, the continuum-based shape sensitivity analysis using the isogeometric approach is derived in the curvilinear coordinate systems for arbitrary surface shapes. Note that the curvilinear coordinates compose the “generalized” coordinate systems from which orthogonal and Cartesian systems are reduced with geometric restrictions. The generalized formulations are applied to the shape sensitivity analysis of the geometrically exact shell model in which the

curvilinear coordinates are directly formed on the given NURBS geometries. The precise sensitivity can be obtained by complete formulations of boundary integrals for the shell boundary resultants and their material derivatives. Incorporating structural response and generalized shape sensitivity analyses in the isogeometric framework into the shape optimization problem.

1.2.4 Organization of thesis

In Chapter 2, IGA method is reviewed for describing this research. NURBS curves and surfaces are introduced and their geometric algorithms including refinement schemes. Also, isogeometric shape optimization is simply reviewed for extending isogeometric configuration optimization. The IGA method for plate element and shell element is introduced. To describe shell formulation, GCC system is introduced. In Chapter 3, basic material derivative formulas for configuration DSA including shape and orientation variations are described in rectangular Cartesian coordinate (RCC) and GCC system. And, isogeometric configuration DSA are derived for plate and shell structures. In Chapter 4, built-up structures cause mismatch problem in configuration design optimization. To solve the mismatch problem, the transformed basis function is introduced to impose the continuity condition at the intersection boundary. In Chapter 5, several numerical examples are demonstrated to verify developed method in this thesis. The accuracy of the response and configuration DSA is validated. Also,

a benchmark problem for shell structure, simple plate structure and a real engineering problem are considered for configuration design optimization. In Chapter 6, the concluding remarks are given and the limit of this thesis and the future work are described.

Chapter 2. Isogeometric Analysis

2.1 Review of Isogeometric analysis

IGA method is the methodology for analysis using NURBS basis functions, which usually represent CAD geometry. Instead of polynomial basis functions in a FEM, the use of NURBS basis functions enables exact description of model geometry, which gives more accurate solution in the response analysis.

2.1.1 NURBS basis function

The IGA is represented in terms of the same basis functions used for CAD geometry. The IGA has several advantages over the conventional FEA; the geometric exactness and simple refinements due to the use of NURBS basis functions based on B-splines. Consider a set of tensor products of knot vectors $\boldsymbol{\xi}$ in an n-dimensional parametric space. In the 1-dimensional case, it is written as

$$\boldsymbol{\xi} = \left\{ \xi_1, \xi_2, \cdots, \xi_{n+p+1} \right\}, \tag{2.1}$$

where ξ_i, p and n are the knot vector, the order of the basis function and the number of control points, respectively. The B-spline basis functions can be defined, recursively, as

$$N_i^0(\xi) = \begin{cases} 1 & \text{if } \xi_i \le \xi < \xi_{i+1} \\ 0 & \text{otherwise} \end{cases}, \tag{2.2}$$

and

$$N_i^p(\xi)=\frac{\xi-\xi_i}{\xi_{i+p}-\xi_i}N_i^{p-1}(\xi)+\frac{\xi_{i+p+1}-\xi}{\xi_{i+p-1}-\xi_{i+1}}N_{i+1}^{p-1}(\xi),\quad (p=1,2,3,\ldots). \tag{2.3}$$

A general quadratic B-spline basis functions are shown in Figure 2.1.

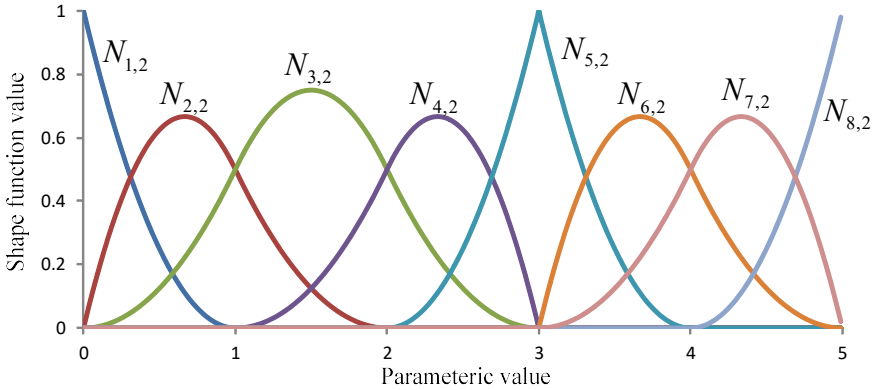

Figure 2.1 Quadratic B-spline basis functions
Ξ={0,0,0,1,2,3,3,4,5,5,5}

The shape functions are completely different from those in the FEM and guarantee *p*-1 continuous derivatives. The B-spline has some useful properties as a basis function such as partition of unity, compactness and non-negativity. Using the B-spline basis function $N_i^p(\xi)$ and weight w_i, the NURBS basis function $R_i^p(\xi)$ is defined as

$$R_i^p(\xi)=\frac{N_i^p(\xi)w_i}{\sum_{j=1}^{n}N_i^p(\xi)w_j}. \tag{2.4}$$

Generally, the IGA using higher order basis functions offers higher regularity than the conventional FEA. The NURBS basis functions satisfy the following properties:

(1) $\sum_{i=1}^{l}R_i^p(\xi)=1$ (Partition of unity),

(2) R_i^p is included in the interval $[\xi_i, \xi_{i+p+1}]$ (Compact support),

(3) $R_i^p(\xi) \geq 0$ (Non-negativity).

A NURBS curve is obtained from the linear combination of NURBS basis function and corresponding control points $\mathbf{B}_i \equiv \mathbf{B}(x_i)$, which are the coefficients for each NURBS basis function. For a given *l* pairs of the *p*-th order NURBS basis function R_i^p and the corresponding projected (weighted) control point, the NURBS curve **C** is obtained by

$$\mathbf{C}(\xi) = \sum_{i=1}^{l} R_i^p(\xi)\mathbf{B}_i \,. \tag{2.5}$$

In higher dimensional spaces, the NURBS surface and solid are defined, respectively, as a tensor product of coordinates as

$$\mathbf{S}(\xi,\eta) = \sum_{i=1}^{l}\sum_{j=1}^{m} R_i^p(\xi) R_j^q(\eta)\, \mathbf{B}_{i,j} \tag{2.6}$$

and

$$\mathbf{S}(\xi,\eta,\zeta) = \sum_{i=1}^{l}\sum_{j=1}^{m}\sum_{k=1}^{n} R_i^p(\xi) R_j^q(\eta) R_k^r(\zeta)\, \mathbf{B}_{ijk} \tag{2.7}$$

where *m* and *n* are the number of control points along the η and ζ directions. And *q* and *r* are the order of basis functions defined at the corresponding knot vectors. For the brevity of expression, Eq. (2.6) in three dimensional problems can be rewritten as

$$\mathbf{S}(\Xi) \equiv \mathbf{S}(\xi,\eta) = \sum_{I}^{CP} W_I(\Xi)\mathbf{B}_I(\mathbf{x}) \tag{2.8}$$

where W_I is introduced for the brevity of expression. *CP* denotes the number of control points and **Ξ** is the parametric domain of surface. The same logic and notations are applicable for one and three dimensional

problems. Besides the aforementioned properties as a basis function, the constructed NURBS basis functions possess the property of affine covariance and p-1 continuous differentiability. If the knots are repeated k-times, the continuity of NURBS basis functions decreases k-times as well. For the details of NURBS geometry, the interested readers may consult Rogers (2000), Piegl and Tiller (1997).

2.1.2 Refinements

In the standard finite element method, the mesh refinements are a core numerical method that the exactness of solution is guaranteed with the refinements. In the isogeometric analysis, the same analogy is adopted. However, the refinement process is directly applied to the geometry such that the resultant geometry and parametrization remain unchanged by refinements. This property is a great advantage of the isogeometric analysis and its details are reviewed.

h-refinement

Although the isogeometric h-refinement is analogous to h-refinement in the standard finite element method, h-refinement process is performed on the parametric space. Since all numerical integration is evaluated in the parametric space, inserting more knots into the original knots results in the refined knots and control points in the level of the analysis as well.

For *h*-refinement, any algorithm inserting knots can be used. As written in the previous chapter, the geometry and the parametrization do not change, but a finer mesh is obtained.

To demonstrate the *h*-refinement process, a simple example is shown. Let us consider the initial knots [0 0 0 1 1 1] with the order 2. From the relationship between the number of knot and the number of basis function, $m = n + p + 1$, the number of basis function is 3, as shown in figure 2.2. If the $\bar{u} = 0.5$ is inserted, the new knot vector is [0 0 0 0.5 1 1 1] and the number of numerical integration interval is changed to 2.

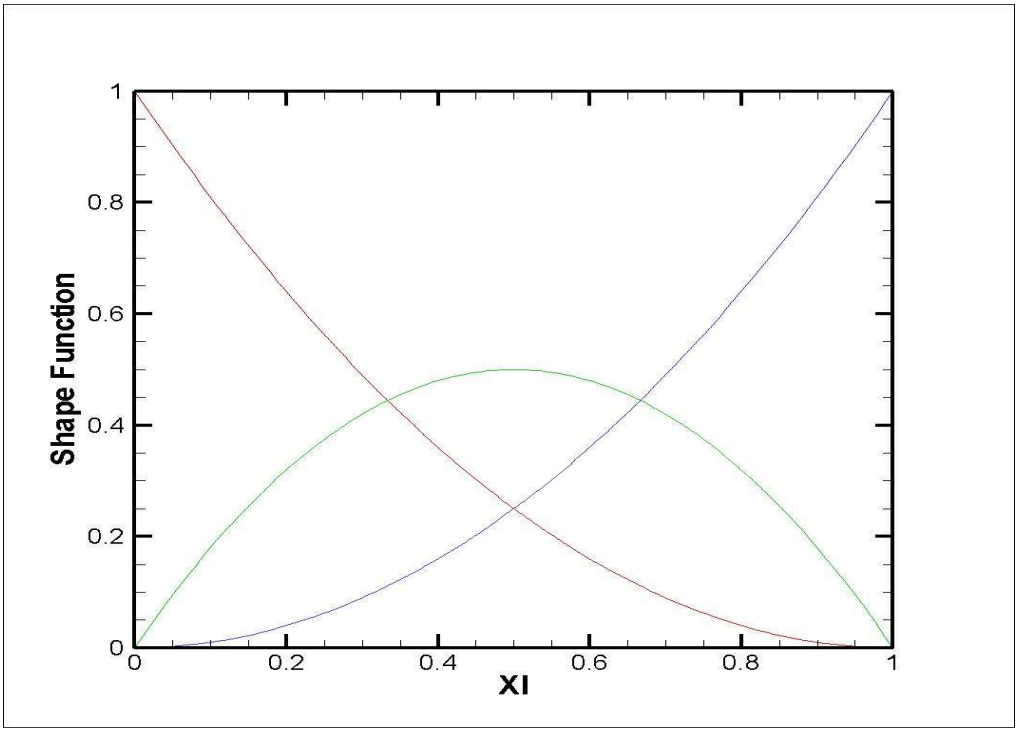

$\Xi = [0 \quad 0 \quad 0 \quad 1 \quad 1 \quad 1]$

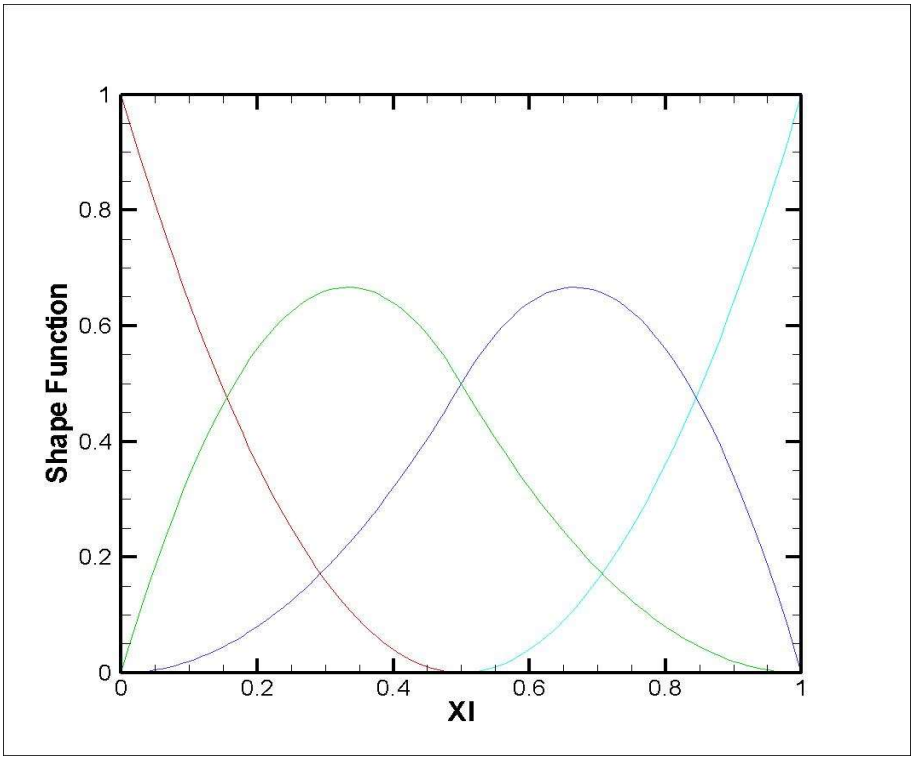

$\Xi = [0 \quad 0 \quad 0 \quad 0.5 \quad 1 \quad 1 \quad 1]$

Figure 2.2 B-spline basis function by *h*-refinement

p-refinement

Increasing the order of basis function is called as p-refinement in the analysis, analogous to the degree elevation in the CAD algorithm. Typically the degree elevation is performed by repeating all discrete knots by the elevation order. The degree elevation process maintains the original geometry and the continuity at each knot remain unchanged, the elevated order minus one, although the order or basis functions is increased.

For the knot in the previous example, [0 0 0 0.5 1 1 1] with the order 2, let us consider *p*-refinement. *P*-refinement is performed by only repeating the knots, then the resulting knot vector is [0 0 0 0 0.5 0.5 1 1 1 1] and basis functions are drawn in figure 2.3. Not apparently shown in figure 2.2, the order of continuity decreases passing the repeated knots, 0.5.

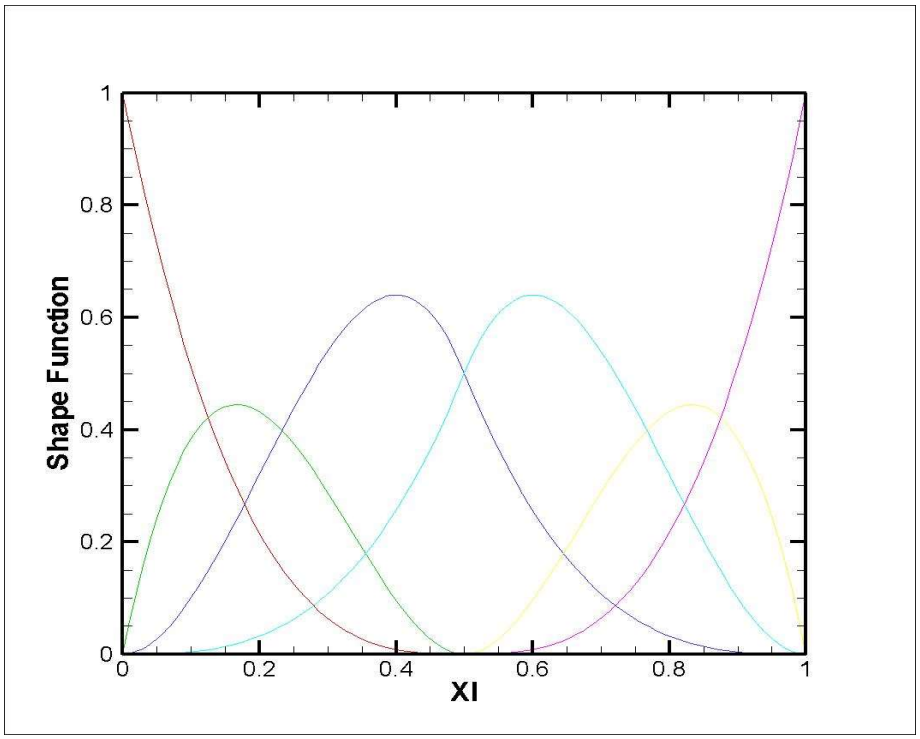

$\Xi = [0 \quad 0 \quad 0 \quad 0 \quad 0.5 \quad 1 \quad 1 \quad 1 \quad 1]$

Figure 2.3 B-spline basis function by *p*-refinement

k-refinement

K-refinement is a new concept in the isogeometric analysis. Basically *k*-refinements correspond to the first degree elevation and the second knot refinement sequentially. By doing in this way, not only the order of basis function is increased but also the parametric mesh is refined without the loss of continuity. The patch-wise continuity is the most important part of the isogeometric analysis and *k*-refinement is superior to p-refinement in the sense of the continuity.

For the previous knot $[0 \quad 0 \quad 0 \quad 1 \quad 1 \quad 1]$ with the order 2, let us consider *k*-refinement. For *k*-refinement, the degree of basis functions is increased by repeating knots and an additional internal knot is inserted. Then the resulting knot is $[0 \quad 0 \quad 0 \quad 0 \quad 0.5 \quad 1 \quad 1 \quad 1 \quad 1]$. Different to p-refinement, the continuity passing through $\bar{u} = 0.5$, does not be deteriorated.

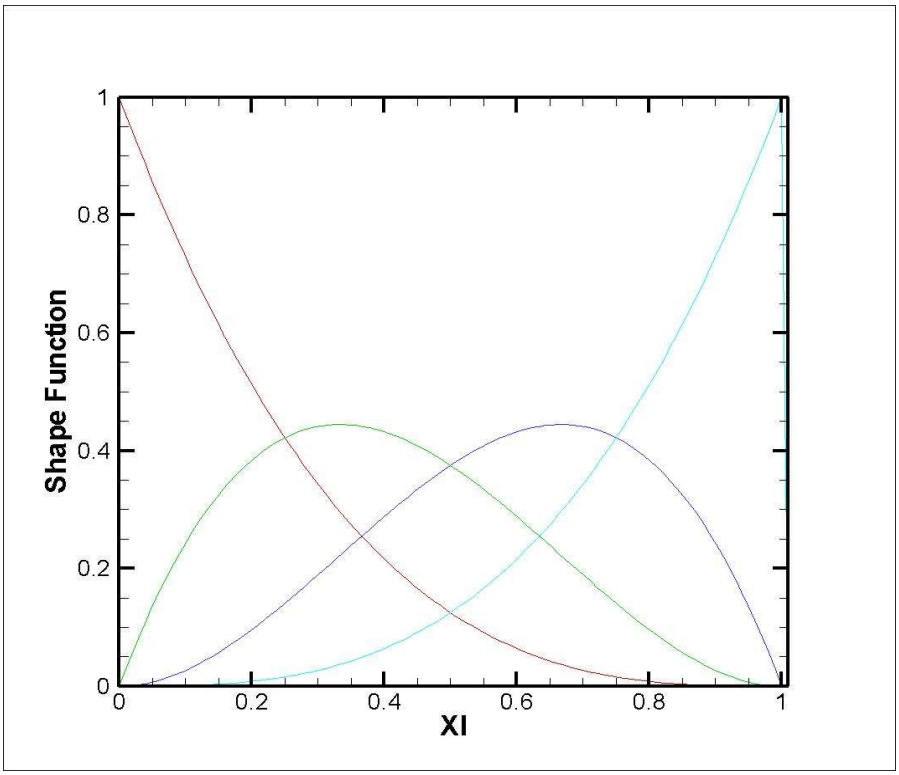

$$\Xi = [0 \quad 0 \quad 0 \quad 0 \quad 0.5 \quad 1 \quad 1 \quad 1 \quad 1]$$

Figure 2.4 B-spline basis function by *k*-refinement

2.1.3 Isogeometric shape optimization

Because IGA has advantages such that it can represent exact geometry and no re-meshing, the IGA method is widely applied for shape design optimization by many researchers. Using IGA, the shape design optimization is performed directly from the CAD model. In the IGA method, the model data such as positions of control points and knot vectors are directly used in the analysis. Therefore, the model data should be extracted from the initial CAD model as shown in Figure 2.5-(a) (Cho and Ha 2009)

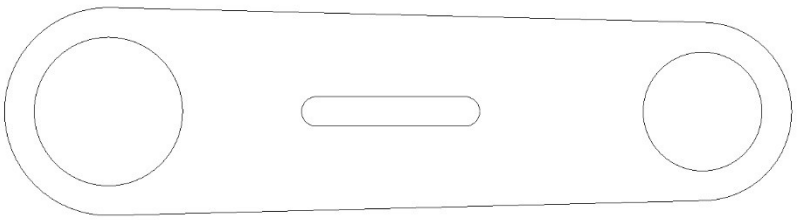

(a) CAD model

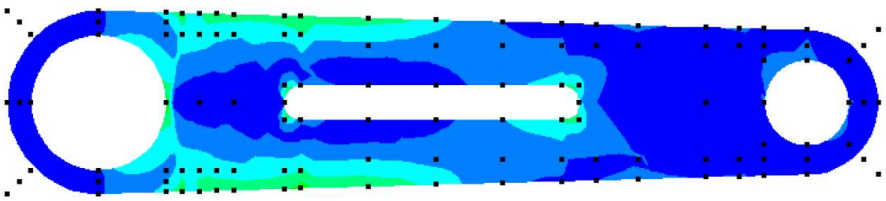

(b) Initial design

Figure 2.5 Torque arm model

Using sweep operation, NURBS surface is generated and we performed IGA directly. Using the isogeometric shape sensitivity, a shape design optimization for minimum material volume is performed for the torque are model shown in Figure 2.5-(b). Based on isogeometric shape sensitivity, the design variables which is the coordinates of boundary control points are updated. In isogeometric shape optimization it is not necessary to regenerate the control mesh. And then, response and sensitivity analysis are performed for the updated design. This process is not performed until the optimal criteria is satisfied. If the optimal criteria is satisfied, the optimal shape is achieved as shown in Figure 2.6, where smooth and symmetric design variation is observed. The whole process of the structural design can be summarized by a schematic design process including system analysis and design optimization given in Figure 2.7.

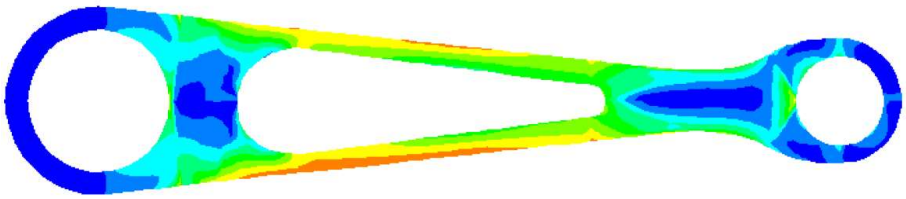

Figure 2.6 Optimal design for torque arm

As shown in Figure 2.7, no mesh regeneration and design parametrization are observed in isogeometric shape optimization. In case of FE-based shape design optimization, it is essential to generate FE mesh at each iteration and to parametrize design variables. Therefore, isogeometric shape optimization has advantage of aspect of efficiency.

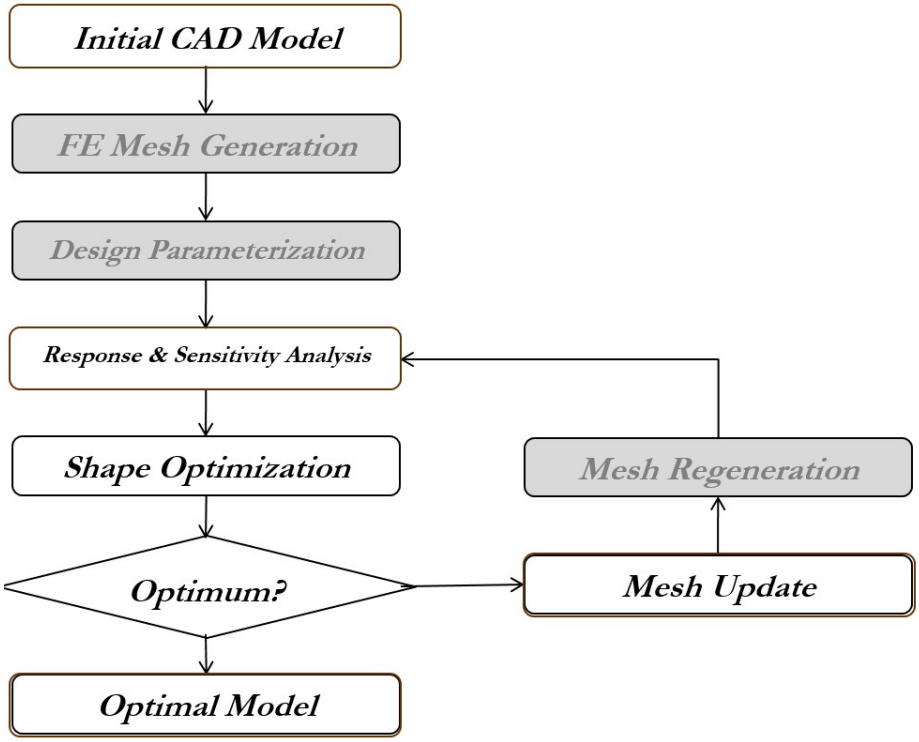

Figure 2.7 Isogeometric optimization process

2.2 Isogeometric analysis of plate structures

2.2.1 Kinematics of Mindlin plate

Consider a general continuum domain $\boldsymbol{\Theta}$ for a Mindlin plate as shown in Figure. 2.8.

$$\Theta = \left\{ \left(x_1, x_2, \zeta \right) \in \Re^3 \left| \zeta \in \left[-\frac{h}{2}, \frac{h}{2} \right], \left(x_1, x_2 \right) \in \Omega \subset \Re^2 \right. \right\} \quad (2.9)$$

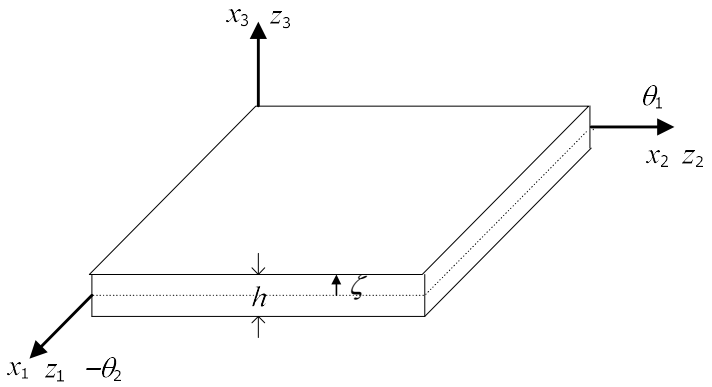

Figure 2.8 Mindlin plate in three dimensional space

According to the Mindlin plate assumptions, the displacement $\hat{\mathbf{z}}$ at any point through thickness are obtained as

$$\hat{z}_1(\hat{x}_1, \hat{x}_2, \hat{x}_3) = u_1(\hat{x}_1, \hat{x}_2) + \zeta\theta_1(\hat{x}_1, \hat{x}_2) \quad (2.10)$$

$$\hat{z}_2(\hat{x}_1, \hat{x}_2, \hat{x}_3) = u_2(\hat{x}_1, \hat{x}_2) + \zeta\theta_2(\hat{x}_1, \hat{x}_2) \quad (2.11)$$

and

$$\hat{z}_3(\hat{x}_1, \hat{x}_2, \hat{x}_3) = w(\hat{x}_1, \hat{x}_2) \quad (2.12)$$

where u_α, w and θ_α are in-plane displacement, out-of-plane displacement and rotational angle at the mid-surface, respectively. Greek

letters such as α, β take values 1 and 2 while Latin italic letters take values from 1 to 3. Thus, a set of nodal displacement in the domain consists of six independent components as

$$\mathbf{d} = [u_1 \quad u_2 \quad w \quad \theta_1 \quad \theta_2 \quad \theta_3]^T , \tag{2.13}$$

where θ_3 is the drilling degrees of freedom for numerical stability. Strains at any points through the plate thickness are expressed as

$$\hat{\varepsilon}_{\alpha\beta}(\mathbf{d}) = \varepsilon_{\alpha\beta}(\mathbf{d}) + \zeta\omega_{\alpha\beta}(\mathbf{d}) , \quad \hat{\varepsilon}_{\alpha 3} = \gamma_\alpha \tag{2.14}$$

where the membrane, curvature, and shear strains at mid-surface are given, respectively, as

$$\varepsilon_{\alpha\beta} = \frac{1}{2}(u_{\alpha,\beta} + u_{\beta,\alpha}) , \tag{2.15}$$

$$\omega_{\alpha\beta} = \frac{1}{2}(\theta_{\alpha,\beta} + \theta_{\beta,\alpha}) \tag{2.16}$$

and

$$\gamma_a = \theta_a + w_{,\alpha} \tag{2.17}$$

where $(\bullet)_{,\alpha}$ denotes partial derivative with respect to the x_α. Using the constitutive law for the linear equation, the relation between strain and stress is represented by

$$\tau^m_{\alpha\beta} = c^m_{\alpha\beta\mu\lambda}\varepsilon_{\mu\lambda} \tag{2.18}$$

$$\tau^b_{\alpha\beta} = c^b_{\alpha\beta\mu\lambda}\omega_{\mu\lambda} \tag{2.19}$$

and

$$\tau^s_{\alpha} = c^s_{\alpha\beta}\gamma_\beta \tag{2.20}$$

where c is the generalized material tensor related to the membrane,

bending and shear actions are expressed, respectively, as

$$c^{m}_{\alpha\beta\mu\lambda} = h\left[\,\mu(\delta_{\alpha\mu}\delta_{\beta\lambda} + \delta_{\alpha\lambda}\delta_{\beta\mu}) + \lambda\delta_{\alpha\beta}\delta_{\mu\lambda}\,\right] \tag{2.21}$$

$$c^{b}_{\alpha\beta\mu\lambda} = \frac{h^3}{12}\left[\,\mu(\delta_{\alpha\mu}\delta_{\beta\lambda} + \delta_{\alpha\lambda}\delta_{\beta\mu}) + \lambda\delta_{\alpha\beta}\delta_{\mu\lambda}\,\right] \tag{2.22}$$

and

$$c^{s}_{\alpha\beta} = h\mu\delta_{\alpha\beta} \tag{2.23}$$

where, λ and μ are the Lamé constants.

2.2.2 Variational equation and isogeometric discretization

Using the principle of virtual work, a variational equation is written as

$$a^{m}(\mathbf{d},\overline{\mathbf{d}}) + a^{b}(\mathbf{d},\overline{\mathbf{d}}) + a^{s}(\mathbf{d},\overline{\mathbf{d}}) = \ell(\overline{\mathbf{d}})\,, \quad {}^{\forall}\overline{\mathbf{d}} \in \overline{Z} \tag{2.24}$$

where the membrane, curvature, and shear strains energy are given, respectively, as

$$a^{m}(\mathbf{d},\overline{\mathbf{d}}) = \int_{\Omega} c^{m}_{\alpha\beta\mu\lambda}\varepsilon_{\alpha\beta}(\mathbf{d})\varepsilon_{\mu\lambda}(\overline{\mathbf{d}})\mathrm{d}\Omega \tag{2.25}$$

$$a^{b}(\mathbf{d},\overline{\mathbf{d}}) = \int_{\Omega} c^{b}_{\alpha\beta\mu\lambda}\omega_{\mu\lambda}(\mathbf{d})\omega_{\alpha\beta}(\overline{\mathbf{d}})\mathrm{d}\Omega \tag{2.26}$$

and

$$a^{s}(\mathbf{d},\overline{\mathbf{d}}) = \int_{\Omega} c^{s}_{\alpha\beta}\gamma_{\beta}(\mathbf{d})\gamma_{\alpha}(\overline{\mathbf{d}})\mathrm{d}\Omega \tag{2.27}$$

Also, load linear equation is represented by

$$\ell(\overline{\mathbf{d}}) = \int_{\Omega} \mathrm{b}_k\,\overline{\mathrm{d}}_k\,\mathrm{d}\Omega + \int_{\Gamma_{\mathrm{N}}} t_k\,\overline{\mathrm{d}}_k\,\mathrm{d}\Gamma \tag{2.28}$$

where b_k are t_k the body force and moment intensity per unit area and the surface force and moment intensity per unit area, respectively. $\overline{Z}$ is a *d*-dimensional variational space defined as

$$\overline{Z} = \{\, \overline{\mathbf{d}} \in \left[H^1(\Omega) \right]^d : \ \overline{\mathbf{d}} = \mathbf{0} \quad \text{on} \ \ \Gamma_D \,\} \tag{2.29}$$

The geometric coordinates are expressed, using the combination of the NURBS basis functions and the corresponding control points $\mathbf{B}_I = \mathbf{B}(\mathbf{x})$, as

$$\mathbf{x}\left(\Xi\right) = \sum_{I}^{CP} W_I(\Xi)\mathbf{B}_I \tag{2.30}$$

Through isoparametric mapping, responses using the combination of the NURBS and the corresponding response coefficients $\mathbf{y}_I = \mathbf{y}(\mathbf{x})$ at control points, as

$$\mathbf{d}\left(\Xi\right) = \sum_{I}^{CP} W_I(\Xi)\mathbf{y}_I \tag{2.31}$$

Note that NURBS basis functions are not interpolatory except for the end points of open knots. Variational space for the response is defined as

$$Y = \{\, \overline{\mathbf{y}} \in \left[H^1(\Omega) \right]^d : \ \overline{\mathbf{d}} = \sum_{J} W_J(\Xi)\overline{\mathbf{y}}_J = \mathbf{0} \quad \text{on} \ \ \Gamma_D \,\} \tag{2.32}$$

Using the isogeometric discretization, Equation (2.24) is expressed as

$$a^m(\mathbf{y},\overline{\mathbf{y}}) + a^b(\mathbf{y},\overline{\mathbf{y}}) + a^s(\mathbf{y},\overline{\mathbf{y}}) = \ell(\overline{\mathbf{y}}) \tag{2.33}$$

where

$$a^m(\mathbf{y},\overline{\mathbf{y}}) = \int_\Omega \sum_{I,K}^{CP} C^m_{\alpha\beta\mu\lambda} W^m_{I,\beta} W^m_{K,\lambda} y_{iI} \overline{y}_{\mu K} \, \mathrm{d}\Omega \tag{2.34}$$

$$a^m(\mathbf{y},\overline{\mathbf{y}}) = \int_\Omega \sum_{I,K}^{CP} C^b_{\alpha\beta\mu\lambda} W^b_{I,\beta} W^b_{K,\lambda} y_{iI} \overline{y}_{\mu K} \, \mathrm{d}\Omega \tag{2.35}$$

and

$$a^s(\mathbf{y},\overline{\mathbf{y}}) = \int_\Omega \sum_{I,K}^{CP} C^s_{\alpha\beta} W^s_I W^s_K y_{\alpha I} \overline{y}_{\beta K} \, \mathrm{d}\Omega \tag{2.36}$$

Also, load linear equation is represented by

$$\ell(\overline{\mathbf{y}}) = \int_\Omega \sum_{I}^{CP} W^p_I b_\alpha \overline{y}_{\alpha I} \, \mathrm{d}\Omega + \int_{\Gamma_t} \sum_{I}^{CP} \widehat{W}^p_I t_\alpha \overline{y}_{\alpha I} \, \mathrm{d}\Gamma_t \tag{2.37}$$

2.3 Isogeometric analysis of shell structures

2.3.1 Generalized curvilinear coordinate system

Any point in space is determined by the position vector $\hat{\mathbf{x}} = \hat{x}_1\mathbf{e}_1 + \hat{x}_2\mathbf{e}_3 + \hat{x}_3\mathbf{e}_3$ in a rectangular Cartesian coordinate system with the fixed base vector $\mathbf{e}_1, \mathbf{e}_2, \mathbf{e}_3$ and the coordinate $(\hat{x}_1, \hat{x}_2, \hat{x}_3)$ and can be expressed in terms of curvilinear coordinate (x_1, x_2, x_3) as

$$\hat{\mathbf{x}} = \hat{\mathbf{x}}(x_1, x_2, x_3). \tag{2.37}$$

The tangent vectors to the coordinate curves at $\hat{\mathbf{x}}$ called covariant base vectors are given by

$$\mathbf{g}_i = \frac{\partial \hat{\mathbf{x}}}{\partial x_i}, \tag{2.38}$$

where $\mathbf{g}_i$ emanate from the position vector $\hat{\mathbf{x}}$ and are directed towards the site of increasing coordinate x_i. Contravariant base vectors $\mathbf{g}^i$ are introduced to satisfy the relationship between reciprocal pairs of general base: $\mathbf{g}^i \cdot \mathbf{g}_j = \delta^i_j$. The dot product of covariant and contravariant base vectors define the coefficient of metric tensor, such as

$$g_{ij} = \mathbf{g}_i \cdot \mathbf{g}_j = \frac{\partial \hat{x}_k}{\partial x_i}\frac{\partial \hat{x}_k}{\partial x_j} \tag{2.39}$$

and

$$g^{ij} = \mathbf{g}^i \cdot \mathbf{g}^j = \frac{\partial x_i}{\partial \hat{x}_k}\frac{\partial x_j}{\partial \hat{x}_k} \tag{2.40}$$

The determinants of coefficient of metric tensor relate to the square of determinant of the Jacobian matrix,

$$\left|g_{ij}\right| = \left|\frac{\partial \hat{x}_i}{\partial x_j}\right| = \left|\mathbf{J}\right|^2 \tag{2.41}$$

we have the covariant derivative of vector as

$$\frac{\partial \mathbf{v}}{\partial x_j} = v_i \Big\|_j \mathbf{g}^j = \left(\frac{\partial v_i}{\partial x_j} - v_k \Gamma_{ij}^k\right)\mathbf{g}^i \tag{2.42}$$

where the second-kind Christoffel symbols to represent the partial derivative of base vectors as

$$\Gamma_{ij}^k = \frac{\partial \mathbf{g}_i}{\partial x_j}\cdot \mathbf{g}^k = -\frac{\partial \mathbf{g}^k}{\partial x_j}\cdot \mathbf{g}_i \,. \tag{2.43}$$

Consider the surface area $d\Gamma_1$ of a face of the differential parallelepiped on which x_1 is constant. On $d\Gamma_1$ the tangential curves are aligned with the coordinate curves x_2 and x_3 while x_1 is constant, and thus $\mathbf{g}^1$ is normal to the surface $d\Gamma_1$. Similarly on the other surface, $\mathbf{g}^2$ and $\mathbf{g}^3$ are normal, respectively. The surface area $d\Gamma_1$ is then calculated as

$$\begin{aligned} d\Gamma_1 &= \left\|\mathbf{g}_2 \times \mathbf{g}_3\right\| dx_2 dx_3 \\ &= \sqrt{g^{11}}\left|\mathbf{J}\right| dx_2 dx_3 \end{aligned} \tag{2.44}$$

and similarly for the other surface. The volume $d\Omega$ of the parallelepiped is

$$d\Omega = \left\| \mathbf{g}_1 \cdot (\mathbf{g}_2 \times \mathbf{g}_3) \right\| dx_1 dx_2 dx_3$$

$$= \left| \mathbf{J} \right| dx_1 dx_2 dx_3 \tag{2.45}$$

2.3.2 Kinematics of deformable shell

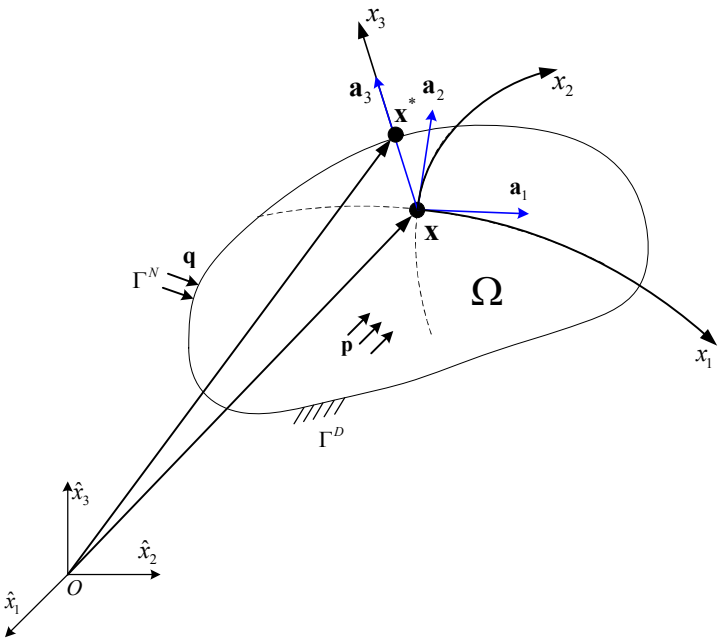

Figure 2.9 Neutral surface of shell in GCC

In this section, we summarize the kinematics of Naghdi`s shell shortly (1963). Also, we employ the NURBS representation of the curvilinear coordinates to derive geometrically exact shell formulation in isogeometric framework. Figure 2.9 depicted the physical shell middle surface. The position vector $\hat{\mathbf{x}}^*$ is material point in domain Ω which is represented by introducing the local curvilinear coordinate system

$x_1 - x_2 - x_3$ for the middle surface. The position vector $\hat{\mathbf{x}}^*$ is decomposed into the position vector $\hat{\mathbf{x}}$ on the neutral surface of the shell and the component along unit normal vector $\mathbf{a}_3$ to the neutral surface. The position vector $\hat{\mathbf{x}}^*$ is then given as

$$\mathbf{x}^*\left(x_1, x_2, x_3\right) = \mathbf{x}\left(x_1, x_2\right) + x_3\mathbf{a}_3\left(x_1, x_2\right), \tag{2.46}$$

and the corresponding covariant base vectors are defined as

$$\mathbf{g}_\alpha \equiv \mathbf{x}^*_{,\alpha} = \mathbf{a}_\alpha + x_3\mathbf{a}_{3,\alpha} = \mathbf{a}_\alpha - b_\alpha^\beta a_\beta x_3, \tag{2.47}$$

where $(\cdot)_{,\alpha}$ denotes partial derivative with respect to the curvilinear coordinate x_α. Also, $\mathbf{a}_\alpha = \mathbf{x}_{,x_\alpha}$ and $\mathbf{a}^\alpha$ are covariant and contravariant base vectors on the neutral surface, respectively. b_α^β is the mixed curvature tensor. The covariant and contravariant components of the surface metric tensors are given as

$$a_{\alpha\beta} = \mathbf{a}_\alpha \cdot \mathbf{a}_\beta, \qquad a^{\alpha\beta} = \mathbf{a}^\alpha \cdot \mathbf{a}^\beta. \tag{2.48}$$

And the covariant curvature tensor and the mixed curvature tensor can be calculated using covariant and contravariant component of the surface metric tensor as

$$b_{\alpha\beta} = -\mathbf{a}_\alpha \cdot \mathbf{a}_{3,\beta} = \mathbf{a}_3 \cdot \mathbf{a}_{\alpha,\beta} \tag{2.49}$$

and

$$b_\beta^\alpha = b_{\gamma\beta} a^{\alpha\gamma} \tag{2.50}$$

Thus strain tensors in the shell tangent plane are

$$E_{\alpha\beta} = \frac{1}{2}(g'_{\alpha\beta} - g_{\alpha\beta})$$

$$= \frac{1}{2}(a'_{\alpha\beta} - a_{\alpha\beta}) - (b'_{\alpha\beta} - b_{\alpha\beta}) + \frac{1}{2}(b'_{\alpha\mu}b'^{\mu}_{\beta} - b_{\alpha\mu}b^{\mu}_{\beta})(x_3)^2 \quad (2.51)$$

It is assumed that $E_{\alpha\beta}$ is linear through the thickness x_3. Strain measure $E_{\alpha\beta}$ is expressed simply as follows:

$$E_{\alpha\beta} \cong \varepsilon_{\alpha\beta} + x_3\omega_{\alpha\beta} \quad (2.52)$$

where

$$\varepsilon_{\alpha\beta} = \frac{1}{2}(a'_{\alpha\beta} - a_{\alpha\beta}) \quad (2.53)$$

and

$$\omega_{\alpha\beta} = \frac{1}{2}(b'_{\alpha\beta} - b_{\alpha\beta}) \quad (2.54)$$

Similarly, the transverse shear measure can be obtained as

$$\gamma_a = 2E_{\alpha 3} = g'_{\alpha 3} - g_{\alpha 3} \quad (2.55)$$

Using the facts that $a_{\alpha 3} = a^{\alpha 3} = 0$ and $a_{33} = a^{33} = 1$, the determinant of metric tensor is expressed as

$$\left|\mathbf{J}\right|^2 = \begin{vmatrix} a_{11} & a_{12} & 0 \\ a_{21} & a_{22} & 0 \\ 0 & 0 & 1 \end{vmatrix} = \left|a_{\alpha\beta}\right| \quad (2.56)$$

and

$$\frac{1}{\left|\mathbf{J}\right|^2} = \begin{vmatrix} a^{11} & a^{12} & 0 \\ a^{21} & a^{22} & 0 \\ 0 & 0 & 1 \end{vmatrix} = \left|a^{\alpha\beta}\right|. \quad (2.57)$$

We consider the shear deformable shell model called Naghdi`s shell

model. The displacement vector is assumed as

$$\mathbf{z}^{*} = u_{\alpha}\mathbf{a}^{\alpha} + x_3\theta_{\alpha}\mathbf{a}^{\alpha} + w\mathbf{a}_3 = \left(u_{\alpha} + x_3\theta_{\alpha}\right)\mathbf{a}^{\alpha} + w\mathbf{a}_3, \quad (2.58)$$

where u_{α} and w are response components of in-plane and out-of-plane displacement, respectively and θ_{α} are rotational angle measure. In addition, it is assumed that transverse shear measure γ_{α} is constant through the thickness x_3. Thus membrane, bending, and shear strain measures are obtained as

$$\varepsilon_{\alpha\beta} = \frac{1}{2}\left(u_{\alpha}\|_{\beta} + u_{\beta}\|_{\alpha} - 2b_{\alpha\beta}w\right), \quad (2.59)$$

$$\omega_{\alpha\beta} = \frac{1}{2}\left(\theta_{\alpha}\|_{\beta} + \theta_{\beta}\|_{\alpha}\right), \quad (2.60)$$

and

$$\gamma_{\alpha} = w_{,\alpha} + \theta_{\alpha} + b_{\alpha}^{\beta}u_{\beta}, \quad (2.61)$$

$(\cdot)_{\alpha}\|_{\beta}=(\cdot)_{\alpha,\beta}-\Gamma_{\alpha\beta}^{\mu}(\cdot)^{\mu}$ means covariant differentiation in which $\Gamma_{\alpha\beta}^{\mu}=a_{\alpha,\beta}\cdot a^{\mu}$ is Christoffel symbol defined at the neutral surface. For homogeneous elastic isotropic materials, material tensors are represented by

$$C^{\alpha\beta\mu\lambda} = \frac{E}{2(1+\nu)}\left(a^{\alpha\mu}a^{\beta\lambda} + a^{\alpha\lambda}a^{\beta\mu} + \frac{2\nu}{1-\nu}a^{\alpha\beta}a^{\mu\lambda}\right) \quad (2.62)$$

and

$$C^{\alpha 3\beta 3} = \frac{E}{2(1+\nu)}a^{\alpha\beta}, \quad (2.63)$$

where E is Young`s modulus and $\nu$ is Poisson`s ratio. The vector of response coefficients is useful, such as

$$\mathbf{d} \equiv [u_1 \quad u_2 \quad w \quad \theta_1 \quad \theta_2]^T \tag{2.64}$$

According to the response coefficient vector **d**, the distributed load intensity vector **p** and the boundary resultant vector **q** can be defined as

$$\mathbf{p} \equiv [p_1 \quad p_2 \quad p_3 \quad 0 \quad 0]^T \tag{2.65}$$

and

$$\mathbf{q} \equiv [N_1 \quad N_2 \quad Q \quad M_1 \quad M_2]^T . \tag{2.66}$$

where p_α and p_3 are in-surface distributed load intensities and out-of-surface distributed load intensity, respectively. N_α and Q are in-surface stretching resultants and a shear resultant, respectively. M_α are moment resultants.

Applying the above constitutive equations and using the principle of virtual work, an equilibrium equation is expressed as

$$a_\Omega\left(\mathbf{d}, \overline{\mathbf{d}}\right) = l_\Omega\left(\overline{\mathbf{d}}\right), \ {}^\forall\overline{\mathbf{d}} \in \overline{Z}, \tag{2.67}$$

where $\overline{Z}$ is a variational space defined by

$$\overline{Z} = \left\{ \overline{\mathbf{z}} \in [H^1(\Omega)]^d \ : \overline{\mathbf{z}} = 0 \text{ on } \Gamma^D \right\}. \tag{2.68}$$

The strain energy bilinear form and load linear form can be respectively written as

$$a_\Omega\left(\mathbf{z}, \overline{\mathbf{z}}\right) \equiv \int_\Omega \left[C^{\alpha\beta\mu\lambda}\varepsilon_{\alpha\beta}\varepsilon_{\mu\lambda} + \frac{h^2}{12} C^{\alpha\beta\mu\lambda}\omega_{\alpha\beta}\omega_{\mu\lambda} + C^{\alpha 3 \beta 3}\gamma_\alpha\gamma_\beta \right] h\left|\mathbf{J}\right| d\Omega \tag{2.69}$$

and

$$l_\Omega\left(\overline{\mathbf{z}}\right) = \int_\Omega \overline{\mathbf{z}}^T \mathbf{p}\left|\mathbf{J}\right| d\Omega + \int_\Gamma \overline{\mathbf{z}}^T \mathbf{q}\sqrt{a}\left|\mathbf{J}\right| d\Gamma \tag{2.70}$$

Through isoparametric mapping, Equation (2.31) can be rewritten as

$$\mathbf{d}\left(\boldsymbol{\Xi}\right) = \sum_{I}^{CP} W_I(\boldsymbol{\Xi})\mathbf{y}_I \tag{2.71}$$

where $\mathbf{y}_I = [u_{1I} \quad u_{2I} \quad w_I \quad \theta_{1I} \quad \theta_{2I}]^T$ is slightly different from the response of Equation (2.31) because the drilling degrees of freedom is not considered at the GCC based shell formulation. Then, Equation (2.67) can be rewritten as

$$a_\Omega\left(\mathbf{y},\overline{\mathbf{y}}\right) = l_\Omega\left(\overline{\mathbf{y}}\right), \ {}^{\forall}\overline{\mathbf{d}} = \sum_{I}^{CP} W_I(\boldsymbol{\Xi})\mathbf{y}_I \in \overline{Z}, \tag{2.72}$$

And energy bilinear form is expressed as similarly to Equation (2.33)

$$a^m(\mathbf{y},\overline{\mathbf{y}}) + a^b(\mathbf{y},\overline{\mathbf{y}}) + a^s(\mathbf{y},\overline{\mathbf{y}}) = \ell(\overline{\mathbf{y}}) \tag{2.73}$$

where

$$a^m(\mathbf{y},\overline{\mathbf{y}}) = \int_\Omega \sum_{I,K}^{CP} \overline{\mathbf{y}}_K^T (\mathbf{B}_m^K)^T \mathbf{D}_m \mathbf{B}_m^I \mathbf{y}_I \mathrm{d}\Omega \tag{2.74}$$

$$a^b(\mathbf{y},\overline{\mathbf{y}}) = \int_\Omega \sum_{I,K}^{CP} \overline{\mathbf{y}}_K^T (\mathbf{B}_b^K)^T \mathbf{D}_b \mathbf{B}_b^I \mathbf{y}_I \mathrm{d}\Omega \tag{2.75}$$

and

$$a^s(\mathbf{y},\overline{\mathbf{y}}) = \int_\Omega \sum_{I,K}^{CP} \overline{\mathbf{y}}_K^T (\mathbf{B}_s^K)^T \mathbf{D}_s \mathbf{B}_s^I \mathbf{y}_I \mathrm{d}\Omega \tag{2.76}$$

in which the subscripts *m*, *b*, and *s* are the indications for membrane, bending and transverse shear, respectively. In the strain measures, the differential operators $\mathbf{B}_m$, $\mathbf{B}_b$ and $\mathbf{B}_s$ include not only partial derivatives with respect to x_1 and x_2 but also the second-kin Christoffel symbols. To help the comprehension, membrane, bending and shear measures are given in the matrix form in detail as follows.

$$\begin{Bmatrix} \varepsilon_{11} \\ \varepsilon_{22} \\ 2\varepsilon_{12} \end{Bmatrix} = \begin{bmatrix} \dfrac{\partial}{\partial x_1} - \Gamma_{11}^1 & -\Gamma_{11}^2 & -b_{11} \\ -\Gamma_{22}^1 & \dfrac{\partial}{\partial x_2} - \Gamma_{22}^2 & -b_{22} \\ \dfrac{\partial}{\partial x_2} - 2\Gamma_{12}^1 & \dfrac{\partial}{\partial x_1} - 2\Gamma_{12}^2 & -2b_{12} \end{bmatrix} \begin{Bmatrix} u_1 \\ u_2 \\ w \end{Bmatrix} \tag{2.77}$$

$$\begin{Bmatrix} \omega_{11} \\ \omega_{22} \\ 2\omega_{12} \end{Bmatrix} = \begin{bmatrix} \dfrac{\partial}{\partial x_1} - \Gamma_{11}^1 & -\Gamma_{11}^2 \\ -\Gamma_{22}^1 & \dfrac{\partial}{\partial x_2} - \Gamma_{22}^2 \\ \dfrac{\partial}{\partial x_2} - 2\Gamma_{12}^1 & \dfrac{\partial}{\partial x_1} - 2\Gamma_{12}^2 \end{bmatrix} \begin{Bmatrix} \theta_1 \\ \theta_2 \end{Bmatrix} \tag{2.78}$$

and

$$\begin{Bmatrix} \gamma_1 \\ \gamma_2 \end{Bmatrix} = \begin{bmatrix} b_1^1 & b_1^2 & \dfrac{\partial}{\partial x_1} & 1 & 0 \\ b_2^1 & b_2^2 & \dfrac{\partial}{\partial x_2} & 0 & 1 \end{bmatrix} \begin{Bmatrix} u_1 \\ u_2 \\ w \\ \theta_1 \\ \theta_2 \end{Bmatrix} \tag{2.79}$$

Also, load linear equation is represented by

$$\ell(\overline{\mathbf{y}}) = \int_{\Omega} \sum_{I}^{CP} W_I \overline{\mathbf{y}}_I^T \mathbf{p} \left|\mathbf{J}\right| \mathrm{d}\Omega + \int_{\Gamma_N} \sum_{I}^{CP} \tilde{W}_I \overline{\mathbf{y}}_I^T \mathbf{q} \sqrt{a} \left|\mathbf{J}\right| \mathrm{d}\Gamma \tag{2.80}$$

where $\tilde{W}_I$ is the modified NURBS basis function for the boundary integral in GCC.

Chapter 3. Isogeometric Configuration Design Sensitivity Analysis

3.1 Configuration design sensitivity analysis

3.1.1 Material derivatives in rectangular Cartesian coordinates

Shape variation

Consider the variation of domain from an original domain Ω to a perturbed one Ω_τ as shown in Figure 3.1

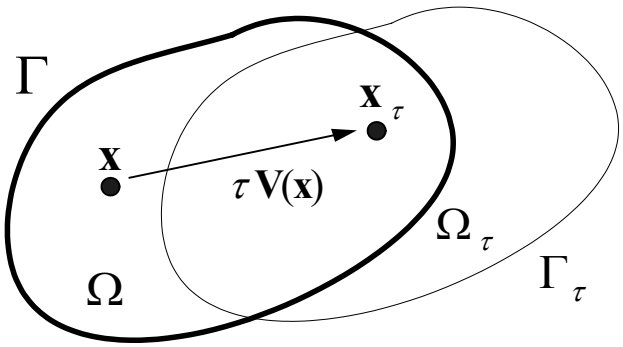

Figure 3.1 Shape variation of domain

Suppose that one parameter τ defines a transformation T. The mapping $T:\mathbf{x}\to\mathbf{x}_\tau$, $\mathbf{x}\in\Omega$ is given by

$$\mathbf{x}_\tau \equiv T(\mathbf{x},\tau) \tag{3.1}$$

and

$$\Omega_\tau \equiv T(\Omega,\tau)\,. \tag{3.2}$$

where Ω_τ, Γ_τ and $\mathbf{x}_\tau$ are design domain, design boundary and

material point in perturbed design, respectively. The shape design velocity field that is equivalent to a mapping rate can be defined as

$$\mathbf{V}_{\Omega}(\mathbf{x}) \equiv \frac{d\mathbf{x}_{\tau}}{d\tau} = \frac{dT(\mathbf{x},\tau)}{d\tau}. \tag{3.3}$$

Assuming the transformation as a linear mapping $\mathbf{T}(\mathbf{x},\tau) = \mathbf{x} + \tau\mathbf{V}_{\Omega}(\mathbf{x})$, the point-wise material derivative of response $\mathbf{z}$ at $\mathbf{x} \in \Omega$ is expressed as

$$\dot{\mathbf{z}}_{\Omega} \equiv \frac{d}{d\tau}\mathbf{z}_{\tau}(\mathbf{x} + \tau\mathbf{V}_{\Omega}(\mathbf{x}))\Big|_{\tau=0} = \mathbf{z}' + \nabla\mathbf{z}^{T}\mathbf{V}_{\Omega}, \tag{3.4}$$

where $\mathbf{z}'$ is the partial derivative of $\mathbf{z}$ with respect to the shape design parameter τ and $\nabla\mathbf{z}$ is the gradient of $\mathbf{z}$. For the following domain functional ψ_1 and boundary functional ψ_2 as the performance measures,

$$\psi_1 = \int_{\Omega} f(\mathbf{x}) d\Omega \tag{3.5}$$

and

$$\psi_2 = \int_{\Gamma} g(\mathbf{x}) d\Gamma. \tag{3.6}$$

The first order variations of Equations (3.5) and (3.6) with respect to the shape design parameter τ are derived as

$$\psi_1' \equiv \int_{\Omega} \left\{ f'(\mathbf{x}) + \nabla f(\mathbf{x})^{T}\mathbf{V}(\mathbf{x}) + f(\mathbf{x}) div\mathbf{V}(\mathbf{x}) \right\} d\Omega \tag{3.7}$$

and

$$\psi_2' \equiv \int_{\Gamma} \left\{ g'(\mathbf{x}) + \left(\nabla g(\mathbf{x})^{T}\mathbf{n} + \kappa g(\mathbf{x}) \right)\mathbf{V}^{T}\mathbf{n} \right\} d\Gamma \tag{3.8}$$

where $\kappa = div\mathbf{n}$ is the curvature of Γ. For more details, interested readers may refer to Choi and Kim (2006)

Orientation variation

Two basic assumptions are used throughout the formulation of orientation design sensitivity; the design component rotates without shape variations and only a small design perturbation is taken into account. Consider the orientation change of a surface design component that rotates in a three dimensional space from the initial domain Ω to perturbed one Ω_τ, as shown in Figure 3.2. The local coordinate system is fixed coordinate system is fixed on the component with the x_3-axis normal to the surface

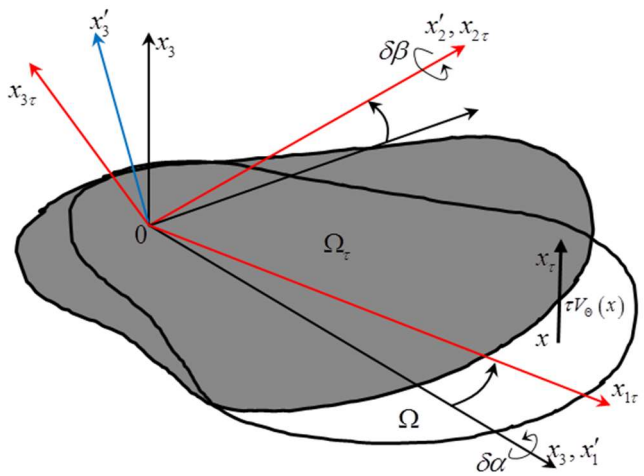

Figure 3.2 Orientation variation of surface design component

Suppose that only one parameter τ defines the transformation T_Ω. An orientation design velocity field is defined as $V_\theta(\mathbf{x}) = [0 \quad 0 \quad V_3(\mathbf{x})]^T$. The components of orientation design velocity field in in-plane directions vanish since the movement $\tau V_3(\mathbf{x})$ in the normal direction only change in the orientation of surface design component. Define a regular extension of $\mathbf{z}_\tau$ to the initial local coordinate system

$x_1 - x_2 - x_3$ as

$$\mathbf{z}_\tau(\mathbf{x}) \equiv \mathbf{z}_\tau(\mathbf{x}_\tau) \tag{3.9}$$

A perturbed solution $\mathbf{z}_\tau$ at two different locations $\mathbf{z}_\tau$ and $\mathbf{z}_\tau$ can be written as

$$\mathbf{z}_\tau(\mathbf{x}_\tau) = \mathbf{A}(\delta\alpha, \delta\beta)\mathbf{z}_\tau(\mathbf{x}) \tag{3.10}$$

where $\delta\alpha$ and $\delta\beta$ are the Euler angles about the x_1 and x_2' axes. These angles rotate about the coordinates in the order $x_i \to x_i' \to x_{i\tau}$. For a small design perturbation of the surface component, the following approximation is valid.

$$\delta\alpha = \tau V_{3,2}, \quad \delta\beta = -\tau V_{3,1} \tag{3.11}$$

Note that both $\mathbf{z}_\tau(\mathbf{x}_\tau)$ and $\mathbf{z}_\tau(\mathbf{x})$ are evaluated in the same $x_1 \to x_2 \to x_3$ local coordinate system and $\mathbf{A}(\delta\alpha, \delta\beta)$ is a rotational transformation matrix given as

$$A(\delta\alpha, \delta\beta) = \begin{bmatrix} 1 & 0 & 0 & 0 & 0 & 0 \\ 0 & \cos\delta\alpha & -\sin\delta\alpha & 0 & 0 & 0 \\ 0 & \sin\delta\alpha & \cos\delta\alpha & 0 & 0 & 0 \\ 0 & 0 & 0 & 1 & 0 & 0 \\ 0 & 0 & 0 & 0 & \cos\delta\alpha & -\sin\delta\alpha \\ 0 & 0 & 0 & 0 & \sin\delta\alpha & \cos\delta\alpha \end{bmatrix}$$

$$\times \begin{bmatrix} \cos\delta\beta & 0 & \sin\delta\beta & 0 & 0 & 0 \\ 0 & 1 & 0 & 0 & 0 & 0 \\ -\sin\delta\beta & 0 & \cos\delta\beta & 0 & 0 & 0 \\ 0 & 0 & 0 & \cos\delta\beta & 0 & \sin\delta\beta \\ 0 & 0 & 0 & 0 & 1 & 0 \\ 0 & 0 & 0 & -\sin\delta\beta & 0 & \cos\delta\beta \end{bmatrix} \tag{3.12}$$

The point-wise derivative of displacement with respect to the orientation defined as

$$\dot{\mathbf{z}}_\theta(\mathbf{x}) = \lim_{\tau \to 0}\left[\frac{\mathbf{A}(\delta\alpha, \delta\beta)\mathbf{z}_\tau(\mathbf{x}) - \mathbf{z}(\mathbf{x})}{\tau}\right]$$
$$= \left[\mathbf{A}(\delta\alpha, \delta\beta)\frac{d\mathbf{z}_\tau(\mathbf{x})}{d\tau}\right]\Bigg|_{\tau=0} + \frac{d\mathbf{A}(\delta\alpha, \delta\beta)}{d\tau}\Bigg|_{\tau=0}\mathbf{z}(\mathbf{x}) = \mathbf{z}'_\theta(\mathbf{x}) + \tilde{\mathbf{V}}_\theta\mathbf{z}(\mathbf{x}) \quad (3.13)$$

where

$$\tilde{\mathbf{V}}_\theta \equiv \frac{dA(\delta\alpha, \delta\beta)}{d\tau}\Bigg|_{\tau=0} = \begin{bmatrix} 0 & 0 & -V_{3,1} & 0 & 0 & 0 \\ 0 & 0 & -V_{3,2} & 0 & 0 & 0 \\ V_{3,1} & V_{3,2} & 0 & 0 & 0 & 0 \\ 0 & 0 & 0 & 0 & 0 & -V_{3,1} \\ 0 & 0 & 0 & 0 & 0 & -V_{3,2} \\ 0 & 0 & 0 & V_{3,1} & V_{3,2} & 0 \end{bmatrix} \quad (3.14)$$

Consider the performance measure in Equation (3.5). The first order variation with respect to the orientation change is derived as

$$\psi'_{V_\theta} = \int_{\Omega_\tau} f'_{V_\theta}(\mathbf{x})d\Omega \quad (3.15)$$

It is interesting to note that Equation (3.15) is different from the shape derivative of the same functional obtained in Equation. (3.5). For more details, interested readers may refer to Cho and Choi (2000)

3.1.2 Material derivatives in curvilinear coordinates

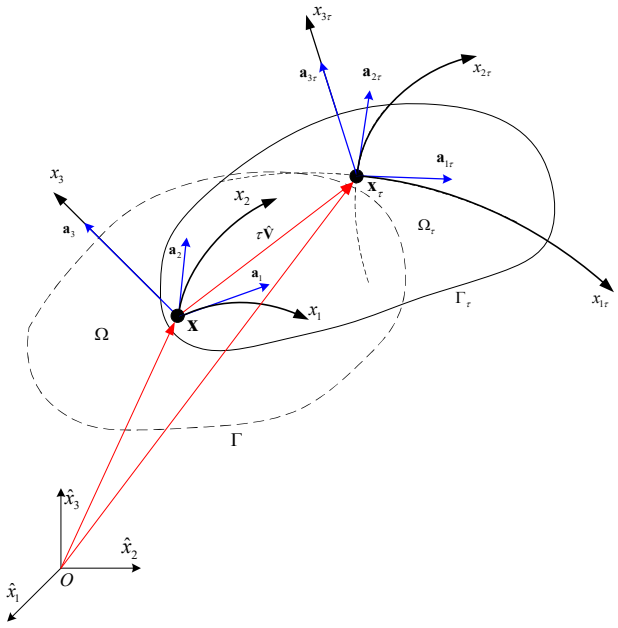

Figure 3.3 Design variation of domain of shell structure

Figure 3.3 shows the design variation of a shell structure in three-dimensional space. $x_{1\tau} - x_{2\tau} - x_{3\tau}$ frame is a local orthogonal curvilinear coordinate system in the perturbed design Ω_τ. $\{\mathbf{a}_{1\tau}, \mathbf{a}_{2\tau}, \mathbf{a}_{3\tau}\}$ are the orthonormal covariant base vectors. Assume that only one parameter τ defines a mapping $T : \hat{\mathbf{x}} \to \hat{\mathbf{x}}_\tau,\ \hat{\mathbf{x}} \in \Omega$ given by

$$\left.\begin{aligned} \hat{\mathbf{x}}_\tau &\equiv T(\hat{\mathbf{x}}, \tau) \\ \Omega_\tau &\equiv T(\Omega, \tau) \end{aligned}\right\} \tag{3.16}$$

Considering τ as time, a design velocity field can be defined as

$$\hat{\mathbf{V}} \equiv \left.\frac{d\hat{\mathbf{x}}_\tau}{d\tau}\right|_{\tau=0} \tag{3.17}$$

Then, we express the perturbed position vector $\mathbf{r}_\tau$ at $\mathbf{x}_\tau$ using design velocity, as

$$\mathbf{r}_\tau = \mathbf{r} + \tau \hat{\mathbf{V}} = \mathbf{r} + \tau \mathbf{a}_{123}^T \mathbf{V} \tag{3.18}$$

where, $\mathbf{r}$ represent the corresponding initial position vector at $\mathbf{x}$. $\mathbf{a}_{123} \equiv [\mathbf{a}_1 \quad \mathbf{a}_2 \quad \mathbf{a}_3]^T$ and $\mathbf{V}$ denotes a design velocity component vector which represents the design velocity measured in $x_1 - x_2 - x_3$ frame. For the perturbed design, the tangential derivative $\mathbf{r}_{\tau,x_\alpha}$ is expressed by

$$\begin{aligned} \mathbf{r}_{\tau,x_\alpha} &= \mathbf{r}_{,x_\alpha} + \tau(\mathbf{a}_{123,x_\alpha}^T \mathbf{V} + \mathbf{a}_{123}^T \mathbf{V}_{,x_\alpha}) \\ &= \mathbf{a}_{123}^T (\mathbf{e}_\alpha + \tau \mathbf{V}_{,x_\alpha} - \tau \boldsymbol{\Omega}_\alpha \mathbf{V}) \equiv \mathbf{a}_{123}^T \mathbf{E}_\alpha \end{aligned} \tag{3.19}$$

where, $\boldsymbol{\Omega}_\alpha$ are initial curvature matrix represented by

$$\boldsymbol{\Omega}_1 = \begin{bmatrix} 0 & k_5 & -k_1 \\ -k_5 & 0 & -k_{61} \\ k_1 & k_{61} & 0 \end{bmatrix} \tag{3.20}$$

and

$$\boldsymbol{\Omega}_2 = \begin{bmatrix} 0 & k_4 & -k_{62} \\ -k_4 & 0 & -k_2 \\ k_{62} & k_2 & 0 \end{bmatrix}. \tag{3.21}$$

The components of $\mathbf{E}_\alpha$ are obtained as

$$\mathbf{E}_1 = \begin{Bmatrix} 1 + V_{1,x_1} - \tau k_5 V_2 + \tau k_1 V_3 \\ V_{2,x_1} + \tau k_5 V_1 + \tau k_{61} V_3 \\ V_{3,x_1} - \tau k_1 V_1 - \tau k_{61} V_2 \end{Bmatrix} \tag{3.22}$$

and

$$\mathbf{E}_2 = \begin{Bmatrix} 1 + V_{1,x_2} - \tau k_4 V_2 + \tau k_{62} V_3 \\ V_{2,x_2} + \tau k_4 V_1 + \tau k_2 V_3 \\ V_{3,x_2} - \tau k_{62} V_1 - \tau k_2 V_2 \end{Bmatrix} \tag{3.23}$$

where k_1 and k_2 are the initial bending curvature with respect to x_1 and x_2 axes, k_{61} and k_{62} are the initial twisting curvature with respect to x_1 and x_2 axes, k_4 is the spiral(or drilling) curvature of the

x_2 axis with respect to the x_3 axis and k_5 is the spiral curvature of the x_1 axis with respect to the x_3 axis. The detailed derivation of initial curvature matrix is described in Appendix A.

Shape variation

A component of material point of the perturbed domain along the $\mathbf{x}_{\alpha\tau}$ axis is expressed by that of material point of the initial domain along the $\mathbf{x}_{\alpha}$ as

$$\mathbf{x}_{\tau} = \mathbf{x} + \tau \mathbf{V}_{\Omega} \tag{3.24}$$

The point-wise material derivative of response $\mathbf{z}$ at $\mathbf{x} \in \Omega$ is expressed as

$$\dot{\mathbf{z}}_{\Omega} \equiv \frac{d}{d\tau} \mathbf{z}_{\tau}(\mathbf{x} + \tau \mathbf{V}_{\Omega}(\mathbf{x}))\Big|_{\tau=0} = \mathbf{z}' + \nabla \mathbf{z}^{T} \mathbf{V}_{\Omega}, \tag{3.25}$$

Equation (3.25) is similar to Equation (3.2) except for $\mathbf{V}_{\Omega}$. This term is represent by material derivative of tangential variation of material point in curvilinear coordinates.

Orientation variation

For the orientation variation, the transformation relation between two sets of covariant base vector $\{\mathbf{a}_1, \mathbf{a}_2, \mathbf{a}_3\}$ and $\{\mathbf{a}_{1\tau}, \mathbf{a}_{2\tau}, \mathbf{a}_{3\tau}\}$ can be expressed by

$$\mathbf{a}_{123\tau} = \mathbf{\Lambda}_{\tau} \mathbf{a}_{123} \tag{3.31}$$

where transformation matrix is expressed as

$$\mathbf{a}_{\alpha\tau} = \frac{\mathbf{E}_{\alpha}}{\|\mathbf{E}_{\alpha}\|} \mathbf{a}_{\alpha} \tag{3.32}$$

and

$$\mathbf{a}_{3\tau} = \left(\frac{\mathbf{E}_1}{\|\mathbf{E}_1\|} \times \frac{\mathbf{E}_2}{\|\mathbf{E}_2\|} \right) \mathbf{a}_3 \tag{3.33}$$

Then, taking the material derivative of Equation (3.31) leads to

$$(\mathbf{a}_{123})^{\cdot} = \frac{d}{d\tau} \mathbf{\Lambda}_{\tau} \Big|_{\tau=0} \mathbf{a}_{123} \equiv \mathbf{V}_{\Theta}^{T} \mathbf{a}_{123} \tag{3.34}$$

where

$$\mathbf{V}_{\Theta} = \begin{bmatrix} 0 & 0 & (V_{3,x_1} - k_1 V_1 - k_{61} V_2) \\ 0 & 0 & (V_{3,x_2} - k_{62} V_1 - k_2 V_2) \\ -(V_{3,x_1} - k_1 V_1 - k_{61} V_2) & -(V_{3,x_2} - k_{62} V_1 - k_2 V_2) & 0 \end{bmatrix} \tag{3.35}$$

Using the relation $\mathbf{a}^{123} = [\mathbf{a}_{123}]^{-1}$ Eq. (3.32) The material derivative of contravariant base vector is derived as

$$(\mathbf{a}^{123})^{\cdot} = \mathbf{a}^{123} \frac{d}{d\tau} (\mathbf{\Lambda}_{\tau}^{T}) \Big|_{\tau=0} = \mathbf{a}^{123} \mathbf{V}_{\theta} \tag{3.36}$$

3.2 Isogeometric sensitivity of plate structures

In the configuration DSA using the first order variation, the material derivatives and the first variance of response are expressed as the superposition of shape and orientation variations

$$\dot{\mathbf{z}} = \dot{\mathbf{z}}_{\Omega} + \dot{\mathbf{z}}_{\theta} \tag{3.37}$$

and

$$\mathbf{z}' = \mathbf{z}'_{\Omega} + \mathbf{z}'_{\theta} \tag{3.38}$$

Although both Equations (3.3) and (3.13) contain partial derivatives, the convective terms are in different form. The former involves the gradient of the displacement, whereas the latter involves the derivative of the design velocity

3.1.2 Configuration sensitivity : Direct differentiation Method

Taking the first order variation of the variational equation (2.24) with respect to design parameter τ, we have the followings

$$a\left(\mathbf{d}', \overline{\mathbf{d}}\right) + a\left(\mathbf{d}, \overline{\mathbf{d}}'\right) + a'_{ex}\left(\mathbf{d}, \overline{\mathbf{d}}\right) = l\left(\overline{\mathbf{d}}'\right) + l'_{ex}\left(\overline{\mathbf{d}}\right) \tag{3.39}$$

where

$$a(\mathbf{d}', \overline{\mathbf{d}}) = \int_{\Omega} c^{m}_{\alpha\beta\mu\lambda} u'_{\alpha,\beta} \overline{u}_{\mu,\lambda} \mathrm{d}\Omega + \int_{\Omega} c^{b}_{\alpha\beta\mu\lambda} \theta'_{\alpha,\beta} \overline{\theta}_{\mu,\lambda} \mathrm{d}\Omega$$
$$+ \int_{\Omega} c^{s}_{\alpha\beta} (w'_{,\alpha} - \theta'_{\alpha})(\overline{w}_{,\beta} - \overline{\theta}_{\beta}) \mathrm{d}\Omega , \tag{3.40}$$

$$a(\mathbf{d}, \overline{\mathbf{d}}') = \int_{\Omega} c^{m}_{\alpha\beta\mu\lambda} u_{\alpha,\beta} \overline{u}'_{\mu,\lambda} \mathrm{d}\Omega + \int_{\Omega} c^{b}_{\alpha\beta\mu\lambda} \theta_{\alpha,\beta} \overline{\theta}'_{\mu,\lambda} \mathrm{d}\Omega$$
$$+ \int_{\Omega} c^{s}_{\alpha\beta} (w_{,\alpha} - \theta_{\alpha})(\overline{w}'_{,\beta} - \overline{\theta}'_{\beta}) \mathrm{d}\Omega \tag{3.41}$$

$$a'_{ex}\left(\mathbf{d},\overline{\mathbf{d}}\right)=\int_{\Omega}[c^{m}_{\alpha\beta\mu\lambda}u_{\alpha,\beta}\overline{u}_{\mu,\lambda}V_{m}]_{,m}+[c^{b}_{\alpha\beta\mu\lambda}\theta_{\alpha,\beta}\overline{\theta}_{\mu,\lambda}V_{m}]_{,m}\mathrm{d}\Omega$$

$$+\int_{\Omega}[c^{s}_{\alpha\beta}(w_{,\alpha}-\theta_{\alpha})(\overline{w}_{,\beta}-\overline{\theta}_{\beta})V_{m}]_{,m}\mathrm{d}\Omega \tag{3.42}$$

$$l\left(\overline{\mathbf{d}}'\right)=\int_{\Omega}\mathrm{b}_{k}\overline{\mathrm{d}}'_{k}\mathrm{d}\Omega+\int_{\Gamma_{\mathrm{N}}}t_{k}\overline{\mathrm{d}}'_{k}\mathrm{d}\Gamma \tag{3.43}$$

and

$$l'_{ex}\left(\overline{\mathbf{d}}\right)=\int_{\Omega}[\mathrm{b}_{k}\overline{\mathrm{d}}_{k}V_{m}]_{,m}\mathrm{d}\Omega$$

$$+\int_{\Gamma_{\mathrm{N}}}(t_{k}\overline{\mathrm{d}}_{k})_{,m}V_{m}\mathrm{d}\Gamma+\int_{\Gamma_{\mathrm{N}}}\kappa(t_{k}\overline{\mathrm{d}}_{k})V_{m}\mathrm{n}_{m}\mathrm{d}\Gamma \tag{3.44}$$

Using the fact that $\mathbf{z}'=\dot{\mathbf{z}}-\nabla\mathbf{z}^{T}\mathbf{V}_{\Omega}-\tilde{\mathbf{V}}_{\theta}\mathbf{z}$ and $\overline{\mathbf{z}}'=\dot{\overline{\mathbf{z}}}-\nabla\overline{\mathbf{z}}^{T}\mathbf{V}_{\Omega}-\tilde{\mathbf{V}}_{\theta}\overline{\mathbf{z}}$, Equation (3.39) is rewritten as

$$a\left(\dot{\mathbf{d}},\overline{\mathbf{d}}\right)+a\left(\mathbf{d},\dot{\overline{\mathbf{d}}}\right)+a'_{c}\left(\mathbf{d},\overline{\mathbf{d}}\right)=l\left(\dot{\overline{\mathbf{d}}}\right)+l'_{c}\left(\overline{\mathbf{d}}\right) \tag{3.45}$$

Since all $^{\forall}\dot{\overline{\mathbf{d}}}\in\overline{Z}$,

$$a\left(\mathbf{d},\dot{\overline{\mathbf{d}}}\right)=l\left(\dot{\overline{\mathbf{d}}}\right)\ \text{ for }\ ^{\forall}\dot{\overline{\mathbf{d}}}\in\overline{Z} \tag{3.46}$$

Therefore, the design sensitivity formulation using a direct differentiation method is derived as

$$a\left(\dot{\mathbf{d}},\overline{\mathbf{d}}\right)=l'_{c}\left(\overline{\mathbf{d}}\right)-a'_{c}\left(\mathbf{d},\overline{\mathbf{d}}\right) \tag{3.47}$$

where

$$a'_{c}(\mathbf{d},\overline{\mathbf{d}})\equiv a'_{ex}(\mathbf{d},\overline{\mathbf{d}})-a(\nabla\mathbf{d}^{T}\mathbf{V}_{\Omega},\overline{\mathbf{d}})-a(\mathbf{d},\nabla\overline{\mathbf{d}}^{T}\mathbf{V}_{\Omega})-a(\tilde{\mathbf{V}}_{\theta}\mathbf{d},\overline{\mathbf{d}})-a(\mathbf{d},\tilde{\mathbf{V}}_{\theta}\overline{\mathbf{d}}) \tag{3.48}$$

and

$$\ell'_{c}(\boldsymbol{\lambda})\equiv\ell'_{ex}(\boldsymbol{\lambda})-\ell(\nabla\boldsymbol{\lambda}^{T}\mathbf{V}_{\Omega})-\ell(\tilde{\mathbf{V}}_{\theta}\boldsymbol{\lambda}) \tag{3.49}$$

Each term of Equations (3.48) and (3.49) can be represented by

$$a'_{ex}(\mathbf{d},\overline{\mathbf{d}})=\int_{\Omega}c^{m}_{\alpha\beta\mu\lambda}u_{\alpha,\beta}\overline{u}_{\mu,\lambda}V_{m,m}+c^{b}_{\alpha\beta\mu\lambda}\theta_{\alpha,\beta}\overline{\theta}_{\mu,\lambda}V_{m,m}+c^{s}_{\alpha\beta}(w_{,\alpha}+\theta_{\alpha})(\overline{w}_{,\alpha}+\overline{\theta}_{\alpha})V_{m,m}d\Omega \tag{3.50}$$

$$a(\nabla \mathbf{d}^T \mathbf{V}_\Omega, \bar{\mathbf{d}}) = \int_\Omega c^m_{\alpha\beta\mu\lambda} u_{\alpha,m} V_{m,\beta} \bar{u}_{\mu,\lambda} + c^b_{\alpha\beta\mu\lambda} \theta_{\alpha,m} V_{m,\beta} \lambda_{\mu,\lambda} + c^s_{\alpha\beta} w_{,m} V_{m,\alpha} (\bar{w}_{,\beta} + \bar{\theta}_\beta) d\Omega \quad (3.51)$$

$$a(\mathbf{d}, \nabla \bar{\mathbf{d}}^T \mathbf{V}_\Omega) = \int_\Omega c^m_{\alpha\beta\mu\lambda} u_{\alpha,\beta} \bar{u}_{\mu,m} V_{m,\lambda} + c^b_{\alpha\beta\mu\lambda} \theta_{\alpha,\beta} \bar{\theta}_{\mu,m} V_{m,\lambda} + c^s_{\alpha\beta} (w_{,\alpha} + \theta_\alpha) \bar{w}_{3,m} V_{m,\beta} d\Omega \quad (3.52)$$

$$a(\tilde{\mathbf{V}}_\theta \mathbf{d}, \bar{\mathbf{d}}) = \int_\Omega c^m_{\alpha\beta\mu\lambda} (\tilde{\mathbf{V}}_\theta \mathbf{d})_{\alpha,\beta} \bar{u}_{\mu,\lambda} + c^b_{\alpha\beta\mu\lambda} (\tilde{\mathbf{V}}_\theta \mathbf{d})_{\alpha,\beta} \bar{\theta}_{\mu,\lambda} d\Omega$$

$$+ \int_\Omega c^s_{\alpha\beta} \left\{ (\tilde{\mathbf{V}}_\theta \mathbf{d})_{3,\alpha} + (\tilde{\mathbf{V}}_\theta \mathbf{d})_\alpha \right\} (\bar{w}_{,\beta} + \theta_\beta) d\Omega \quad (3.53)$$

$$a(\mathbf{d}, \tilde{\mathbf{V}}_\theta \bar{\mathbf{d}}) = \int_\Omega c^m_{\alpha\beta\mu\lambda} u_{\alpha,\beta} (\tilde{\mathbf{V}}_\theta \bar{\mathbf{d}})_{\mu,\lambda} + c^b_{\alpha\beta\mu\lambda} \theta_{\alpha,\beta} (\tilde{\mathbf{V}}_\theta \bar{\mathbf{d}})_{\mu,\lambda} d\Omega$$

$$+ \int_\Omega c^s_{\alpha\beta} (w_{,\alpha} + \theta_\alpha) \left\{ (\tilde{\mathbf{V}}_\theta \bar{\mathbf{d}})_{3,\beta} + (\tilde{\mathbf{V}}_\theta \bar{\mathbf{d}})_\beta \right\} d\Omega \quad (3.54)$$

$$\ell'_{ex}(\bar{\mathbf{d}}) = \int_\Omega (\mathbf{b}^T \bar{\mathbf{d}}) div \mathbf{V}_\Omega d\Omega + \int_{\Gamma^N} (\mathbf{t}^T \boldsymbol{\lambda}) div \mathbf{n} \mathbf{V}_\Omega^T \mathbf{n} d\Gamma \quad (3.55)$$

$$\ell(\nabla \bar{\mathbf{d}}^T \mathbf{V}_\Omega) = \int_\Omega \nabla (\mathbf{b}^T \bar{\mathbf{d}})^T \mathbf{V}_\Omega d\Omega + \int_{\Gamma^N} \nabla (\mathbf{t}^T \bar{\mathbf{d}})^T \mathbf{n} \mathbf{V}_\Omega^T \mathbf{n} d\Gamma \quad (3.56)$$

and

$$\ell(\tilde{\mathbf{V}}_\theta \bar{\mathbf{d}}) = \int_\Omega \mathbf{b}^T \tilde{\mathbf{V}}_\theta \bar{\mathbf{d}} d\Omega + + \int_{\Gamma^N} \mathbf{t}^T \tilde{\mathbf{V}}_\theta \bar{\mathbf{d}} d\Gamma \quad (3.57)$$

3.1.3 Configuration sensitivity : Adjoint variable method

To derive an adjoint equation, consider the general performance functional, in an integral form, as

$$\psi(\mathbf{d}) = \int_{\Omega} F(\mathbf{d}) d\Omega + \int_{\Gamma} G(\mathbf{d}) d\Gamma \tag{3.58}$$

and define a Lagrangian as

$$L(\mathbf{d}, \boldsymbol{\lambda}) = \psi(\mathbf{d}) + \ell(\boldsymbol{\lambda}) - a(\mathbf{d}, \boldsymbol{\lambda}) \tag{3.59}$$

where $\lambda \in \bar{Z}$ is the solution of the following a adjoint system.

$$a(\boldsymbol{\lambda}, \bar{\boldsymbol{\lambda}}) = \ell(\bar{\boldsymbol{\lambda}}), \quad {}^{\forall}\bar{\boldsymbol{\lambda}} \in \bar{Z} \tag{3.60}$$

Taking the first order variation of the Lagrangian leads to

$$[L(\mathbf{d}, \boldsymbol{\lambda})]' = [\psi(\mathbf{d})]' + [\ell(\boldsymbol{\lambda})]' - [a(\mathbf{d}, \boldsymbol{\lambda})]'$$

$$= \psi'_{ex}(\mathbf{d}) + \psi(\mathbf{d}') + \ell'_{ex}(\boldsymbol{\lambda}) + \ell(\boldsymbol{\lambda}') - a'_{ex}(\mathbf{d}, \boldsymbol{\lambda}) - a(\mathbf{d}', \boldsymbol{\lambda}) - a(\mathbf{d}, \boldsymbol{\lambda}') \tag{3.61}$$

Using the fact that $\mathbf{z}' = \dot{\mathbf{z}} - \nabla \mathbf{z}^T \mathbf{V}_{\Omega} - \tilde{\mathbf{V}}_{\theta} \mathbf{z}$ and $\boldsymbol{\lambda}' = \dot{\boldsymbol{\lambda}} - \nabla \boldsymbol{\lambda}^T \mathbf{V}_{\Omega} - \tilde{\mathbf{V}}_{\theta} \boldsymbol{\lambda}$, Equation (3.61) is rewritten as

$$[L(\mathbf{d}, \boldsymbol{\lambda})]' = \psi'_c(\mathbf{d}) + \ell'_c(\boldsymbol{\lambda}) - a'_c(\mathbf{d}, \boldsymbol{\lambda})$$

$$+ \left\{ \psi(\dot{\mathbf{d}}) - a(\dot{\mathbf{d}}, \boldsymbol{\lambda}) \right\} + \left\{ \ell(\dot{\boldsymbol{\lambda}}) - a(\mathbf{d}, \dot{\boldsymbol{\lambda}}) \right\}, \tag{3.62}$$

where

$$\psi'_c(\mathbf{d}) \equiv \psi'_{ex}(\mathbf{d}) - \psi(\nabla \mathbf{d}^T \mathbf{V}_{\Omega}) - \psi(\tilde{\mathbf{V}}_{\theta} \mathbf{d})$$

$$= \int_{\Omega} \left\{ F(\mathbf{d}) div \mathbf{V}_{\Omega} - F(\nabla \mathbf{d}^T \mathbf{V}_{\Omega}) - F(\tilde{\mathbf{V}}_{\theta} \mathbf{d}) \right\} d\Omega$$

$$+ \int_{\Gamma} \left[\left\{ G(\mathbf{d}) div \mathbf{n} - G(\nabla \mathbf{d}^T \mathbf{n}) \right\} \mathbf{V}_{\Omega}^T \mathbf{n} - G(\tilde{\mathbf{V}}_{\theta} \mathbf{d}) \right] d\Gamma \tag{3.63}$$

$$\ell'_c(\boldsymbol{\lambda}) \equiv \ell'_{ex}(\boldsymbol{\lambda}) - \ell(\nabla\boldsymbol{\lambda}^T\mathbf{V}_\Omega) - \ell(\tilde{\mathbf{V}}_\theta\boldsymbol{\lambda})$$

$$= \int_\Omega \left\{(\mathbf{b}^T\boldsymbol{\lambda})div\mathbf{V}_\Omega - \nabla(\mathbf{b}^T\boldsymbol{\lambda})^T\mathbf{V}_\Omega - \mathbf{b}^T\tilde{\mathbf{V}}_\theta\boldsymbol{\lambda}\right\}d\Omega$$

$$+\int_{\Gamma^N}\left[\left\{(\mathbf{t}^T\boldsymbol{\lambda})div\mathbf{n} - \nabla(\mathbf{t}^T\boldsymbol{\lambda})^T\mathbf{n}\right\}\mathbf{V}_\Omega^T\mathbf{n} - \mathbf{t}^T\tilde{\mathbf{V}}_\theta\boldsymbol{\lambda}\right]d\Gamma \quad (3.64)$$

and

$$a'_c(\mathbf{d},\boldsymbol{\lambda}) \equiv a'_{ex}(\mathbf{d},\boldsymbol{\lambda}) - a(\nabla\mathbf{d}^T\mathbf{V}_\Omega,\boldsymbol{\lambda}) - a(\mathbf{d},\nabla\boldsymbol{\lambda}^T\mathbf{V}_\Omega) - a(\tilde{\mathbf{V}}_\theta\mathbf{d},\boldsymbol{\lambda}) - a(\mathbf{d},\tilde{\mathbf{V}}_\theta\boldsymbol{\lambda})$$

$$= \int_\Omega c^m_{ijkl}\left\{d_{i,j}\lambda_{k,l}V_{m,m} - d_{i,m}V_{m,j}\lambda_{k,l} - d_{i,j}\lambda_{k,m}V_{m,l} - (\tilde{\mathbf{V}}_\theta\mathbf{d})_{i,j}\lambda_{k,l} - d_{i,j}(\tilde{\mathbf{V}}_\theta\boldsymbol{\lambda})_{k,l}\right\}d\Omega$$
$$+\int_\Omega c^b_{ijkl}\left\{d_{i,j}\lambda_{k,l}V_{m,m} - d_{i,m}V_{m,j}\lambda_{k,l} - d_{i,j}\lambda_{k,m}V_{m,l} - (\tilde{\mathbf{V}}_\theta\mathbf{d})_{i,j}\lambda_{k,l} - d_{i,j}(\tilde{\mathbf{V}}_\theta\boldsymbol{\lambda})_{k,l}\right\}d\Omega$$
$$+\int_\Omega c^s_{ij}\left\{(d_{3,i}+\theta_i)(\lambda_{3,j}+\lambda_j)V_{m,m} - d_{3,m}V_{m,i}(\lambda_{3,j}+\lambda_j) - (d_{3,i}+\theta_i)\lambda_{3,m}V_{m,j}\right\}d\Omega$$
$$-\int_\Omega c^s_{ij}\left[\left\{(\tilde{\mathbf{V}}_\theta\mathbf{d})_{3,i} + (\tilde{\mathbf{V}}_\theta\mathbf{d})_i\right\}(\lambda_{3,j}+\lambda_j) + (d_{3,i}+\theta_i)\left\{(\tilde{\mathbf{V}}_\theta\boldsymbol{\lambda})_{3,j} + (\tilde{\mathbf{V}}_\theta\boldsymbol{\lambda})_j\right\}\right]d\Omega \quad (3.65)$$

For the brevity of the problem, the external loads are assumed independent of shape and orientation variations. Using the fact that $a(\mathbf{d},\dot{\boldsymbol{\lambda}}) = l(\dot{\boldsymbol{\lambda}}),\ {}^\forall\dot{\boldsymbol{\lambda}} \in Z$ and, since $a(\bullet,\bullet)$ is an self-adjoint operator, $a(\dot{\mathbf{d}},\boldsymbol{\lambda}) = a(\mathbf{d},\dot{\boldsymbol{\lambda}}) = l(\dot{\mathbf{d}}), \equiv \psi(\dot{\mathbf{d}}),\ {}^\forall\dot{\mathbf{d}} \in \bar{Z}$ Equation (3.62) is rewritten as

$$[L(\mathbf{d},\boldsymbol{\lambda})]' = \psi'_c(\mathbf{d}) + \ell'_c(\boldsymbol{\lambda}) - a'_c(\mathbf{d},\boldsymbol{\lambda}) \quad (3.66)$$

Without consider the design dependence of NURBS basis functions, the material derivatives of the response and the adjoint response are obtained as

$$\dot{\mathbf{d}} = \sum W_I(\boldsymbol{\Xi})\dot{\mathbf{y}}_I \quad (3.67)$$

and

$$\dot{\boldsymbol{\lambda}} = \sum W_I(\boldsymbol{\Xi})\dot{\boldsymbol{\mu}}_I \quad (3.68)$$

For the discretization of the terms related to the orientation changes in

Equations (3.64)-(3.66), new variables are introduced s

$$\mathbf{d}^{\theta} \equiv \tilde{\mathbf{V}}_{\theta}\mathbf{d} = \sum W_I(\boldsymbol{\Xi})\mathbf{y}_I^{\theta} \tag{3.69}$$

and

$$\boldsymbol{\lambda}^{\theta} \equiv \tilde{\mathbf{V}}_{\theta}\boldsymbol{\lambda} = \sum W_I(\boldsymbol{\Xi})\boldsymbol{\mu}_I^{\theta} \tag{3.70}$$

To distinguish the basis functions in the domain integral, the basis function in the boundary integral is denoted as $\widehat{W_I}(\boldsymbol{\Xi})$. Variational spaces for the response and adjoints response are defined, respectively, as

$$Y = \{\ \overline{\mathbf{y}} \in \left[H^1(\Omega)\right]^d :\ \overline{\mathbf{d}} = \sum_J W_J(\boldsymbol{\Xi})\overline{\mathbf{y}}_J = \mathbf{0} \quad \text{on} \quad \Gamma^D\ \} \tag{3.71}$$

and

$$\Theta = \{\ \boldsymbol{\mu} \in \left[H^1(\Omega)\right]^d :\ \boldsymbol{\lambda} = \sum_J W_J(\boldsymbol{\Xi})\boldsymbol{\mu}_J = \mathbf{0} \quad \text{on} \quad \Gamma^D\ \} \tag{3.72}$$

Also, for the brevity of the problem, the integrands of performance functional are assumed to be linear to the response, i.e. $F(\mathbf{d}) = f_i d_i$ and $G(\mathbf{d}) = g_i d_i$. Using the isogeomtric discretization, Eq. (3.25) is expressed as

$$[L(\mathbf{y},\boldsymbol{\mu})]' = \psi_c'(\mathbf{y}) + \ell_c'(\boldsymbol{\mu}) - a_c'(\mathbf{y},\boldsymbol{\mu}) \tag{3.73}$$

where

$$\psi_c'(\mathbf{y}) = \int_{\Omega} \sum_{I,M}^{CP} \left\{ \left(W_I^P W_{M,m}^P - W_{I,m}^P W_M^P \right) f_i y_{iI} V_{mM} - f_i W_I^P y_{iI}^{\theta} \right\} d\Omega$$

$$+ \int_{\Gamma} \sum_{I,M}^{CP} \left\{ \left(\widehat{W}_I^P \widehat{W}_M^P n_{k,k} - \widehat{W}_{I,k}^P \widehat{W}_M^P n_k \right) g_i y_{iI} n_m V_{mM} - \widehat{W}_I^P g_i y_{iI}^{\theta} \right\} d\Gamma \tag{3.74}$$

$$\ell'_c(\boldsymbol{\mu}) = \int_\Omega \sum_{I,M}^{CP} \left\{ \left(W_I^{\,p} W_{M,m}^{\,p} - W_{I,m}^{\,p} W_M^{\,p} \right) b_i \mu_{iI} V_{mM} - W_I^{\,p} b_i \mu_{iI}^{\theta} \right\} d\Omega$$

$$+ \int_{\Gamma^N} \sum_{I,M}^{CP} \left\{ \left(\widehat{W}_I^{\,p} \widehat{W}_M^{\,p} n_{k,k} - \widehat{W}_{I,k}^{\,p} \widehat{W}_M^{\,p} n_k \right) t_i \mu_{iI} n_m V_{mM} - t_i \widehat{W}_I^{\,p} \mu_{iI}^{\theta} \right\} d\Gamma \quad (3.75)$$

and

$$a'_c(\mathbf{y}, \boldsymbol{\mu}) = \int_\Omega \sum_{I,K,N}^{CP} c_{ijkl}^{m} \begin{Bmatrix} \left(W_{I,j}^{m} W_{K,l}^{m} W_{N,n}^{m} - W_{I,n}^{m} W_{K,l}^{m} W_{N,j}^{m} - W_{I,j}^{m} W_{K,n}^{m} W_{N,l}^{m} \right) y_{iI} \mu_{kK} V_{nN} \\ -\left(W_{I,j}^{m} W_{K,l}^{m} y_{iI}^{\theta} \mu_{kK} + W_{I,j}^{m} W_{K,l}^{m} y_{iI} \mu_{kK}^{\theta} \right) \end{Bmatrix} d\Omega$$

$$+ \int_\Omega \sum_{I,K,N}^{CP} c_{ijkl}^{b} \begin{Bmatrix} \left(W_{I,j}^{b} W_{K,l}^{b} W_{N,n}^{b} - W_{I,n}^{b} W_{K,l}^{b} W_{N,j}^{b} - W_{I,j}^{b} W_{K,n}^{b} W_{N,l}^{b} \right) y_{iI} \mu_{kK} V_{nN} \\ -\left(W_{I,j}^{b} W_{K,l}^{b} y_{iI}^{\theta} \mu_{kK} + W_{I,j}^{b} W_{K,l}^{b} y_{iI} \mu_{kK}^{\theta} \right) \end{Bmatrix} d\Omega$$

$$+ \int_\Omega \sum_{I,K,N}^{CP} c_{ij}^{s} \begin{Bmatrix} (W_{I,i}^{s} y_{3I} + W_I^{s} y_{iI})(W_{K,j}^{s} \mu_{3K} + W_K^{s} \mu_{jK}) W_{N,n}^{s} V_{nN} \\ -W_{I,m}^{s} y_{3I} W_{N,i}^{s} V_{mN} (W_{K,j}^{s} \mu_{3K} + W_K^{s} \mu_{jK}) \\ -(W_{I,i}^{s} y_{3I} + W_I^{s} y_{iI}) W_{K,m}^{s} \mu_{3K} W_{N,j}^{s} V_{mN} \end{Bmatrix} d\Omega$$

$$- \int_\Omega \sum_{I,K,N}^{CP} c_{ij}^{s} \begin{Bmatrix} (W_{I,i}^{s} y_{3I}^{\theta} + W_I^{s} y_{iI}^{\theta})(W_{K,j}^{s} \mu_{3K} + W_K^{s} \mu_{jK}) \\ +(W_{I,i}^{s} y_{3I} + W_I^{s} y_{iI})(W_{I,j}^{s} \mu_{3I}^{\theta} + W_I^{s} \mu_{jI}^{\theta}) \end{Bmatrix} d\Omega \quad (3.76)$$

3.3 Isogeometric sensitivity of shell structures

The equilibrium equation for the perturbed design is

$$a_{\Omega_\tau}(\mathbf{z}_\tau, \overline{\mathbf{z}}_\tau) = \ell_{\Omega_\tau}(\mathbf{z}_\tau, \overline{\mathbf{z}}_\tau), \quad \forall \overline{\mathbf{z}}_\tau \in \overline{Z}_\tau \tag{3.77}$$

where, $\overline{Z}_\tau$ is the variational space on the perturbed design, and the subscript Ω_τ is used to denote dependence of these terms on the configuration design .The point-wise material derivative of displacement component vector which measured in $x_1 - x_2 - x_3$ frame is defined as

$$\dot{\mathbf{z}} = \mathbf{z}' + \mathbf{z}_{,x_\alpha} \cdot \mathbf{V} \tag{3.78}$$

where $\mathbf{z}'$ is partial derivative of $\mathbf{z}$ with respect to τ. A physical displacement vector, $\hat{\mathbf{z}}_\tau$ on the perturbed design can be expressed as

$$\hat{\mathbf{z}}_\tau = (\mathbf{a}_\tau^{123})^T \mathbf{z}_\tau = \mathbf{\Lambda}_\tau (\mathbf{a}^{123})^T \mathbf{z}_\tau \tag{3.79}$$

Taking the material derivative of Eq.(3.58) and using Eq. (3.34) give

$$(\hat{\mathbf{z}})^{\cdot} = (\mathbf{a}^{123})^T \dot{\mathbf{z}} + \mathbf{V}_\Xi (\mathbf{a}^{123})^T \mathbf{z} \tag{3.80}$$

The material derivatives of the membrane, bending and shear strain tensors are obtained as

$$\dot{\varepsilon}_{\alpha\beta}(\mathbf{z}) = sym\left[\dot{u}_{\alpha,\beta} - \dot{\Gamma}^{\mu}_{\alpha\beta} u_\mu - \Gamma^{\mu}_{\alpha\beta}\dot{u}_\mu - \dot{b}_{\alpha\beta} w - b_{\alpha\beta}\dot{w}\right] = \varepsilon_{\alpha\beta}(\dot{\mathbf{z}}) + \varepsilon^V_{\alpha\beta}(\mathbf{z}), \tag{3.81}$$

$$\dot{\omega}_{\alpha\beta}(\mathbf{z}) = sym\left(\dot{\theta}_{\alpha,\beta} - \dot{\Gamma}^{\mu}_{\alpha\beta}\theta_\mu - \Gamma^{\mu}_{\alpha\beta}\dot{\theta}_\mu\right) = \omega_{\alpha\beta}(\dot{\mathbf{z}}) + \omega^V_{\alpha\beta}(\mathbf{z}) \tag{3.82}$$

and

$$\dot{\gamma}_\alpha(\mathbf{z}) = \dot{w}_{,\alpha} + \dot{\theta}_\alpha + \dot{b}^\beta_\alpha u_\beta + b^\beta_\alpha \dot{u}_\beta = \gamma_\alpha(\dot{\mathbf{z}}) + \gamma^V_\alpha(\mathbf{z}) \tag{3.83}$$

where $\varepsilon(\dot{\mathbf{z}})$, $\omega(\dot{\mathbf{z}})$ and $\gamma(\dot{\mathbf{z}})$ implicitly depend on the design through $\dot{\mathbf{z}}$. $\varepsilon^V(\mathbf{z})$, $\omega^V(\mathbf{z})$ and $\gamma^V(\mathbf{z})$ represent the explicitly dependent terms that can be calculated from both the state variable $\mathbf{z}$ and the design velocity $\mathbf{V}$. Note that the operations of partial derivative with respect to

the NURBS parametric coordinates and the material derivative are commutative. The material derivative of variational equation for structural elasticity problem is given as

$$\begin{aligned}[a(\mathbf{z},\overline{\mathbf{z}})]' &= a(\dot{\mathbf{z}},\overline{\mathbf{z}}) + a(\mathbf{z},\dot{\overline{\mathbf{z}}}) + a'_V(\mathbf{z},\overline{\mathbf{z}}) \\ &= \ell(\dot{\overline{\mathbf{z}}}) + \ell'_V(\overline{\mathbf{z}}) = [\ell(\overline{\mathbf{z}})]'\end{aligned} \tag{3.84}$$

The following relation holds such as $\hat{\overline{\mathbf{z}}} \in \overline{Z}$, $\dot{\hat{\overline{\mathbf{z}}}} \in \overline{Z}$ and $\dot{\hat{\overline{\mathbf{z}}}} = \dot{\overline{z}}_i \mathbf{g}^i + \overline{z}_i \dot{\mathbf{g}}^i$.

Since $\hat{\overline{\mathbf{z}}} = \overline{z}_i \mathbf{g}^i = 0$ on Γ^D and the base vector $\mathbf{g}^i$ are linearly independent, $\overline{z}_i = 0$ on Γ^D. Therefore $\overline{\mathbf{z}} \in \overline{Z}$, and following equation is valid

$$a(\mathbf{z},\dot{\overline{\mathbf{z}}}) = \ell(\dot{\overline{\mathbf{z}}}) \tag{3.85}$$

The design sensitivity formulation using a direct differentiation method is finally derived as

$$\begin{aligned}a(\dot{\mathbf{z}},\overline{\mathbf{z}}) &= \ell'_V(\overline{\mathbf{z}}) - a'_V(\mathbf{z},\overline{\mathbf{z}}) \\ &= \ell'_V(\overline{\mathbf{z}}) - \{a'_{mV}(\mathbf{z},\overline{\mathbf{z}}) + a'_{bV}(\mathbf{z},\overline{\mathbf{z}}) + a'_{sV}(\mathbf{z},\overline{\mathbf{z}})\}\end{aligned} \tag{3.86}$$

Here, *m*, *b* and *s* mean explicitly dependent terms of membrane, bending and shear respectively which can be expressed as

$$\begin{aligned}a'_{mV}(\mathbf{z},\overline{\mathbf{z}}) = &\int_\Omega \left[\dot{C}^{\alpha\beta\mu\lambda}\varepsilon_{\alpha\beta}(\mathbf{z})\varepsilon_{\mu\lambda}(\overline{\mathbf{z}})\right] h|\mathbf{J}|d\Omega \\ &-\int_\Omega \left[C^{\alpha\beta\mu\lambda}(\dot{\Gamma}^\mu_{\alpha\beta}u_\mu + \dot{b}_{\alpha\beta}w)\varepsilon_{\mu\lambda}(\overline{\mathbf{z}})\right] h|\mathbf{J}|d\Omega \\ &-\int_\Omega \left[C^{\alpha\beta\mu\lambda}\varepsilon_{\alpha\beta}(\mathbf{z})(\dot{\Gamma}^\mu_{\alpha\beta}\overline{u}_\mu + \dot{b}_{\alpha\beta}\overline{w})\right] h|\mathbf{J}|d\Omega \\ &+\int_\Omega \left[C^{\alpha\beta\mu\lambda}\varepsilon_{\alpha\beta}(\mathbf{z})\varepsilon_{\mu\lambda}(\overline{\mathbf{z}})\right] h div\mathbf{V}|\mathbf{J}|d\Omega\end{aligned} \tag{3.87}$$

$$\begin{aligned}a'_{bV}(\mathbf{z},\overline{\mathbf{z}}) = &\int_\Omega \left[\dot{C}^{\alpha\beta\mu\lambda}\omega_{\alpha\beta}(\mathbf{z})\omega_{\mu\lambda}(\overline{\mathbf{z}}) - C^{\alpha\beta\mu\lambda}\dot{\Gamma}^\mu_{\alpha\beta}\theta_\mu\omega_{\mu\lambda}(\overline{\mathbf{z}}) - C^{\alpha\beta\mu\lambda}\omega_{\alpha\beta}(\mathbf{z})\dot{\Gamma}^\mu_{\alpha\beta}\overline{\theta}_\mu\right]\frac{h^3}{12}|\mathbf{J}|d\Omega \\ &+\int_\Omega \left[C^{\alpha\beta\mu\lambda}\omega_{\alpha\beta}(\mathbf{z})\omega_{\mu\lambda}(\overline{\mathbf{z}})\right]\frac{h^3}{12} div\mathbf{V}|\mathbf{J}|d\Omega\end{aligned} \tag{3.88}$$

and

$$a'_{sV}(\mathbf{z},\overline{\mathbf{z}}) = \int_{\Omega}\left[\dot{C}^{\alpha 3\beta 3}\gamma_{\alpha}(\mathbf{z})\gamma_{\beta}(\overline{\mathbf{z}}) + C^{\alpha 3\beta 3}\dot{b}^{\beta}_{\alpha}u_{\beta}\gamma_{\beta}(\overline{\mathbf{z}}) + C^{\alpha 3\beta 3}\gamma_{\alpha}(\mathbf{z})\dot{b}^{\beta}_{\alpha}\overline{u}_{\beta}\right]h\left|\mathbf{J}\right|d\Omega + \int_{\Omega}\left[\dot{C}^{\alpha 3\beta 3}\gamma_{\alpha}(\mathbf{z})\gamma_{\beta}(\overline{\mathbf{z}})\right]h div\mathbf{V}\left|\mathbf{J}\right|d\Omega \tag{3.89}$$

The explicitly dependent part of load linear form is obtained as

$$\ell'_{V}(\overline{\mathbf{z}}) = \int_{\Omega}\overline{\mathbf{z}}^{T}(\nabla\mathbf{p}\cdot\mathbf{V} + \mathbf{p}div\mathbf{V})\left|\mathbf{J}\right|d\Omega \tag{3.90}$$

Chapter 4. Isogeometric Configuration Design Optimization

4.1 Transformed basis function for mismatch problems

In the IGA, the control points representing CAD geometry using NURBS basis functions is directly used to analyze the mathematical model. The IGA prevents the loss of higher order geometric information such as the normal vector and curvature at boundary. Hence, more accurate configuration design sensitivity can be obtained and consequently lead to a more accurate result in configuration optimization. Nevertheless, a mismatch problem could occur at the interface of patches in case the control points are selected as design variables for built-up structures.

Figure 4.1-(a) shows the intersection of patches which is designed to perfectly fit in the initial design. However, the design variables of control points vary during the process of isogeometric configuration optimization, which could result in the mismatch problem of patches at the intersection due to the non-interpolatory property of NURBS basis functions in the IGA as shown in Figure 4.1-(b). The intersection of NURBS surface (patch 2) has C^0-continuity since the control point is located in vertex of NURBS surface. Hence, the physical boundary of NURBS surface (patch 2) coincides the control points. However, the intersection of NURBS surface (patch 1) has C^1-continuity condition because the control point is located in not the vertex point of NURBS

surface but any place of the edge of NURBS surface. Therefore, the control point of intersection between patch 1 and patch 2 does not match the physical boundary of NURBS surface (patch 1) due to the property of NURBS model which does not have boundary interpolation as shown in Figure 4.1-(b). In case of this mismatch problem, it is not proper for this optimal to manufacture directly. It is necessary to propose an alternative to solve this problem when the configuration design optimization of built-up structures is performed using isogeometric framework.

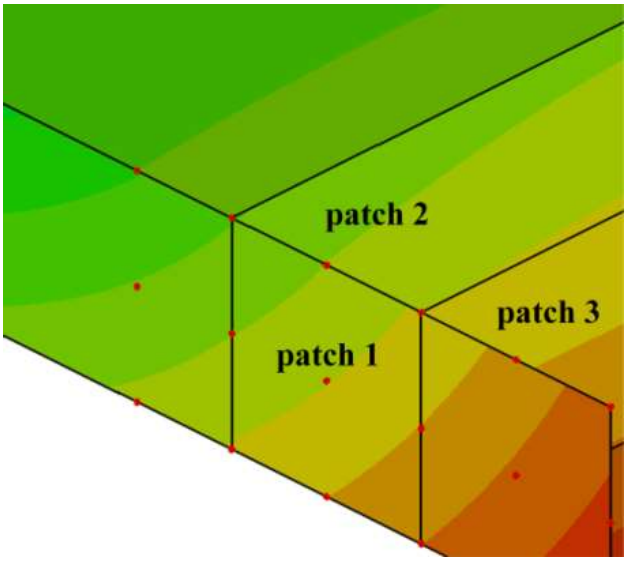

(a) Initial design

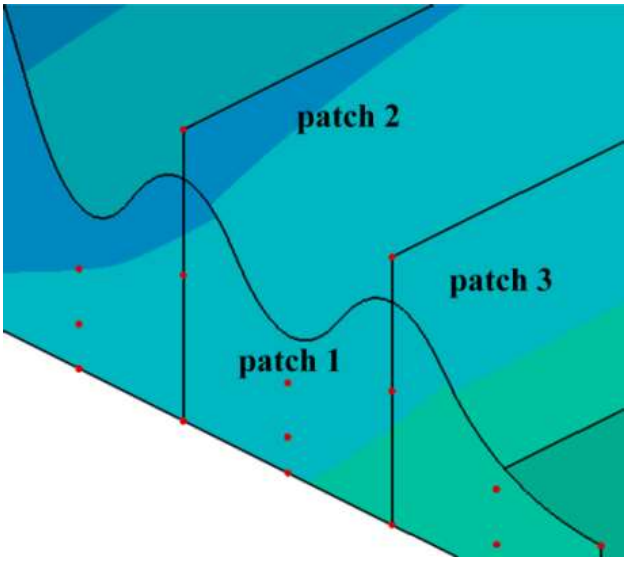

(b) Optimal design

Figure 4.1 Mismatch problem at intersection

To overcome this difficulty, there are two approaches:

(1) *Enforcement of constraint conditions*

(2) *Imposition of Kronecker delta property on NURBS*

In the first approach, the constraint conditions $\mathbf{S}_{patch\_i}(\xi,\eta)-\mathbf{S}_{patch\_j}(\xi,\eta)\le\varepsilon$ at the intersection of the patches i and j can be added in the original optimization problem. The constraint conditions are imposed as an equality constraint in design optimization problem. However, this approach has a drawback that leads to the reduction of design space by restricting the movement of design variables to enforce the match of patches within the tolerance.

As an alternative approach, the basis function can be modified to possess the Kronecker delta property in two ways.

Repeated knots

The way is to use the repeated knots or the division of patches at the intersection point. However, the use of repeated knots has a drawback such that if the knots are repeated *k*-times, the continuity decreased *k*-times as well. Therefore, the use of repeated knots allows a C^0-continuity at the intersection points, sacrificing the inter-element continuity which is one of the major advantages in the IGA.

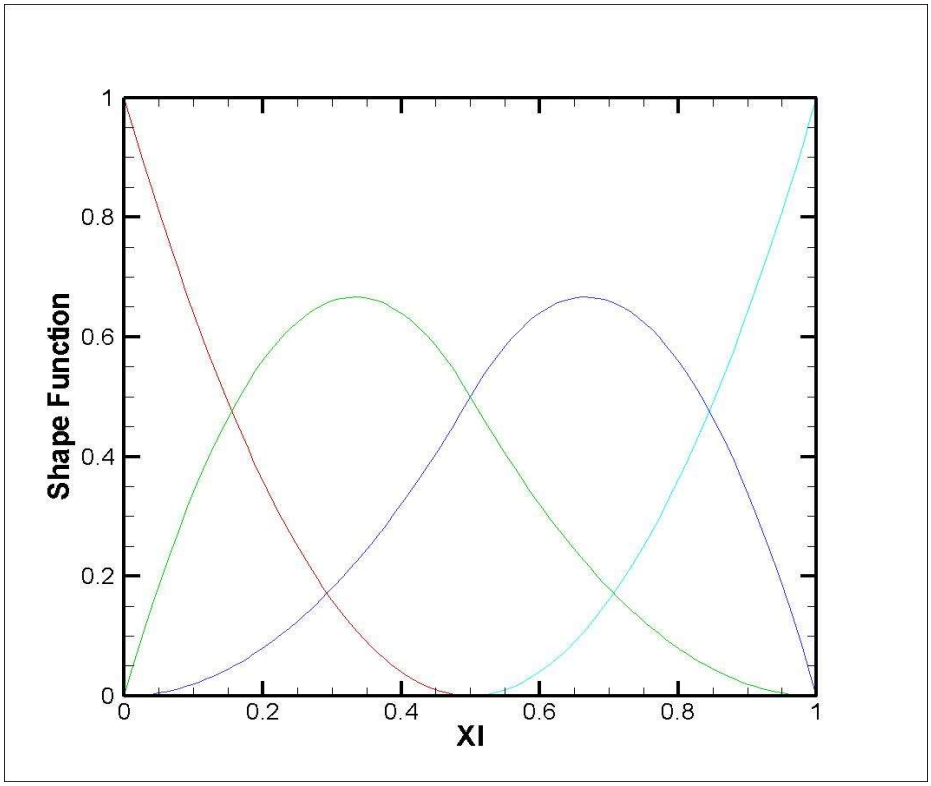

(a) $\Xi = [0 \quad 0 \quad 0 \quad 0.5 \quad 1 \quad 1 \quad 1]$

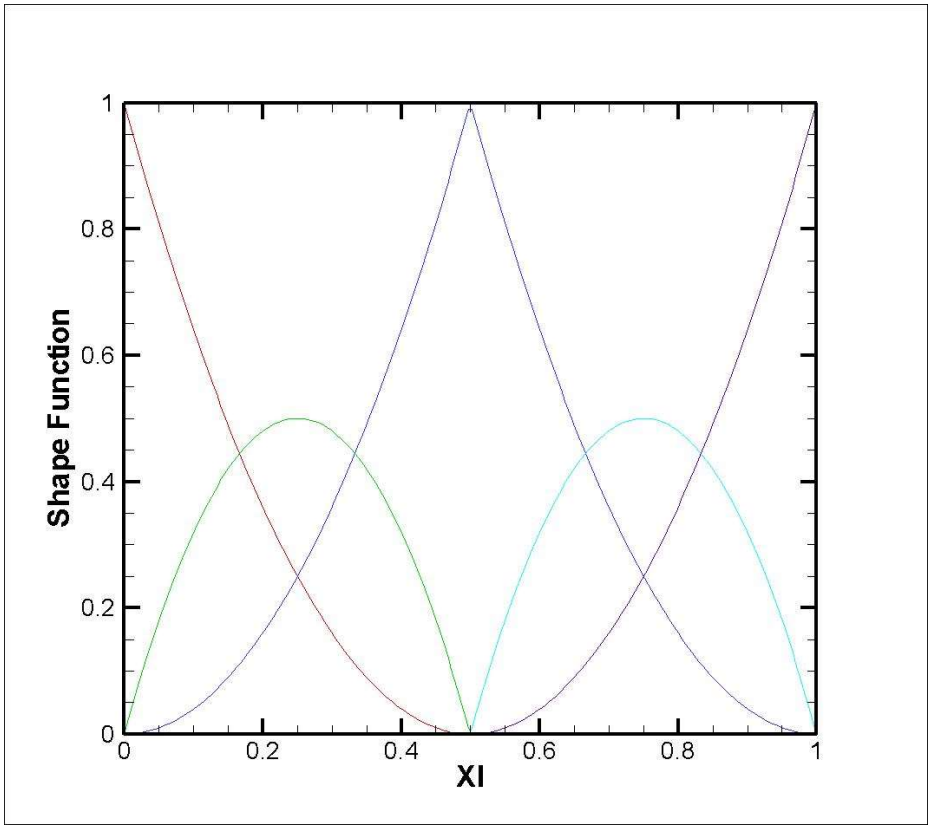

(b) $\Xi = [0 \quad 0 \quad 0 \quad 0.5 \quad 0.5 \quad 1 \quad 1 \quad 1]$

Figure 4.2 Knot insertion for repeated knot

As shown in Figure 4.2 the knot insertion is used for repeated knot. Through the knot insertion, the Kronecker delta property is obtained. Therefore, the physical boundary corresponding $\xi = 0.5$ passes through control point.

Transformed basis function

The method is to transform the NURBS to possess the Kronecker delta property at the intersection boundary. In this way, the related control point is located at the right physical point. The performances of the aforementioned approaches will be compared in the following section of numerical examples.

We briefly introduce the mixed transformation of NURBS basis functions with details found in the reference (Koo *et al.* 2013). The response field is divided into the interior and the boundary term as

$$\mathbf{z}(\boldsymbol{\Xi}) = \sum_{I}^{\text{int}} W_I^{\text{int}}(\boldsymbol{\Xi})\mathbf{d}_I^{\text{int}} + \sum_{I}^{bnd} W_I^{bnd}(\boldsymbol{\Xi})\mathbf{d}_I^{bnd} \tag{4.1}$$

where W_I^{int} and $\mathbf{d}_I^{\text{int}}$ denoted the interior basis function and the response coefficient, respectively. W_I^{bnd} and $\mathbf{d}_I^{bnd}$ denoted the basis function and the response coefficient on the boundary, respectively. Using the property that the interior basis functions are eliminated at the boundary, the response at the boundary nodes can be presented as

$$\mathbf{z}(\mathbf{x}_J) = \sum_{I}^{bnd} W_I^{bnd}(\boldsymbol{\Xi}_{\mathbf{x}_J})\mathbf{d}_I^{bnd} \tag{4.2}$$

where $\mathbf{X}_J$ denotes the physical collocation point where the response value is designated. $\boldsymbol{\Xi}_{\mathbf{x}_J}$ denotes the parametric collocation point corresponding to the physical one $\mathbf{X}_J$. The relationship between the response and the response coefficient at a collocation position on the boundary is expressed, in a matrix form, as

$$\mathbf{z}^b = \mathbf{A}^T\mathbf{d}^{bnd} \tag{4.3}$$

where $\mathbf{A}^T$ is non-singular and serves as a matrix that transform the

response coefficient at the boundary $\mathbf{d}^{bnd}$ to the physical response $\mathbf{z}^b$ that represents the actual response vector on the boundary. From the inverse relationship of Equation (4.3) and $\mathbf{d}^{bnd} = \mathbf{A}^{-T}\mathbf{z}^b$, the full response field in Equation (4.1) becomes

$$\mathbf{z}(\Xi) = \sum_{I}^{\text{int}} W_I^{\text{int}}(\Xi)\mathbf{d}_I^{\text{int}} + \sum_{I}^{bnd} W_I^{bnd}(\Xi)\sum_{I} \mathbf{A}_{IJ}^{-T}\mathbf{z}_J^b \equiv \sum_{I} \omega_I \delta_I \quad (4.4)$$

where ω_I and δ_I denote a generalized basis function and a generalized response coefficient, respectively.

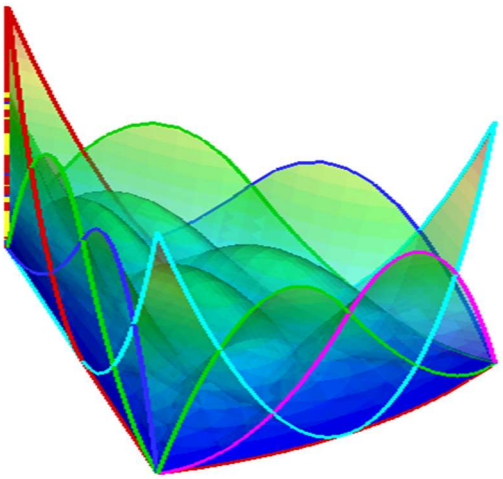

(a) NURBS

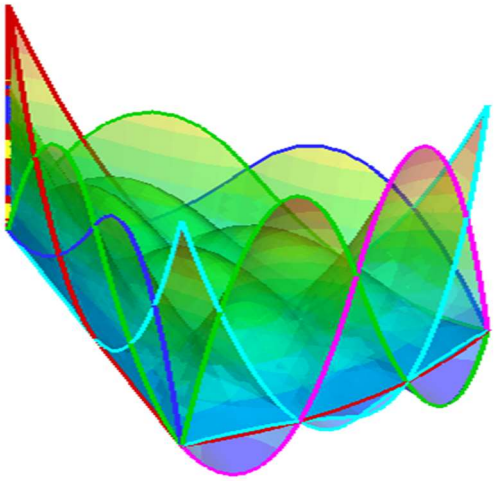

(b) Transformed NURBS

Figure 4.3 Transformation of NURBS basis function

4.2 Design parametrization

In shape optimization, the decision of the nodal coordinates of FE model is natural but could result in many difficulties such as too many design variables, unrealistic design due to an irregular boundary, and the difficulty for maintaining adequate FE mesh during the optimization.

But, in the isogeometric-based configuration design optimization, the design boundary is already expressed by NURBS curved. According to the movement of boundary control points, the design boundary varies very smoothly without a numerical instability. Therefore, an additional boundary parameterization is not necessary unlike the FE-based configuration design optimization. Nevertheless, in order to obtain realistic and manufactural designs, the geometry representation method can be utilized. If parametrization method is not used, in case of plate element, configuration design variation make curved element such as shell structure. It is important to parameterize design variables to maintain flat element. In the isogeometric-based configuration design optimization, the following representations can be introduced as Figure 4.3 and 4.4

In case of translation, the degrees of freedom out of plate direction share one design variable as

$$x_1 = x_2 = x_3 = x_4 = DV_1 \tag{4.5}$$

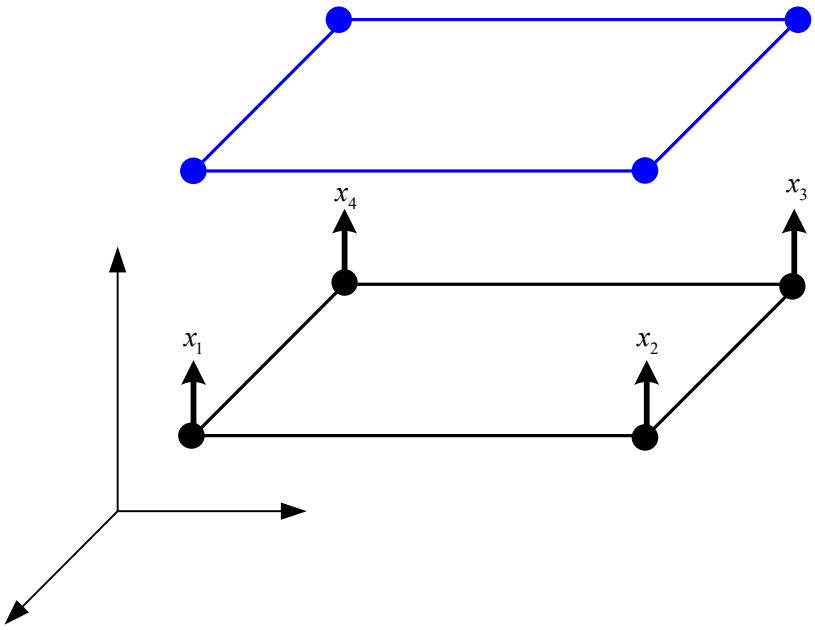

Figure 4.4 Translation

In case of flat element which has width a and length b , the degrees of freedom have following relation as

$$x_1 = dV_1,\ x_3 = dV_2 \tag{4.6}$$

$$x_2 = \frac{b}{\sqrt{a^2 + b^2}}(dV_2 - dV_1) + dV_1 \tag{4.7}$$

$$x_4 = \frac{a}{\sqrt{a^2 + b^2}}(dV_2 - dV_1) + dV_1 \tag{4.8}$$

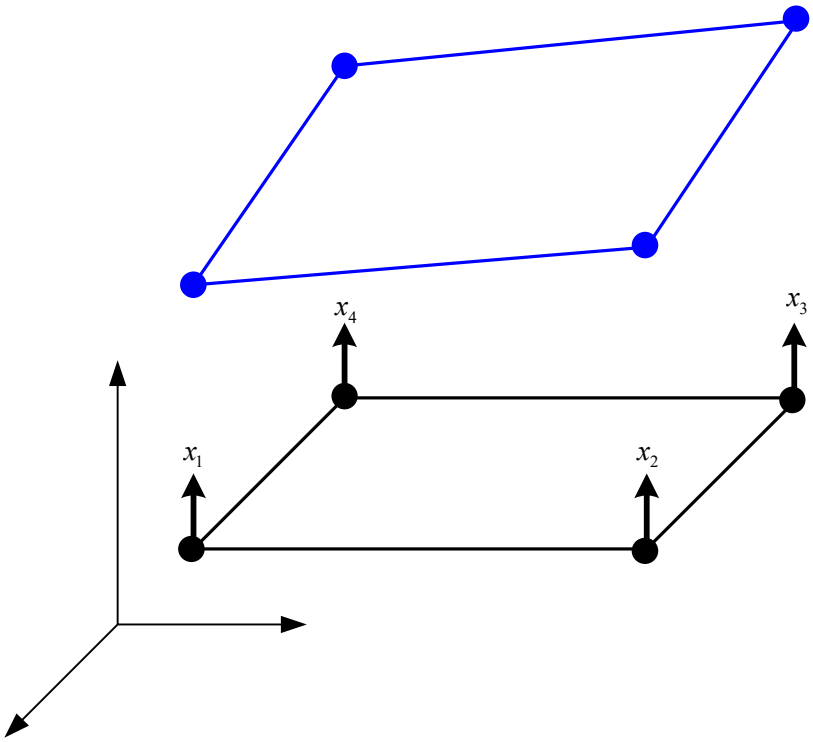

Figure 4.5 Flat element

4.3 General formulation for design optimization

The objective of design optimization is to find the optimal design. The formulation of optimization problem is state as finding the set of design variables u_i such that

$$\text{Minimize } \Psi(u_i, \mathbf{z}(u_i)) \tag{4.5}$$

subject to the equality constraints

$$h(u_i, \mathbf{z}(u_i)) = 0 \tag{4.6}$$

and the inequality constraints

$$g(u_i, \mathbf{z}(u_i)) \le 0 \tag{4.7}$$

with the side constraints

$$u_i^{lower} \le u_i \le u_i^{upper} \tag{4.8}$$

where Ψ is the objective function, and u_i^{lower} and u_i^{upper} are the sets of lower and upper bounds of design variables. In the examples of this thesis, a gradient based design optimization method is utilized in a configuration design optimization problem by using configuration design sensitivity analysis.

Among gradient-based design optimization methods, the modified method of feasible direction (MMFD) is used in this thesis. The optimization tool using MMFD requires the objective function and constrain values with their gradient values. The code for response and sensitivity is developed and linked to the optimization tool.

Chapter 5. Numerical Examples

Unless specified, all the numerical examples in this paper are modeled employing quadratic NURBS basis functions and the following material properties: Young's modulus $E = 10^5 N/m^2$, Poisson's ratio $\upsilon = 0.3$ and thickness $h = 0.1m$.

5.1 Convergence test

Flat surface in RCC

The purpose of this example is the verification of the accuracy of the developed isogeometric sensitivity in comparison with the finite difference sensitivity as well as the exact solution. Consider an annulus shown in Figure 5.1-(a), where a clamped boundary condition is imposed along the inner circle and a distributive load of $P = 0.01N/m^2$ is applied to the surface of the annulus. The outer and inner radii of the model are $a = 10m$ and $a/2 = 5m$, respectively. To evaluate the shape design sensitivity, the design perturbation and the corresponding design velocity field are shown in Figure 5.1-(b), where the initial design (thin circle) is perturbed by 0.1% of the circle radii to obtain the perturbed design (thick circle).

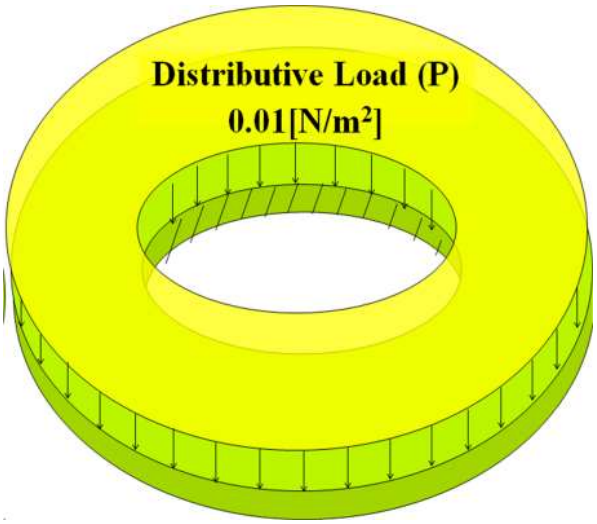

(a) Problem description

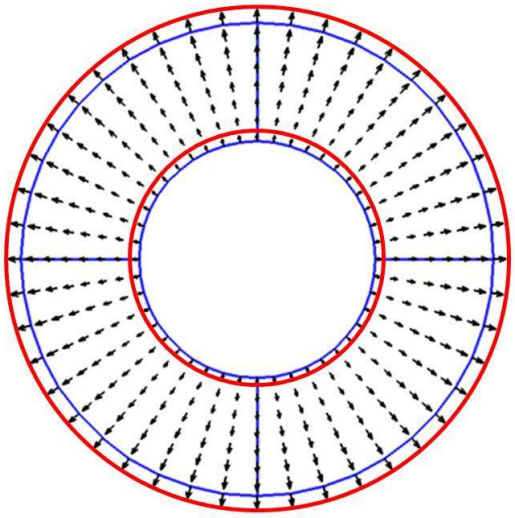

(b) Design velocity field

Figure 5.1 Annulus model

The maximum deflection occurs along the outer circle. The analytic (exact) solution and the shape design sensitivity with respect to the outer radius are given by

$$w = 0.0938 \frac{Pa^4}{Eh^3} \tag{5.1}$$

and

$$\frac{\partial w}{\partial a} = 0.3752 \frac{Pa^3}{Eh^3} \tag{5.2}$$

The log scale errors of the linear FEA, quadratic FEA, and quadratic IGA from the analytic (exact) one are shown in Figure 5.2. The convergence rate of the IGA is superior to that of the FEAs.

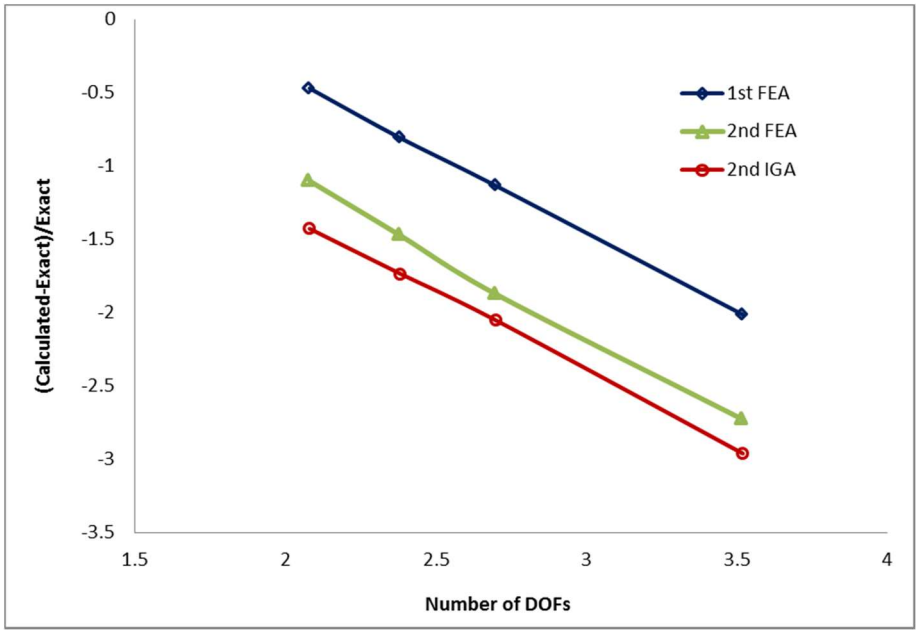

Figure 5.2 Errors in maximum deflection

Table 5.1 compares the obtained analytical and the analytic (exact) sensitivities. Compared with the finite difference sensitivity, the analytical sensitivity shows excellent agreement in both approaches of FEA (99.85%) and IGA (99.86%). However, in comparison with the

exact sensitivity, the FE sensitivity (88.59%) does not show good agreement whereas the isogeometric sensitivity (98.74%) does as shown in the last column. In the finite element model, the geometry is represented by the piecewise linear approximation and thus discretization errors are included

Table 5.1 Comparison of analytical sensitivities

Method	Analytical sensitivity	Finite difference sensitivity (a)	Agreement with (a)	Exact sensitivity (b)	Agreement with (b)
FEA	0.03323	0.0332	99.85%	0.03752	88.59%
IGA	0.03704	0.0371	99.86%		98.74%

Curved surface in GCC

Consider the problem of a pinched hemispherical shell as shown in Figure 5.3-(a). An hole has been introduced at the top of the hemispherical shell. Taking advantage of the symmetry in *x*- and *y*-axes of the problem, a quarter model of the domain is considered in Figure 5.3-(b). For the comparison of convergence performance to the exact solution, we consider the following two methods; FEA and IGA. The radius of the hemisphere is 10, thickness is 0.04, Young`s modulus is $E = 6.825 \times 10^7$ and Poisson`s ratio is $\nu = 0.3$. In these conditions, analytic displacement at the tip is known as 0.094.

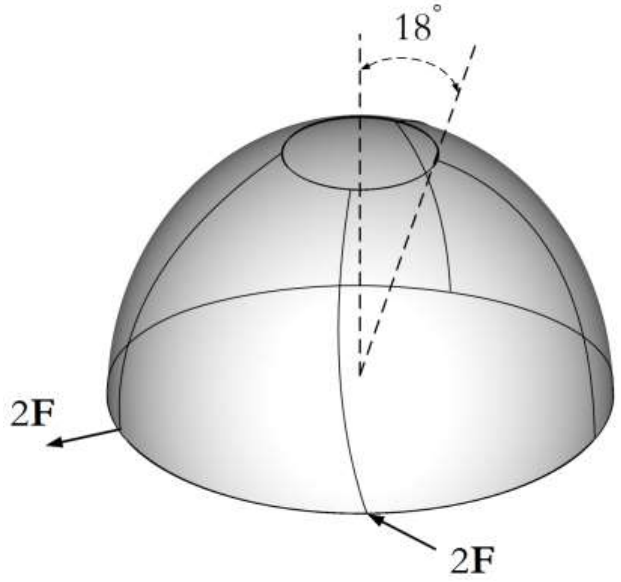

(a) Pinched hemisphere

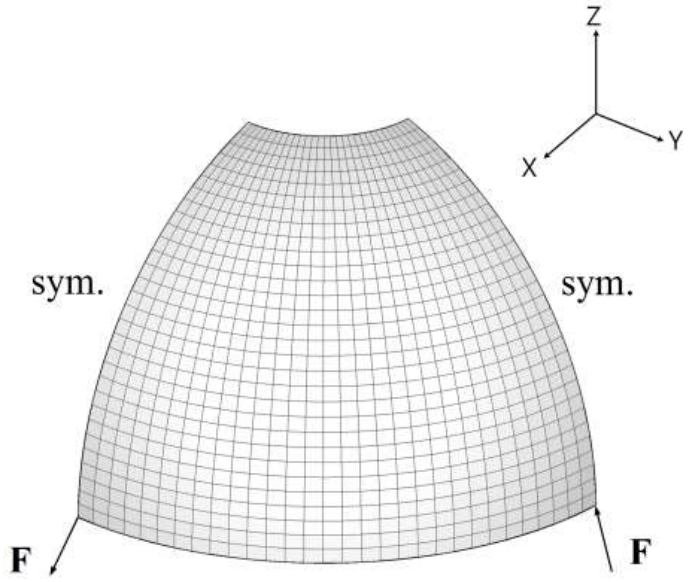

(b) A quarter model

Figure 5.3 Pinched hemisphere shell

Using quadratic and linear Lagrange polynomials and quadratic NURBS, the convergence performances of two methods are compared by increasing the number of DOFs in the numerical models. Figure 5.4

shows convergence rate with normalized solution. 1st order FEA shows bad convergence rate due to the large geometrical error. 2nd order FEA shows better convergence rate than 1st order FEA case but it is less accurate than 2nd order IGA case which is geometrically exact and have higher inter element continuity. From this result, we can say that isogeometric shell analysis using curvilinear coordinates gives reliable accuracy.

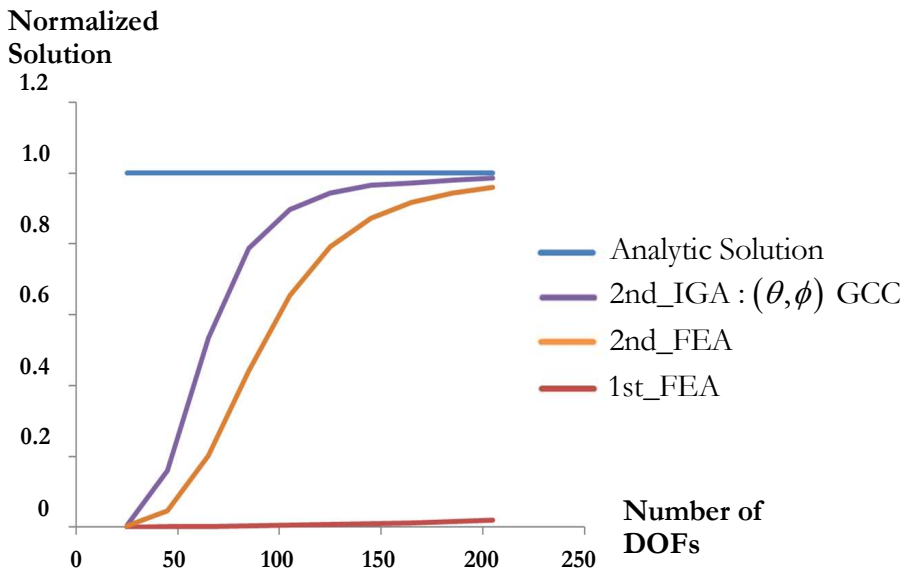

Figure 5.4 The comparison of convergence rate of pinched hemispherical shell

5.2 Sensitivity verification for higher order geometric effects

The purpose of this example is to investigate the impact of higher order geometric effects on plate bending problems the higher order geometric effect of isogeometric approach on the shape sensitivity are investigated by comparing it with FE sensitivity. Recall the boundary integral term in Equations (3.23) and (3.25). in the sensitivity equation. The expression includes the first order derivative of geometry for the normal vector and the second order derivative for the curvatures ($\kappa = div\mathbf{n}$). In the case of FE sensitivity, the normal vector is inaccurate and the curvature is missing due to the piecewise linear approximation of geometry. However, in the case of isogeometric sensitivity, the curvature and normal vector can be computed exactly due to the use of higher order NURBS for the exact representation of geometry. To verify the higher order geometric effects, consider a quarter annulus subjected to the traction along the outer circle Figure 5.5-(a)

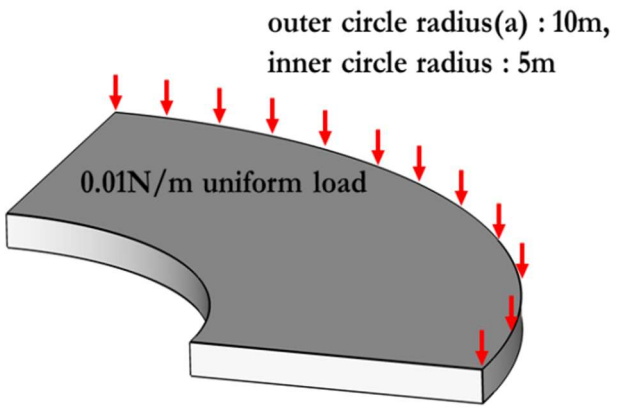

(a) Problem description

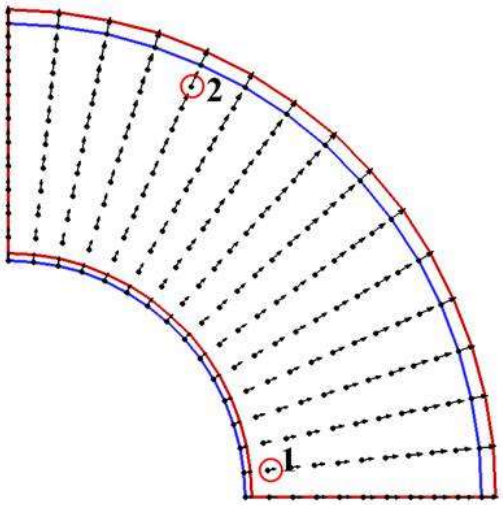

(b) Design velocity field

Figure 5.5 A quarter annulus

A clamped boundary condition is imposed along the inner arc and a uniform traction of $0.01N/m$ is applied along the outer arc. To evaluate the configuration design sensitivity, the design perturbation and the corresponding design velocity field are shown in Figire 5.5-(b) , where the initial design (thin arc) is perturbed by 0.1% the radii to obtain the perturbed design (thick arc). The displacements at the nodes 1 and 2 are selected as performance measures as shown in Figure 5.5-(b). As shown in Table 5.2, the agreement between the FE sensitivity (b) and the finite difference on (a) is not quite good.

Table 5.2 Higher order geometric effects in FE sensitivity

DOFs	Finite difference sensitivity (a)	Finite element sensitivity (b)	Agreement (b)/(a)	Finite element sensitivity (c) (with curvature)	Agreement (c)/(a)
1-z_3	1.5496E-05	7.7376E-06	43.93%	1.5463E-05	99.78%
1-θ_x	2.0173E-05	6.7485E-06	33.45%	2.0134E-05	99.81%
1-θ_y	-1.4996E-05	-5.0447E-07	33.64%	-1.4968E-06	99.81%
2-z_3	1.3941E-04	6.9432E-05	49.80%	1.3910E-04	99.78%
2-θ_x	2.5090E-05	8.2829E-06	33.01%	2.5042E-05	99.81%
2-θ_y	-8.6389E -06	-2.8343E-06	32.81%	-8.6224E-06	99.81%

To investigate the impact of curvature on the configuration sensitivity, the calculated curvature (0.1 for this case) is included in the computation of FE sensitivity As expected, the FE sensitivity considering the curvature (c) also has good agreement with finite difference one (a). In Table 5.4, the isogeometric configuration sensitivities of response coefficients corresponding to the nodes 1 and 2 in Figure 5.5-(b) are compared with the finite difference ones using the IGA. The isogeometric configuration sensitivity has excellent agreement with the finite difference on since the isogeometric approach could provide the exact normal vector and curvature.

Table 5.3 Verification of isogeometric sensitivity

DOFs	Finite difference sensitivity	Isogeometric sensitivity	Agreement
1-z_3	2.39762E-04	2.38800E-04	99.60%
1-θ_x	5.01996E-05	4.99808E-05	99.56%
1-θ_y	-2.76308E-05	-5.0447E-07	99.56%
2-z_3	4.43086E-04	-2.75105E-05	99.60%
2-θ_x	3.09569E-05	3.08220E-05	99.56%
2-θ_y	-6.32689E-05	-6.29931E-05	99.56%

5.3 Verification of configuration design sensitivity

Configuration DSA in RCC

In this example, the effect of orientation variation is included in the total shape variations. Consider the platform model which consists of two plates in Figure 5.6. The platform is fixed at the wall shown in Figure 5.6-(a) is subjected to a uniform vertical load on the horizontal plate. δa in Figure 5.6-(b) is selected as a design parameter. The length of the horizontal plate is selected as a design parameter. The displacement at the center of the horizontal plate (a dot in Figure 5.6(a)) is a performance measure. As the design is perturbed, the plate are subjected to both shape and orientation change as shown Figure 5.6(b).

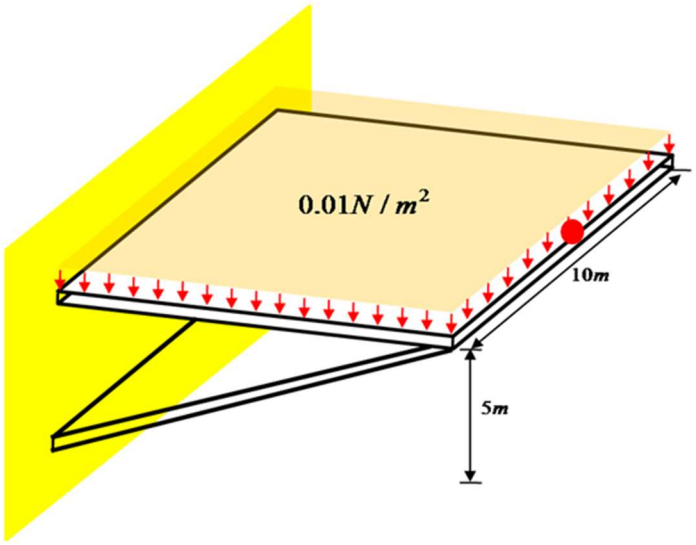

(a) Platform model

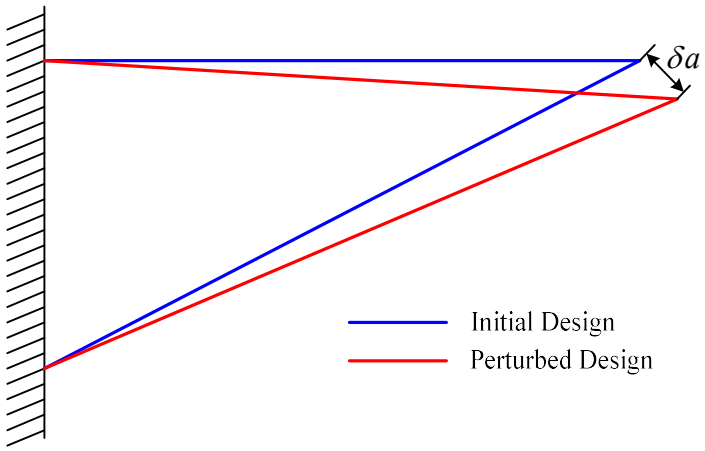

(b) Design perturbation

Figure 5.6 Configuration design sensitivity analysis

Table 5.4 compares the isogeometric configuration sensitivity of the performance measure with the finite differencing. Excellent agreements are observed at all the degrees of freedom as shown in the last column, It turns out that the contribution of orientation changes is not small throughout the whole configuration sensitivity.

Table 5.4 Verification of isogeometric configuration sensitivity in RCC

DOFs	Finite difference sensitivity (a)	Isogeometric sensitivity (b)	Shape contribution	Orientation contribution	Agreement (b)/(a)
z_1	3.5959E-09	3.5687E-09	3.0611E-10	3.2626E-09	99.24%
z_2	-3.2114E-10	-3.1860E-10	8.4952E-11	-4.0355E-10	99.21%
z_3	-6.1871E-08	-6.1852E-08	-5.7875E-08	-3.9769E-09	99.97%
θ_x	2.4049E-07	2.4049E-07	1.2344E-08	2.2815E-07	100.00%
θ_y	-1.3374E-08	-1.3474E-08	-1.3867E-08	3.9273E-10	100.75%
θ_z	-1.5406E-08	-1.5205E-08	1.2092E-10	-1.5326E-08	98.70%

Configuration DSA in GCC

The verification model is the same as convergence test model in section 5.1. For configuration sensitivity verification, every control points are perturbed randomly. Figure 5.7 shows design variation between initial design and perturbed design. Under randomly perturbed design velocity field, the configuration design sensitivity of displacement is evaluated.

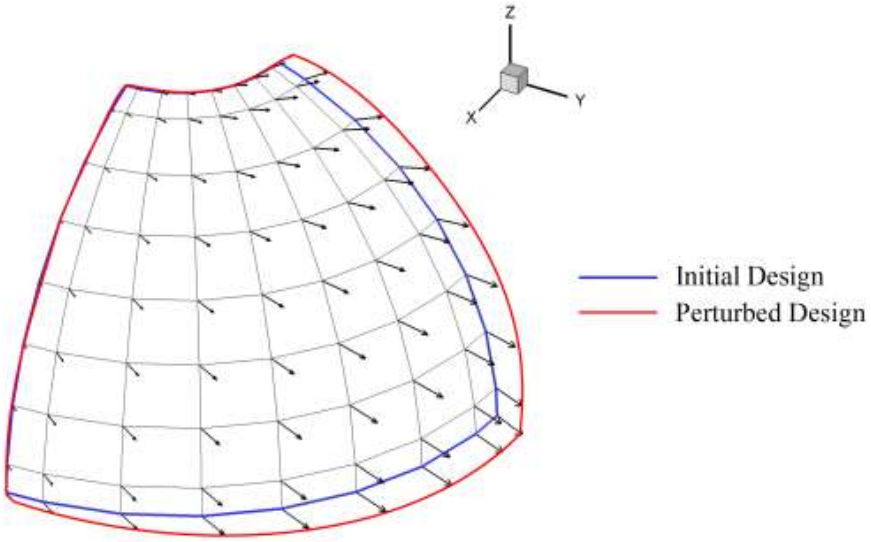

Figure 5.7 Configuration design variation and velocity field

Table 5.5 compares the isogeometric configuration sensitivity of the performance measure with the finite differencing. Excellent agreements are observed at all the degrees of freedom as shown in the last column, It turns out that the contribution of orientation changes is not small throughout the whole configuration sensitivity.

Table 5.5 Verification of isogeometric configuration sensitivity in GCC

DOFs	Finite difference sensitivity (a)	Isogeometric sensitivity(b)	Shape contribution	Orientation contribution	Agreement (b)/(a)
1	2.021E-03	2.056E-03	1.764E-04	1.880E-03	101.73%
2	1.763E-27	1.762E-27	-4.698E-28	2.232E-27	99.94%
3	-2.964E-03	-2.974E-03	-2.783E-03	-1.912E-04	100.34%
4	1.729E-02	1.729E-02	8.875E-04	1.640E-02	100.00%
5	-2.357E-28	-2.356E-28	-2.425E-28	6.867E-30	99.96%

5.4 Design optimization of shell structures

Configuration design optimization problem of parabolic arch under distributed load is considered. The objective of configuration optimization is to minimize the total strain energy. The optimal shape for an arch under distributed load is known as parabola where bending moments vanish and the loads are carried by membrane forces only. There is infinite number of quadratic parabolas to be spanned between two points, and we want to find the optimal height of the parabola on the given width. Kiendl et al. (2014) discussed the exact optimal height of parabola. The total strain energy for the parabolic arch is derived as

$$W = \frac{q^2}{EA}\int_{-b}^{b}\left(\frac{b^4}{4a^2}+x^2\right)\sqrt{1+\frac{4a^2}{b^4}x^2}\,dx \tag{5.3}$$

Detailed derivation of equation (5.3) and its derivatives can be found in Appendix B.

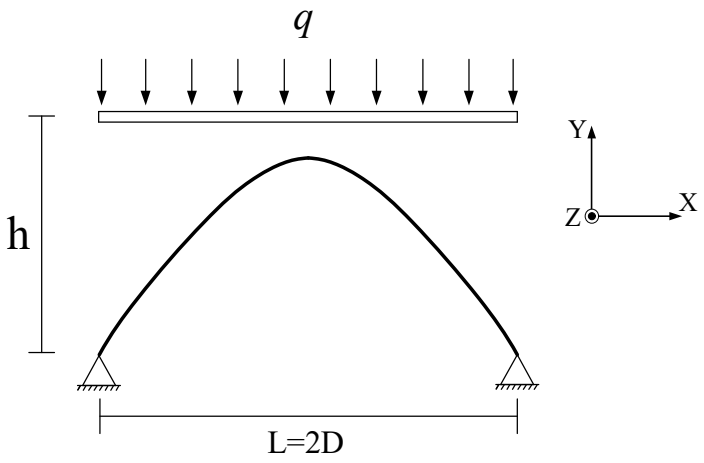

Figure 5.8 Parabolic arch under constant load with optimal arch height

The problem parameters are: D is 5m, q is 1N/m and thickness is 0.01m. To guarantee constant state throughout the z-direction, Poisson`s ratio υ is set to zero and Total number of DOFs is 105. Design variables are shown as Figure 5.9.

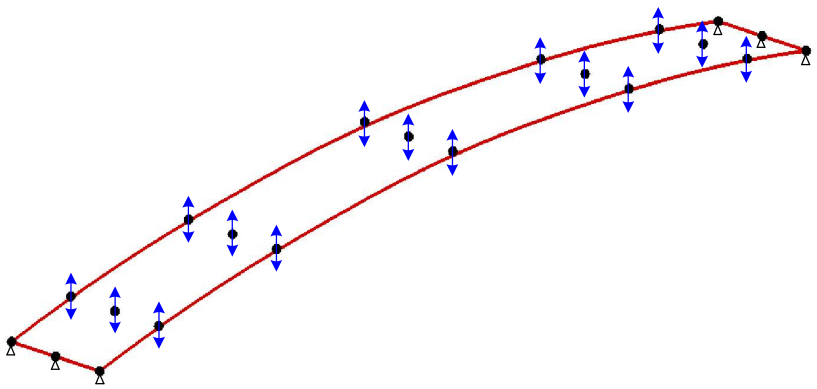

Figure 5.9 Design variables

The control points are updated by the optimization algorithm, based on the configuration sensitivities. The control points along the z-direction have design parametrization with same design updates. Initial design is shown as Figure 5.10-(a). In Figure 5.10-(b), optimal design is represented and exact optimal height is obtained as

$$h_{optimal} = 1.09558D \tag{5.4}$$

Since this example is known as $D = 5m$, optimal height is 5.4779(m) Detailed process to derive optimal height is described to Appendix B.

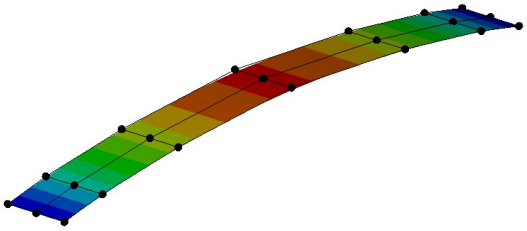

(a) Initial design

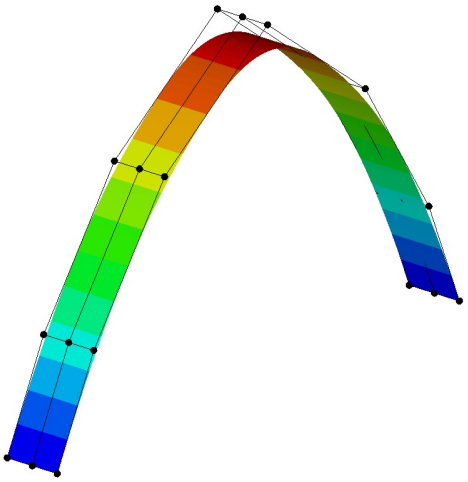

(b) Optimal design

Figure 5.10 Optimization results

Its corresponding optimization history is given in Figure 5.11. The number of iteration is 14. The compliance of optimal design properly approaches to exact compliance of parabolic arch with optimal height. The compliance of optimal design in Figure 5.10-(b) is numerically compared with exact solution driven by mathematical formulation.

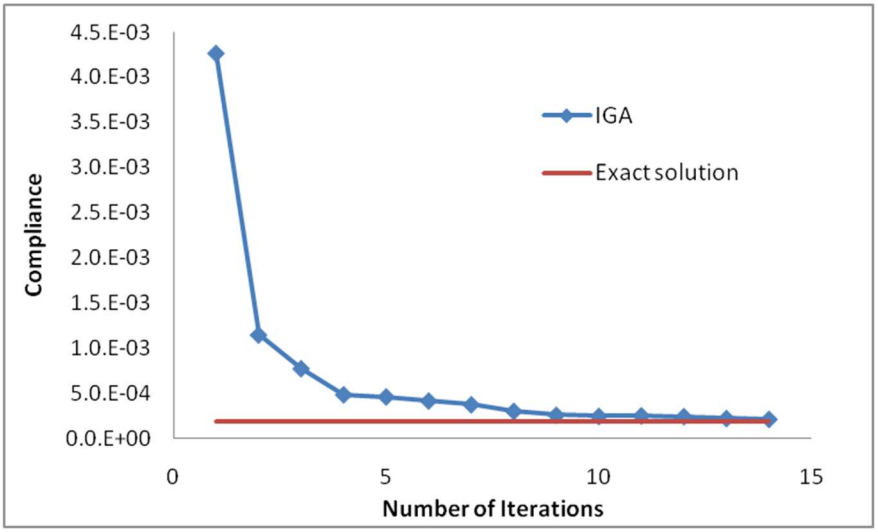

Figure 5.11 Optimization history

To validate configuration design optimization used in isogeometric framework, parabola arch beam problem is used as the benchmark problem because the benchmark problem for shell structures does not exist at design optimization problem. Therefore, as shown in Figure 5.9, the same design variations are imposed along the *z*-direction to be varied like beam elements in spite of shell structure. In Figure 5.10-(b), the optimal design is optimized under beam assumption. In case of shell structure, to check whether the model in Figure 5.8-(b) becomes optimal design, the configuration design optimization is performed considering the model in Figure 5.10-(b) as the initial design. For comparing the initial design, it is subject to the volume constraint that is less than the initial volume. During optimization, compliance is changing at every iteration step. The optimization problem is stated as

$$\text{Minimize } \mathbf{C} = \int_{\Omega} \mathbf{f}^T \mathbf{z}(u)\, d\Omega + \int_{\Gamma_t} \mathbf{T}^T \mathbf{z}(u)\, d\Gamma_t \tag{5.5}$$

$$\text{Subject to } V = \int_{\Omega} d\Omega \le V_{initial} \tag{5.6}$$

$$u_i^{lower} \le u_i \le u_i^{upper} \tag{5.7}$$

Unlike to design variables in Figure 5.9, the various design variations are observed as shown in figure 5.12.

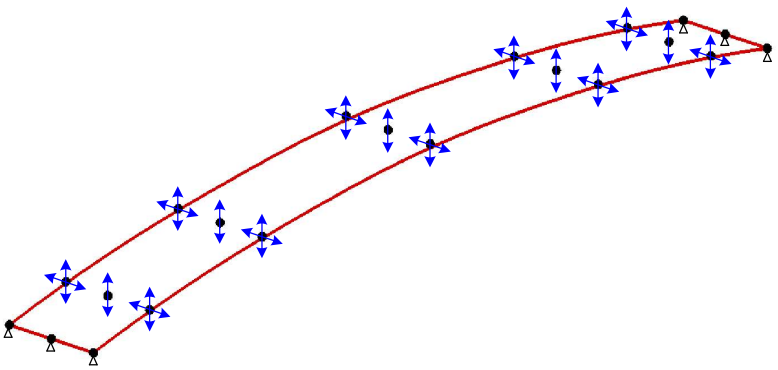

Figure 5.12 Design variables

After several iteration, the optimal design is achieved as shown in Figure 5.13, where smooth and symmetric design variation is observed. All the initial values of design variables are set to zero and the side constraints are determined through feasible design perturbations preserving the order of the control points.

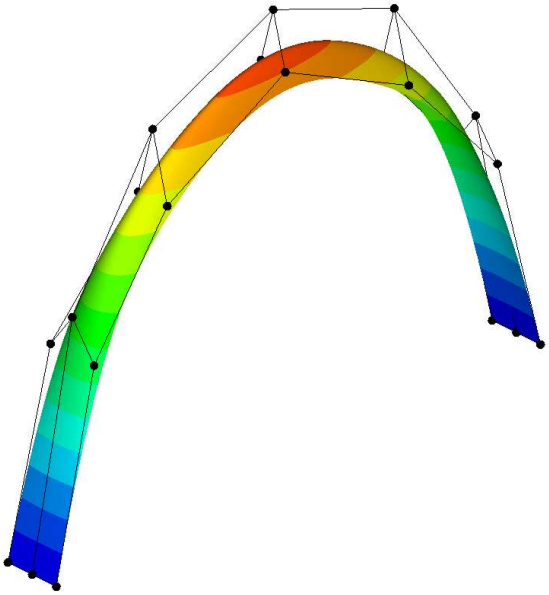

Figure 5.13 Optimal design

As shown in Table 5.6, Optimal design (b) in Figure 5.13 has lower compliance than optimal design (a) in Figure 5.10-(b). The degree of freedom of design improves that shell structure has better design than beam structures.

Table 5.6 Compliance comparison of initial and optimal design

	Initial design	Optimal design(a)	Optimal design(b)
Compliance	4.4854E-03	3.8734E-04	3.5195E-04

5.5 Design optimization of built-up structures

Configuration optimization of built-up structure

The objective of this design optimization is to find an optimal shape that minimizes the compliance of the system under the constraint of allowable material volume using the obtained isogeometric configuration design sensitivity. The configuration design optimization problem is stated as

$$\text{Minimize } \mathbf{C} = \int_{\Omega} \mathbf{f}^T \mathbf{z}(u)\, d\Omega + \int_{\Gamma_t} \mathbf{T}^T \mathbf{z}(u)\, d\Gamma_t \tag{5.8}$$

$$\text{Subject to } V = \int_{\Omega} d\Omega \le V_{\max} \tag{5.9}$$

$$u_i^{lower} \le u_i \le u_i^{upper} \tag{5.10}$$

where $V_{\max}$ is the allowable material volume. u_i is the design variable whose lower and upper bounds are $u_i^{lower} = -2$ and $u_i^{upper} = 2$, respectively. The inclined built-up structure shown in Figure 5.14-(a) consists of three plates whose lengths are all equal to 10 *m*.

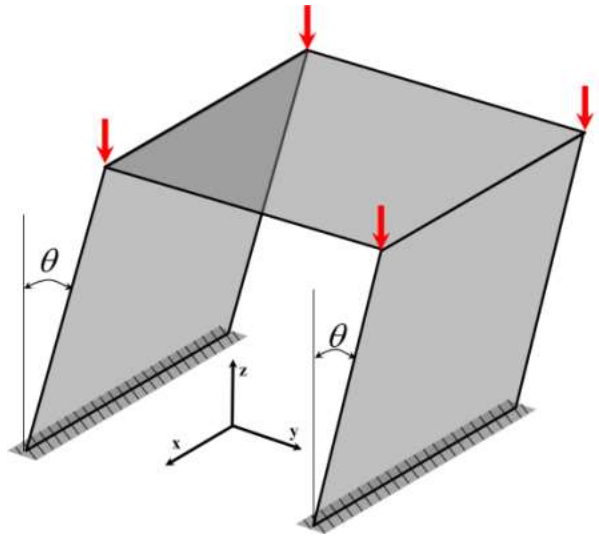

(a) Inclined built-up structure

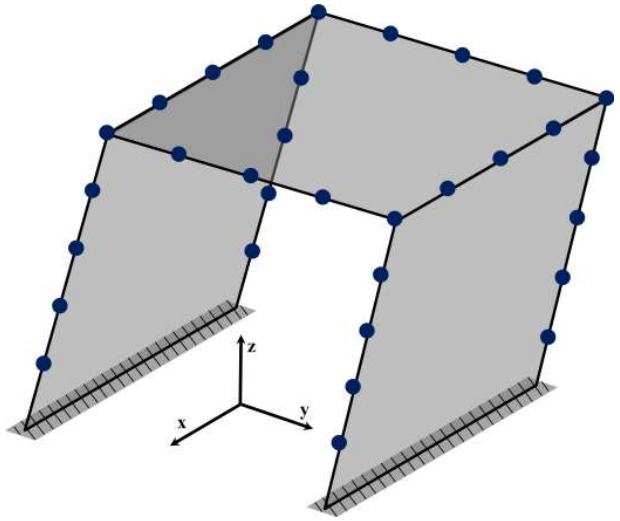

(b) Design variables

Figure 5.14 Configuration optimization problem

The top plate is subjected to concentrated loads of $F = 100N$ at the vertices and the bottom lines of vertical plates are fixed on the ground. To demonstrate the orientation effects, two vertical plates are initially inclined by $\theta = 11.3°$. To avoid the mathematical modeling failure due to the significant distortion of the plate elements, the design variables in

a patch are linearly parameterized in the out-of-plane direction. Figures 5.15-(a) and (b) respectively show the contours of total displacement in the initial and optimal designs after 8 iterations.

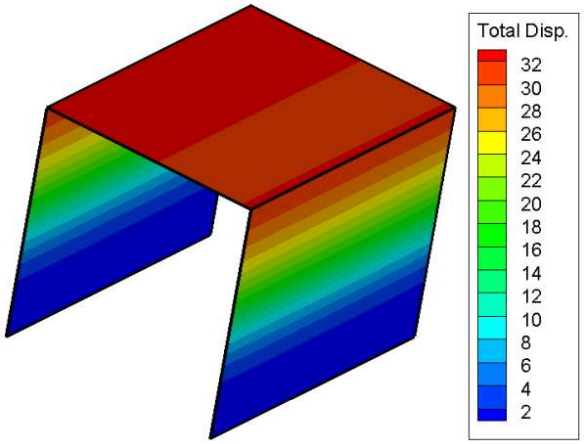

(a) Initial design

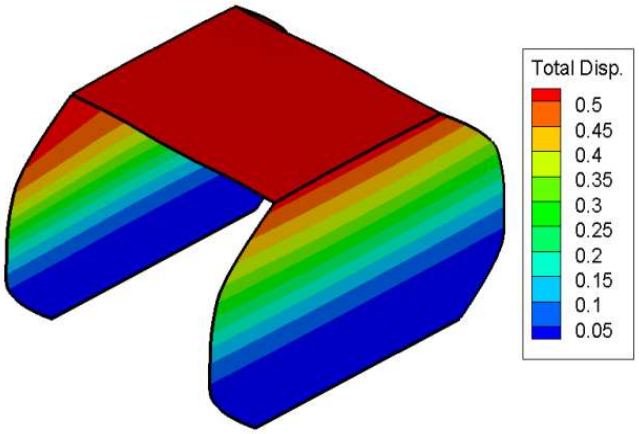

(b) Optimal design

Figure 5.15 Configuration design optimization result

Figure 5.16 shows the optimization history of compliance and inclined angle. Under the condition of same material volume, the structural compliance is decreased by 99.6% in the optimal design. In the optima design, it is observed that the overall displacement level is decreased and the inclined angle vanishes.

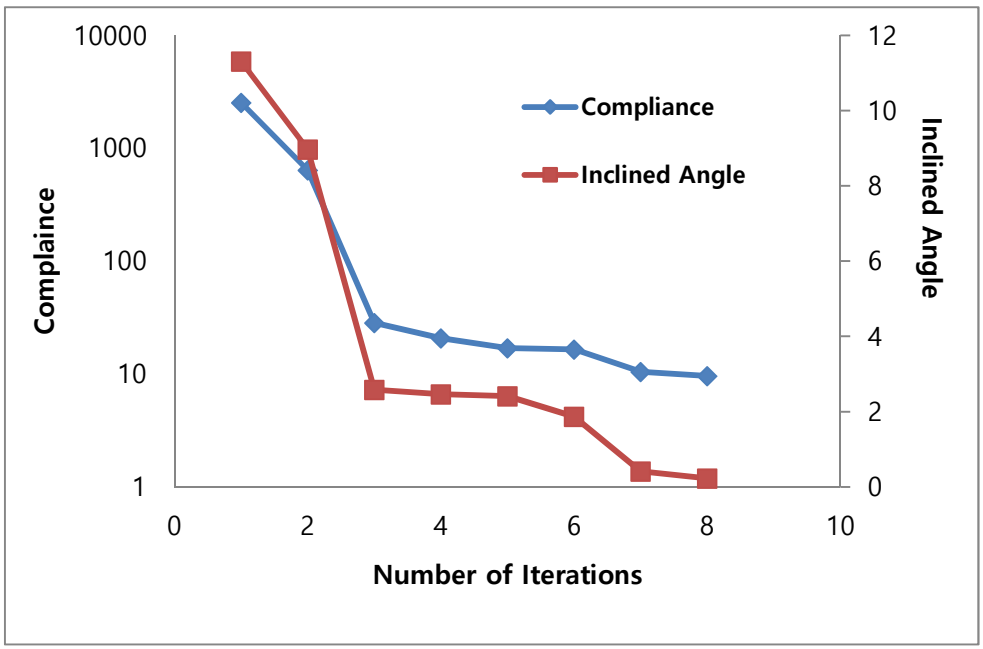

Figure 5.16 Optimization history (compliance, Inclined angle)

Application to general engineering problems: Stiffened plate

The developed optimization method is applied to a stiffened plate model as shown in Figure 5.17-(a). 9 patches, 118 control points, and quadratic NURBS basis functions are used. The bottom plate is subject to the uniform load of $10N/m^2$. The side plates are fixed along the upper edges. The design variables are selected as the global coordinates of the control points in Figure 5.17-(b). The optimization problem is to find the optimal shape such that the compliance is minimized and the initial volume is kept constant. In this example, the following methods are conducted to avoid the mismatch problem at the intersection;

(1) *Constraint condition*

(2) *Repeated knots*

(3) *Transformed basis function*

The optimal shape obtained from any of the methods indicates that the areas of inner hole and side plates are increased. Also the heights of the stiffeners are increased.

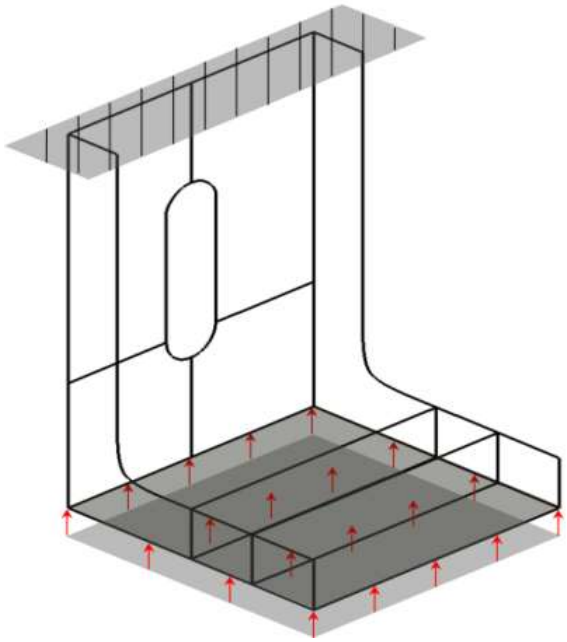

(a) Model description

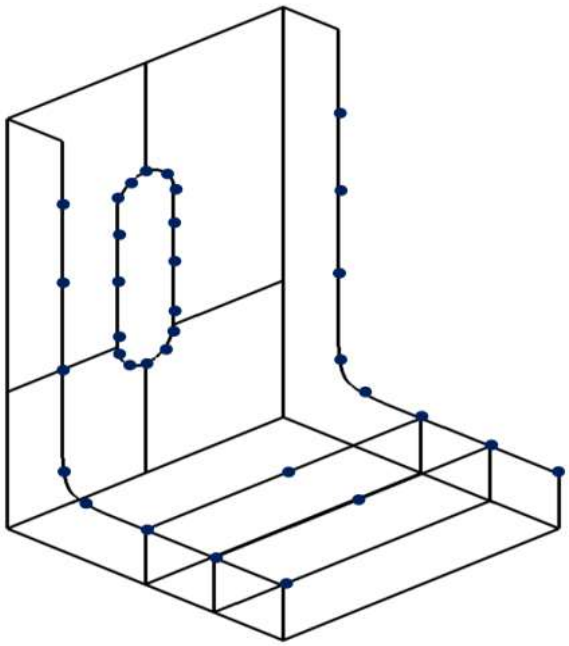

(b) Design variables

Figure 5.17 Stiffened plate

Figure. 5.18-(a) shows the optimal shape and the contour of displacement field when no additional treatment is applied. Some mismatch is observed at the intersection between the side plate and the stiffeners. When a constraint condition is imposed, there is no mismatch at the intersection of the optimal design except that the displacement level is slightly increased as shown in Figure 5.18-(b). Also, as shown in Table 5.7, the optimal design from the constraint condition has an increased compliance (4224.7) that is a biggest value of all the compliance obtained from any other methods. The constraint condition restrains the design variations and thus reduces the DOFs in design space.

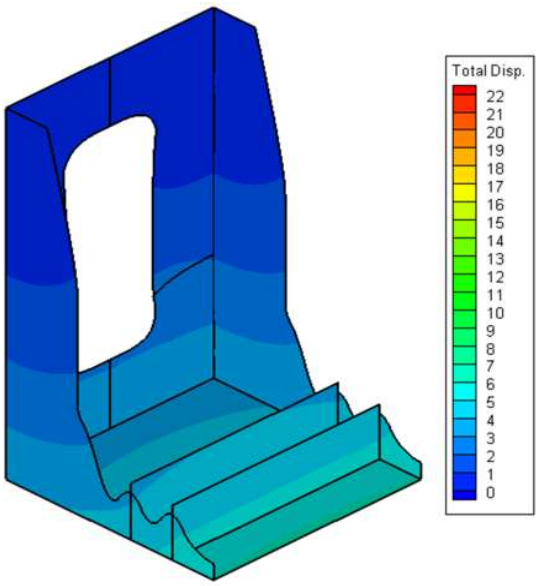

(a) No additional treatment

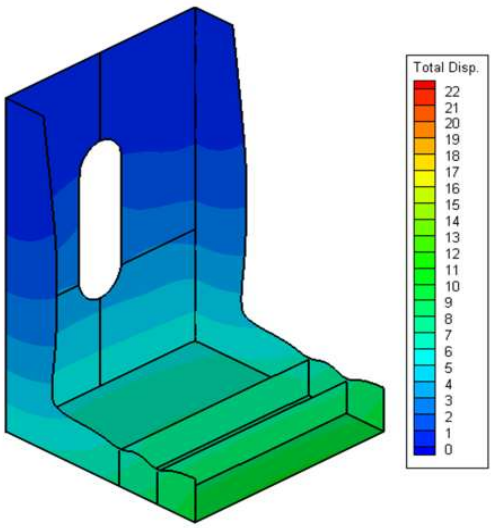

(b) Constraint condition

Figure 5.18 Comparison of optimal shapes and displacement contours

Table 5.7 Compliance comparison in various methods

	No additional treatment	Constraint condition	Repeated knots	Transformed basis function
Initial design	7.0060E+03	7.0060E+03	7.4923E+03	6.9989E+03
Optimal design	2.3873E+03	4.2247E+03	2.8253E+03	2.5299E+03

In the case of repeated knots in Figure 5.19-(a), the mismatch problem is easily resolved but another problem of continuity arises. Geometric continuity is decreased and consequently stress distributions is discontinuous at the intersections of patches. The method of

transformed basis functions keeps the inter-patch continuity and the number of DOFs in design space. Also, we obtain the continuous tress contour and the reduced compliance by 63.9% under the condition of same material volume.

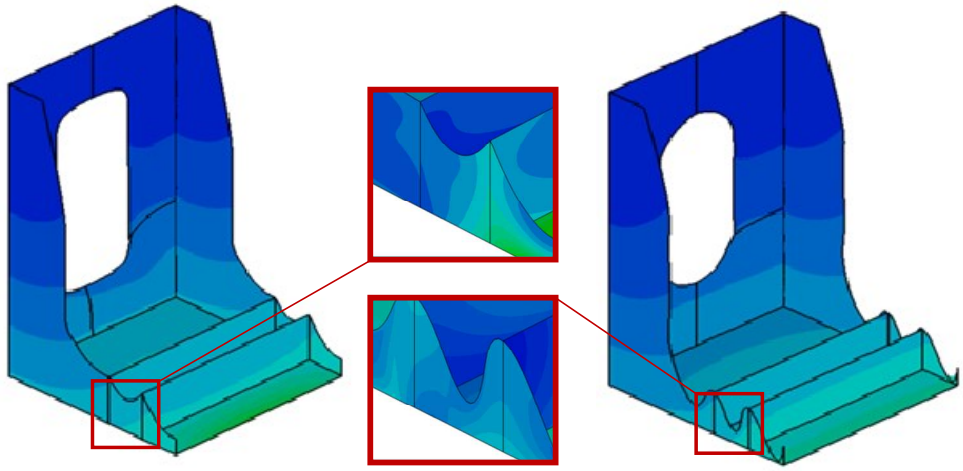

(a) Repeated knots (b) Transformed basis function

Figure 5.19 Comparison of optimal shapes and von-Mises stress contours

Chapter 6. Conclusion and Future Work

6.1 Conclusion

An isogeometric configuration DSA method for Mindlin plates is developed using the material derivative and adjoint approaches and utilized in the design optimization of built-up structures. The configuration design sensitivity includes both shape and orientation variations. In the isogeometric approach, the NURBS basis function in CAD system is directly utilized in the response analysis, which enables the seamless incorporation of higher continuity and exact geometry such as curvature and normal vector into the computational framework. Unlike the conventional FE based configuration optimization, complicated design parametrization is not necessary due to direct use of CAD geometry in the IGA. However, a mismatch problems arises at the intersection of patches. Among various methods conducted to overcome this difficulty, the method of transformed basis functions provides the best performance in terms for continuity and design space

We also derived the configuration design sensitivity formulation for shell structure in curvilinear coordinates using direct differentiation method. The transformation between coordinate systems for original design and for perturbed design is defined. The orientation variation is obtained through the material derivative of transformation matrix for two coordinate system. Therefore, covariant and contravariant base vectors are dependent on the design especially orientation variation.

Several numerical examples are given to illustrate the capabilities of developed method for the shell and plate structures. The problem obtaining optimal height of parabolic arch is solved by introducing configuration design variation. We demonstrate that IGA framework shown better convergence rate than FEA case due to the exact geometry and higher-order geometric information. Also we applied the configuration design optimization to practical example.

6.2 Future works

In RCC, the configuration design sensitivity is formulated using both direct differentiation method and adjoint variable method. But, In GCC, the derived configuration design sensitivities are obtained by direct differentiation method. For the efficiency, configuration sensitivities will be derived by adjoint variable method.

And, numerical examples in this thesis are based on shell structure and built-up structures with plate. In order to apply the isogeometric-based configuration design optimization to more practical problems, built-up structures with plate and shell structures are required. Since the configuration design sensitivities are derived for shell and plate structure, this work can be accomplished readily.

Appendix A

Derivation of initial curvatures

The position vector $\mathbf{r}$ of the observed point $\hat{\mathbf{x}}$ in Figure 3.3 is assumed to be known and given by

$$\mathbf{r} = r_1(x_1, x_2)\mathbf{e}_1 + r_2(x_1, x_2)\mathbf{e}_2 + r_3(x_1, x_2)\mathbf{e}_3 \tag{A.1}$$

Taking the first-order derivative of Equation (A.1) with respect to x_1 and x_2 yields

$$\mathbf{a}_1 = R_{1,x_1}\mathbf{e}_1 + R_{2,x_1}\mathbf{e}_2 + R_{3,x_1}\mathbf{e}_3 \tag{A.2}$$

$$\mathbf{a}_2 = R_{1,x_2}\mathbf{e}_1 + R_{2,x_2}\mathbf{e}_2 + R_{3,x_2}\mathbf{e}_3 \tag{A.3}$$

$$\begin{aligned}\mathbf{a}_3 &= \mathbf{a}_1 \times \mathbf{a}_2 \\ &= (R_{2,x_1}R_{3,x_2} - R_{3,x_1}R_{2,x_2})\mathbf{e}_1 + (R_{3,x_1}R_{1,x_2} - R_{1,x_1}R_{3,x_2})\mathbf{e}_2 \\ &+ (R_{1,x_1}R_{2,x_2} - R_{2,x_1}R_{1,x_2})\mathbf{e}_3\end{aligned} \tag{A.4}$$

Hence, the base vectors of the $x_1 - x_2 - x_3$ frame are related to the base vectors of the $\hat{x}_1 - \hat{x}_2 - \hat{x}_3$ frame by the known transformation matrix as

$$\mathbf{a}_{123} = \mathbf{T}^0\mathbf{e}_{123} \tag{A.5}$$

where $\mathbf{a}_{123} \equiv [\mathbf{a}_1, \mathbf{a}_2, \mathbf{a}_3]^T$, $\mathbf{e}_{123} \equiv [\mathbf{e}_1, \mathbf{e}_2, \mathbf{e}_3]^T$ and

$$\mathbf{T}^0 = \begin{bmatrix} r_{1,x_1} & r_{2,x_1} & r_{3,x_1} \\ r_{1,x_2} & r_{2,x_2} & r_{3,x_2} \\ r_{2,x_1}r_{3,x_2} - r_{3,x_1}r_{2,x_2} & r_{3,x_1}r_{1,x_2} - r_{1,x_1}r_{3,x_2} & r_{1,x_1}r_{2,x_2} - r_{2,x_1}r_{1,x_2} \end{bmatrix} \tag{A.6}$$

Using Equation (A.5) and the identity $[\mathbf{T}^0]^{-1} = [\mathbf{T}^0]^T$, we obtain the relations

$$\frac{\partial \mathbf{a}_m}{\partial x_\alpha} \cdot \mathbf{a}_m = 0 \tag{A.7}$$

and

$$\frac{\partial \mathbf{a}_m}{\partial x_\alpha} \cdot \mathbf{a}_n = -\frac{\partial \mathbf{a}_n}{\partial x_\alpha} \cdot \mathbf{a}_m . \tag{A.8}$$

The partial derivatives of the initial base vector $\mathbf{a}_{123}$ with respect to x_1 and x_2 are expressed as

$$\begin{aligned} \mathbf{a}_{123,x_\alpha} &= (\mathbf{T}^0 \mathbf{e}_{123})_{,x_\alpha} \\ &= \mathbf{T}^0{}_{,x_\alpha} \mathbf{e}_{123} + \mathbf{T}^0 \mathbf{e}_{123,x_\alpha} \\ &= \mathbf{T}^0{}_{,x_\alpha} [\mathbf{T}^0]^{-1} \mathbf{a}_{123} \\ &= \mathbf{T}^0{}_{,x_\alpha} [\mathbf{T}^0]^T \mathbf{a}_{123} \\ &= \mathbf{\Omega}_\alpha \mathbf{a}_{123} \end{aligned} \tag{A.9}$$

where

$$\mathbf{\Omega}_1 = \begin{bmatrix} \mathbf{a}_{1,x_1} \cdot \mathbf{a}_1 & \mathbf{a}_{1,x_1} \cdot \mathbf{a}_2 & \mathbf{a}_{1,x_1} \cdot \mathbf{a}_3 \\ \mathbf{a}_{2,x_1} \cdot \mathbf{a}_1 & \mathbf{a}_{2,x_1} \cdot \mathbf{a}_2 & \mathbf{a}_{2,x_1} \cdot \mathbf{a}_3 \\ \mathbf{a}_{3,x_1} \cdot \mathbf{a}_1 & \mathbf{a}_{3,x_1} \cdot \mathbf{a}_2 & \mathbf{a}_{3,x_1} \cdot \mathbf{a}_3 \end{bmatrix} = \begin{bmatrix} 0 & k_5 & -k_1 \\ -k_5 & 0 & -k_{61} \\ k_1 & k_{61} & 0 \end{bmatrix} \tag{A.10}$$

and

$$\mathbf{\Omega}_2 = \begin{bmatrix} \mathbf{a}_{1,x_2} \cdot \mathbf{a}_1 & \mathbf{a}_{1,x_2} \cdot \mathbf{a}_2 & \mathbf{a}_{1,x_2} \cdot \mathbf{a}_3 \\ \mathbf{a}_{2,x_2} \cdot \mathbf{a}_1 & \mathbf{a}_{2,x_2} \cdot \mathbf{a}_2 & \mathbf{a}_{2,x_2} \cdot \mathbf{a}_3 \\ \mathbf{a}_{3,x_2} \cdot \mathbf{a}_1 & \mathbf{a}_{3,x_2} \cdot \mathbf{a}_2 & \mathbf{a}_{3,x_2} \cdot \mathbf{a}_3 \end{bmatrix} = \begin{bmatrix} 0 & k_4 & -k_{62} \\ -k_4 & 0 & -k_2 \\ k_{62} & k_2 & 0 \end{bmatrix}. \tag{A.11}$$

The Ω_1 and Ω_2 are called initial curvature matrices. The initial curvatures are defined as

$$k_1 \equiv \frac{\partial \mathbf{a}_3}{\partial x_1} \cdot \mathbf{a}_1 = -\frac{\partial \mathbf{a}_1}{\partial x_1} \cdot \mathbf{a}_3 = -\sum_{i=1}^{3} \frac{\partial T_{1i}^0}{\partial x_1} T_{3i}^0 \tag{A.12}$$

$$k_2 \equiv \frac{\partial \mathbf{a}_3}{\partial x_2} \cdot \mathbf{a}_2 = -\frac{\partial \mathbf{a}_2}{\partial x_2} \cdot \mathbf{a}_3 = -\sum_{i=1}^{3} \frac{\partial T_{2i}^0}{\partial x_2} T_{3i}^0 \tag{A.13}$$

$$k_{61} \equiv \frac{\partial \mathbf{a}_3}{\partial x_1} \cdot \mathbf{a}_2 = -\frac{\partial \mathbf{a}_2}{\partial x_1} \cdot \mathbf{a}_3 = -\sum_{i=1}^{3} \frac{\partial T_{2i}^0}{\partial x_1} T_{3i}^0 \tag{A.14}$$

$$k_{62} \equiv \frac{\partial \mathbf{a}_3}{\partial x_2} \cdot \mathbf{a}_1 = -\frac{\partial \mathbf{a}_1}{\partial x_2} \cdot \mathbf{a}_3 = -\sum_{i=1}^{3} \frac{\partial T_{1i}^0}{\partial x_2} T_{3i}^0 \tag{A.15}$$

$$k_5 \equiv -\frac{\partial \mathbf{a}_2}{\partial x_1} \cdot \mathbf{a}_1 = \frac{\partial \mathbf{a}_1}{\partial x_1} \cdot \mathbf{a}_2 = \sum_{i=1}^{3} \frac{\partial T_{1i}^0}{\partial x_1} T_{2i}^0 \tag{A.16}$$

and

$$k_4 \equiv -\frac{\partial \mathbf{a}_2}{\partial x_2} \cdot \mathbf{a}_1 = -\frac{\partial \mathbf{a}_1}{\partial x_2} \cdot \mathbf{a}_2 = -\sum_{i=1}^{3} \frac{\partial T_{1i}^0}{\partial x_2} T_{2i}^0 \tag{A.17}$$

Appendix B

Derivation of optimal height in parabola arch

The strain energy of an arch in pure compression state is

$$W = \int_V \sigma \cdot \varepsilon dV \tag{B.1}$$

with V as the volume σ as the stress, ε as the strains and they can be represented by

$$\sigma = \frac{N}{A} \tag{B.2}$$

$$\varepsilon = \frac{\sigma}{E} = \frac{N}{EA} \tag{B.3}$$

and

$$dV = A \cdot ds \tag{B.4}$$

where N is the normal force, E the Young`s modulus, A the cross-sectional area and ds the infinitesimal arc length. The equation (B.1) can be rewritten as

$$W = \frac{1}{EA}\int_l N^2 ds \tag{B.5}$$

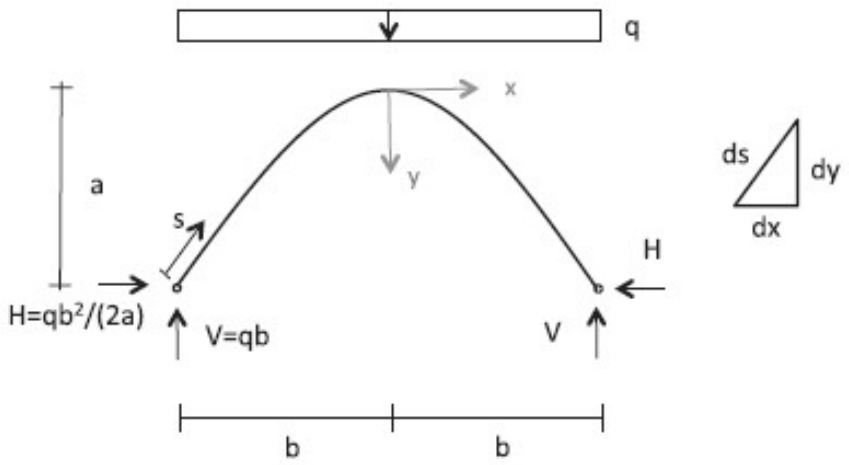

Figure B.0.1 Parabolic arch under constant load

The geometry is described by the parabolic function

$$y = \frac{a}{b}x^2, \tag{B.6}$$

$$\frac{dy}{dx} = \frac{2a}{b^2}x \tag{B.7}$$

and

$$ds = \sqrt{dx^2 + dy^2} = \left(\sqrt{1 + \frac{4a^2}{b^4}x^2}\right)dx \tag{B.8}$$

The normal force is determined by its horizontal and vertical components

$$N_h(x) = -H = -\frac{qb^2}{2a} \tag{B.9}$$

and

$$N_v(x) = -V + q(x+b) = qx \tag{B.10}$$

The normal force can be represented by

$$N(x) = \sqrt{N_h^2(x) + N_h^2(x)} = q\sqrt{\frac{b^4}{4a^2} + x^2} \tag{B.11}$$

Substituting Equations (B.8) and (B.11) into Equation (B.5) yields the strain energy as function of the arch height *a*:

$$W = \frac{q^2}{EA}\int_{-b}^{b}\left(\frac{b^4}{4a^2} + x^2\right)\sqrt{1 + \frac{4a^2}{b^4}x^2}\,dx \tag{B.12}$$

Substituting *b*=1, Equation (B.12) can be rewritten as

$$\begin{aligned} W &= \frac{q^2}{EA}\int_{-1}^{1}\left(\frac{b^4}{4a^2} + x^2\right)\sqrt{1 + \frac{4a^2}{b^4}x^2}\,dx \\ &= \frac{q^2}{EA}\frac{1}{64a^3}\left(12\sqrt{1+4a^2}\,a + 8(a+4a^2)^{\frac{3}{2}}a\right) \\ &\quad -\frac{q^2}{EA}\frac{1}{64a^3}\left(3\ln\left(-2a + \sqrt{1+4a^2}\right) - 3\ln\left(2a + \sqrt{1+4a^2}\right)\right) \end{aligned} \tag{B.13}$$

Derivative of Equation (B.13) with respect to *a* yields

$$\frac{dW}{da}=\frac{q^2}{EA}\frac{1}{64}\frac{\left(-128a^5+80a^3+28a+9\ln\left(-2a+\sqrt{1+4a^2}\right)\right)}{\sqrt{1+4a^2}\left(2a+\sqrt{1+4a^2}\right)\left(2a-\sqrt{1+4a^2}\right)a^4}$$

$$-\frac{q^2}{EA}\frac{1}{64}\frac{\left(9\ln\left(2a+\sqrt{1+4a^2}\right)\sqrt{1+4a^2}\right)}{\sqrt{1+4a^2}\left(2a+\sqrt{1+4a^2}\right)\left(2a-\sqrt{1+4a^2}\right)a^4} \quad \text{(B.14)}$$

The optimum is determined by stationary point

$$\frac{dW}{da}=0 \quad \text{(B.15)}$$

$$a_{optimal}=1.09558 \quad \text{(B.16)}$$

Bibliography

AHMAD, S., ORONS, B. M. & ZIENKIEWICZ, O. C. 1970. Analysis of thick and thin shell structures by curved finite elements. *International Journal for Numerical Method in Engineering.* 2, 419-451.

BAZILEVS, Y., CALO, V.M., HUGHES, T.J.R. & ZHANG, Y. 2008. Isogeometric fluid-structure interaction: Theory, Algorithms and Computation. *Computational Mechanics*, 43, 3-37.

BENSON, D. J., BAZILEVS, Y., HSU, M. C. & HUGHES, T. J. R. 2010. Isogeometric shell analysis: the Reissner-Mindlin shell. *Computer Methods in Applied Mechanics and Engineering*, 199, 276-289.

BOUCLIER, R., ELGUEDI, T. & COMBESCURE, A. 2013. Efficient isogeometric NURBS-based solid-shell elements: mixed formulation and B-method. *Computer Methods in Applied Mechanics and Engineering*, 267, 86-110.

CHO, S. & HA, S. H. 2009. Isogeometric shape design optimization: exact geometry and enhanced sensitivity. *Structural and Multidisciplinary Optimization*, 38, 53-70.

CHO, S. & CHOI, K. K. 2000. Design sensitivity analysis and optimization of non-linear transient dynamics. Part II: Configuration design. *International Journal for Numerical Method in Engineering.* 48, 375-399.

CHOI, J.-H. 2002. Configuration design sensitivity analysis and optimization of beam structures. *Computational Mechanics*, 29, 129-142.

CHOI, M. J. & CHO, S. 2014. Isogeometric shape design sensitivity analysis of stress intensity factors for curved crack problems. *Computer Methods in Applied Mechanics and Engineering*, 279, 469-496.

CHOI, K. K. & KIM, N. H. 2006. *Structural Sensitivity Analysis and Optimization 1: Linear Systems*, Springer.

COTTRELL, J.A., REALI, A., BAZILEVS, Y. & HUGHES, T.J.R. 2006. Isogeometric analysis of structural vibrations. *Computer Methods in Applied Mechanics and Engineering*, 195, 5257-5296.

COTTRELL, J.A., HUGHES, T.J.R. & REALI, A. 2007. Studies of refinement and continuity in isogeometrical structural analysis. *Computer Methods in Applied Mechanics and Engineering*, 196, 264-275.

ECHTER, R., OESTERLE, B. & BISCHOFF, M. 2013. A hierarchic family of isogeometric shell finite elements, *Computer Methods in Applied Mechanics and Engineering*, 254, 170-180.

EVANS, J.A., BAZILEVS, Y., BABUSKA, I. & HUGHES, T.J.R. 2009. *n*-Widths, sup-infs, and optimality ratios for the *k*-version of the isogeometric finite element method, *Computer Methods in Applied Mechanics and Engineering*, 198, 1726-1741.

HOSSEINI, S., REMMERS, J.J.C., VERHOOSEL, C. V. & BORST, R. 2014. An isogeometric continuum shell element for non-linear analysis. *Computer Methods in Applied Mechanics and Engineering*, 271, 1-22.

HUGHES, T. J. R., COTTRELL, J. A. & BAZILEVS, Y. 2005. Isogeometric analysis: CAD, finite elements, NURBS, exact geometry and mesh refinement. *Computer Methods in Applied Mechanics and Engineering,* 194, 4135-4195.

KIENDL, J., BLETZINGER, K.-U., LINHARD, J. & WÜCHNER, R. 2009. Isogeometric shell analysis with Kirchhoff-Love element, *Computer Methods in Applied Mechanics and Engineering*, 198, 3902-3914

KIENDL, J., SCHMIDT, R. & WÜCHNER, R. & BLETZINGER, K.-U. 2014.

Isogeometric shape optimization of shells using semi-analytical sensitivity analysis and sensitivity weighting, *Computer Methods in Applied Mechanics and Engineering*, 274, 148-167.

KIM, N.H., CHOI, K.K., CHEN, J.-S. & BOTKIN, M.E. 2002. Meshfree analysis and design sensitivity analysis for shell structures, *International Journal for Numerical Method in Engineering.* 53, 3902-3914

KOMKOV, V., CHOI, K.K. & HAUG, E.J. 1986. *Design sensitivity analysis of structural system*, Academic press

KOO, B., HA, S-H., KIM, H-S. & CHO, S. 2013. Isogeometric shape design optimization of geometrically nonlinear structures, *Mechanics Based Design of Structures and Machines*, 41, 337-358.

KOO, B., YOON, M. & CHO, S. 2012. Isogeometric shape design sensitivity analysis using transformed basis functions for Kronecker delta property, *Computer Methods in Applied Mechanics and Engineering*, 253, 505-516

LEE, S. -W. & CHO, S. 2015. Isogeometric configuration design optimization of built-up structures. *Structural and Multidisciplinary Optimization, 51*(2), 319-331.

NAGHDI, P.M. 1963. *In Foundations of Elastic Shell Theory*, Progress in Solid Mechanics.

NAGY, A. P., IJSSELMUIDEN, S. T. & ABDALLA, M. M. 2013. Isogeometric design of anisotropic shells: optimal form and material distribution. *Computer methods in applied mechanics and engineering*, 264, 145-162.

PIEGL, L. & TILLER, W. 1997. *The NURBS Book (Monographs in Visual Communication)*, Springer-Verlag.

QIAN, X. 2010. Full analytical sensitivities in NURBS based isogeometric shape optimization. *Computer methods in applied mechanics and engineering*, 29, 2069-

2071.

ROGERS, D.F. 2001. *An Introduction to NURBS with Historical Perspective*, Academic Press.

ROH, H. Y. & CHO, M. 2003. Development of geometrically exact new shell element based on general curvilinear coordinates. *Computer methods in applied mechanics and engineering*, 56, 81-115.

SIMO, J. C., FOX, D. D. 1989. On a stress resultant geometrically exact shell model Part I: formulation and optimal parametrization. *Computer Methods in Applied Mechanics and Engineering*, 72, 267-304.

TAMIZER, T., WRIGGER, P. & HUGHES, T.J.R. 2008. Contact treatment in isogeometric analysis with NURBS. *Computer Methods in Applied Mechanics and Engineering*, 100, 1100-1117.

TWU, S. L. & CHOI, K. K. Configuration design sensitivity analysis of built-up structures. Part I: Theory, *International Journal for Numerical Method in Engineering*, 35, 1127-1150.

WALL, W.A., FRENZEL, M.A. & CYRON, C. 2008. Isogeometric structural shape optimization. *Computer Methods in Applied Mechanics and Engineering*, 197, 2976-2988.

YOON, D.H. 2015. Generalized isogeometric shape sensitivity analysis in curvilinear coordinate system and shape optimization of shell structures. *Structural and Multidisciplinary Optimization, 52* 1069-1088.

YOON, M. & CHO, S. 2013. Isogeometric shape design sensitivity analysis of elasticity problems using boundary integral equations. *Engineering Analysis with Boundary Elements,* 66, 119-128.

YOON, M., HA, S. -H., & CHO, S. 2013. Isogeometric shape design optimization of

heat conduction problems. *International Journal of Heat and Mass Transfer,* 62, 272-285.

ZHANG, Y., BAZILEVS, Y., GOSWAMI, S., BAJAJ, C.L. & HUGHES, T.J.R. 2007. Patient-specific vascular NURBS modeling for isogeometric analysis of blood flow. *Computer Methods in Applied Mechanics and Engineering*, 196, 2943-2959.

일반곡면좌표계에서 조립구조물의 아이소-지오메트릭 배치 최적설계

이 승 욱

산업·조선공학부

공과대학

서울대학교

초 록

아이소-지오메트릭 해석은 2000년 초부터 개발되어온 방법론으로서 CAD에서 쓰이는 NURBS 기저함수를 해석에서 그대로 이용한다는 점에서 기존의 유한요소법에 비해 많은 장점들을 가지고 있다. 기하학적인 모델을 법선 벡터와 곡률과 같은 고차기하정보를 손실 없이 쉽게 아이소-지오메트릭 해석모델로 변환하고 변위를 계산 할 수 있다. 또한 최적설계와 연계되어서 CAD 모델과 해석 모델이 직접적으로 연결 되어 있기 때문에 최적설계로 변경 된 모델을 다시 메시작업을 할 필요 없이 그대로 다시 해석에 사용될 수 있기 때문에 시간적인 효율이 좋다는 장점을 가지고 있다.

하지만 현재 아이소-지오메트릭 최적설계는 간단한 예제에 대해서만 검증되고 있어서 3차원 확장 및 판이나 쉘 같은 요소로 최적설계 요소를 넓히는 것이 중요하다. 그러기 위해서는 판과 쉘에 대한 배치 민감도 해석이 불가피 하며, 3차원 구조물의 최적설계를 위해서 반듯이 수행되어야 한다. 배치 민감도 해석은 기존의 형상 민감도 해석에 방향 민감도 해석을 추가한 개념이다. 이 논문에서는 판과 쉘에 대한 배치 민감도 해석을 수행하였으며, 그 민감도 값을 사용하여 최적설계를 수행 하였다. 특히 판의 경우 조립구조를 구성하여 좀 더 복잡한 예제를 구성할 수 있었다.

그리고 쉘의 경우, 기존의 사람들이 사용하는 형상 민감도를 배치 민감도해석으로 재해석하여 쉘에서도 배치 민감도 해석이 수행 될 수 있음을 보였다. 또한 수치 예제를 통해서 아이소-지오메트릭 해석이 유한요소해석보다 더 정확함을 보였고, 유한요소해석에서 할 수 없는 고차항의 기하학적인 정보를 정확하게 계산 할 수 있음을 보여주었다.

주요어: 아이소-지오메트릭 해석법, 배치 민감도 해석, 조립구조, 배치 설계 최적화, 변형 NURBS 기저 함수

학번: 2010-21111